UNIVERSITÀ
DEGLI STUDI
DI PADOVA

UNIVERSITA' DEGLI STUDI DI PADOVA

DEPARTMENT OF MEDICINE

Ph.D. COURSE IN CLINICAL AND EXPERIMENTAL SCIENCES
I CURRICULUM: CLINICAL METHODOLOGY AND MEDICINE OF PHYSICAL EXERCISE.
DIABETIC, ENDOCRINOLOGICAL AND NEPHROLOGICAL SCIENCES

XXX SERIES

UNDERSTANDING THE MECHANISMS OF ADIPOSE TISSUE EXPANSION IN MULTIPLE SYMMETRIC LIPOMATOSIS AND OBESITY

Coordinator: Ch.mo Prof. Paolo Angeli

Supervisor: Ch.mo Prof. Roberto Vettor

Co-Supervisor: Dr. Gabriella Milan

Ph.D. student: Dr. Marta Sanna

SUMMARY

ABSTRACT

Background: Our Center for The Study and The Integrated Treatment of Obesity (Ce.S.I.T.O) manages patients affected by obesity and, thanks to our Endocrine-Metabolic Laboratory, we focus on translational projects in metabolic diseases. Recently, given our scientific interest on the mechanisms and consequences of adipose tissue (AT) expansion, we also investigate another AT disorders, named Multiple Symmetric Lipomatosis (MSL), characterized by enlarging, symmetric and unencapsulated lipomas. The mechanisms involved in lipomatous tissue (LT) formation are still unknown. As the distribution of LT resembles the anatomic location of brown fat depots, the main hypothesis believes that brown cells fail to completely differentiate, accumulating lipids due to mitochondrial dysfunctions, defective noradrenergic regulation or both. Recently, the *Pten*^{Myf5cKO} mouse model was found to resemble MSL phenotype. PTEN is involved in insulin cascade as an inhibitor factor, whose activity is negatively regulated by protein kinase CK2, thus suggesting that an impairment of insulin pathway could have a role in AT expansion. CK2 is a protein kinase implicated in several essential cellular processes, such as the regulation of insulin signalling cascade. Recently, CK2 has been described to negatively regulate thermogenesis and to inhibit insulin release. Nevertheless, the role of CK2 in AT and its involvement in human obesity development and therapy has been poorly investigated. Our work provides a fine characterization of LT and its precursors from a morphological, molecular and functional point of view. Moreover, we have investigated the role of CK2 in adipocyte glucose homeostasis and CK2 expression and activity in a wide variety of AT alterations: mouse models of obesity, obese patients before and after weight loss and lipomas from MSL patients.

Material and Methods: We collected paired samples of LT and SAT in non-affected area of 5 Type I MSL patients, during lipectomy. H/E staining for adipocyte sizing evaluation and UCP1 IHC were performed in tissue sections. Gene expression profile of white/brown/beige markers was performed in tissues and cellular fractions. Stromal vascular fractions (SVF) were characterized by *ex vivo* cytofluorimetric analysis, proliferation assay and adipogenic and clonogenic potential limiting dilution assay. Moreover, to explore CK2 role in AT biology, glucose uptake assay, western blot, GLUT4 immunofluorescence were performed on *in vitro* differentiated 3T3L1 and human adipocytes in presence of CK2 inhibitors. We analyzed CK2 expression and activity in both visceral (VAT) and subcutaneous AT (SAT) of animal models of obesity (ob/ob) and obesity/diabetes (db/db), of 27 obese patients with different degree of insulin resistance or overt diabetes, in LT, SAT and SFV extracted from the enrolled MSL patients. Finally, CK2 was evaluated also in VAT and/or SAT of 12 patients who had obtained a relevant weight loss after diet or bariatric surgery.

Results: We demonstrated that LT contains slightly smaller univacuolated UCP1 negative adipocytes, expressing similar level of white-specific genes than SAT and negligible level of brown marker UCP1. LT-derived ASCs, defined as CD34+CD31-CD45- fraction, were significantly higher than in SAT. LT-precursors showed a slightly shorter doubling time and a higher clonogenic and adipogenic potential, giving rise to a higher number of clones, able to differentiate to mature adipocytes more efficiently than SAT derived cells.

LT-derived cells also exhibited a greater adipogenic potential than SAT at the clonal level, resulted enriched of adipogenic precursors. We demonstrated that in both human and 3T3L1 adipocytes CK2-inhibition decreased insulin-induced glucose uptake by counteracting Akt-signaling and GLUT4-translocation to the plasma membrane. We showed that CK2 promoted insulin-signaling in mouse AT, liver and skeletal muscle and that *in vivo* acute treatment with CX-4945 impaired tissue insulin signaling activation. Studies in tissues of ob/ob and db/db mice highlighted an up-regulation of CK2 expression and activity only in WAT. CK2 hyper-activation was strongly evident also in SAT and VAT of obese patients, independently from metabolic complications and a relevant weight loss completely normalized CK2 level. Interestingly, CK2 has been also found upregulated in LT in comparison with SAT of MSL patients and in LT-derived SVF.

Conclusions: LT exhibits a typical white AT signature and morphology and is enriched of adipogenic precursors, with a higher proliferating and clonogenic potential compared with paired SAT. This feature could contribute to explain LT benign expansion. We clearly show that CK2 supports insulin signaling in adipocytes, skeletal muscle and liver. Moreover, we demonstrated in different pathological conditions, such as mouse and human obesity and MSL, that CK2 upregulation is a hallmark of expanding AT, independent from metabolic complications and tightly regulated by AT reduction and remodeling. In conclusion, the present work gives molecular insights in the pathogenesis of obesity and MSL, suggesting a new therapeutic target for both rare and common AT disorders.

ABBREVIATIONS

ASCs: adipose derived stem cells
AT: adipose tissue
BAT: brown adipose tissue
BMPs: bone morphogenetic proteins
CD: cluster of differentiation
CIDEA: cell death inducing DFFA like effector A
CK2: protein kinase 2
ELOVL3: Fatty Acyl Chain Elongase 3
ERG1: E26 transformation-specific (ETS) related gene 1
EVA1: Epithelial V-like antigen 1
FLT1: Fms-Like Tyrosine Kinase 1
FML: Familial Multiple Lipomatosis
iNOS: inducible ossido nitrico sintetasi
KDR: Kinase Insert Domain Receptor
LT: lipomatous tissue
mRNA: messenger ribonucleic acid
MSL: Multiple Symmetric Lipomatosis
mtDNA: mitochondrial DNA
NO: nitric oxide
PGC1α: Peroxisome proliferator-activated receptor-gamma coactivator 1 α
Pheo: perirenal adipose tissue of patient affected by Pheochromocytoma
PPARγ2: Peroxisome proliferator activated receptor γ 2
PRDM16: PR domain containing 16
PTEN: Phosphatase and tensin homolog
qRT-PCR: quantitative real time polymerase chain reaction
SAT: subcutaneous adipose tissue
SVF: stromal vascular fraction
UCP1: uncoupling protein 1
us-CRP: high sensitive C reactive protein
WAT: white adipose tissue
VAT: visceral adipose tissue; VAT-E: epididymal adipose tissue
VEGFA: vascular endothelial growth factor A
ZIC1: Zinc Fingers in the Cerebellum 1

INTRODUCTION

MULTIPLE SYMMETRIC LIPOMATOSIS: A RARE ADIPOSE TISSUE DISORDER

Multiple Symmetric Lipomatosis (MSL, OMIM 151800) is a rare adipose tissue (AT) disorder characterized by enlarging, painless, and unencapsulated lipomas, developing symmetrically in the subcutaneous compartment (SAT), disfiguring patient aspect. It was first described in 1846 by Sir Benjamin Brodie, who reported on two patients with symmetrical cervical lipomas [1]; later in 1898 Madelung reported on three patients with symmetrical submental deposition of fat, the 'Madelung's collar' [2]. In 1898 Launois and Bençaude described in several patients lipomatosis clinical features as "symmetrical adenolipomatosis" [3].

An approximate incidence rate of 1:25.000 has been calculated for MSL in the Italian population [4] but it is probably underestimated because of frequent misdiagnosis. The disease mainly affects men than women, with a ratio of about 6 to 1. Mean age at onset varies from 30 to 60 years old according to the cohort [5, 6] without significant differences in men and women [7]. However, MSL has been reported also in children, describing cases of bilateral neck fat masses [8-10]. An epidemiological correlation of MSL with alcohol intake, mainly red wine, has been found [5, 11, 12], although a pathogenetic link has not explained so far.

Phenotypically two types of MSL have been described (Figure 1) according to lipomatous tissue (LT) distribution [7, 12]: type 1 is defined by well circumscribed, grossly round lipomas protruding from the body surface, and a substantially normal Body Mass Index BMI, while in type 2 MSL LT progressively diffuses, involving SAT layer and giving to the patient the appearance of a simple obesity, with a significantly higher BMI compared to type1 MSL [5]. Females almost invariably present a type 2 MSL, with a low occurrence of the Madelung's collar and of accumulation of LT within the mediastinum. Therefore, in females the differential diagnosis of MSL and simple obesity might be more difficult. Evaluating the frequency in a large cohort of 72 MSL patients [5], fat masses occur most frequently at neck (83.3% of the male patients), dorsal area (55%), mammary and subcutaneous abdominal areas (35%), upper limbs (54.1%), lower limbs (28%); distal segments of arms and legs are invariably spared. Sporadic case reports have described other rare localizations of lipomas, such as retro-orbital region [13], tongue [14, 15]; perineal and scrotal area [16].

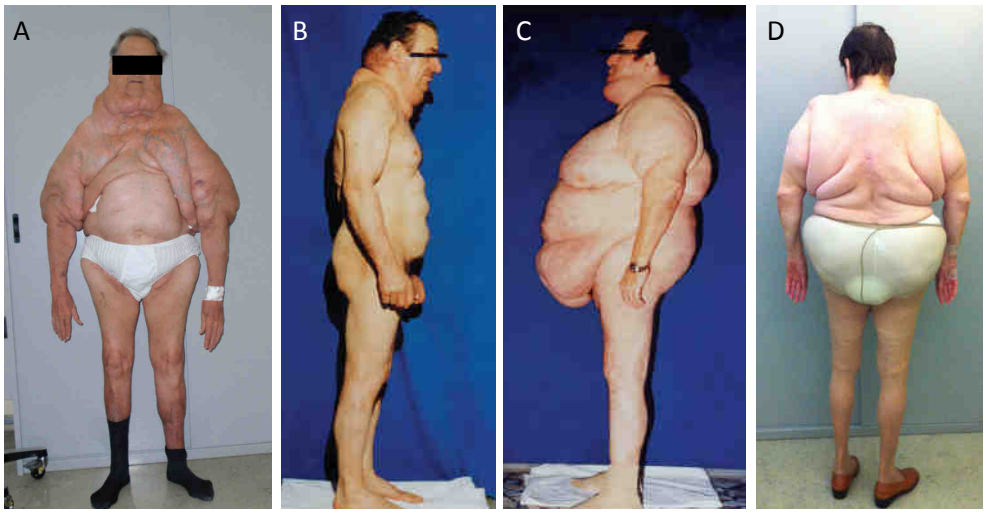

Figure 1. Phenotypes of Multiple Symmetric Lipomatosis. In **A** and **B** Type 1 MSL is represented: patients carry neck, cervical and thoracic involvement by lipomatous tissue (LT), while in **C** and **D** Medelung collar is absent and LT spreads in the context of subcutaneous adipose tissue in an obesity-like manner. Distal part of limbs is typically spared (adapted from [7]).

Relevant MSL clinical complications reside in the consequences of compression by lipomatous masses on close organs and structures: the occupation of mediastinum and peri-pharyngeal spaces could be associated to laryngeal dislocation and compression, requiring tracheostomy, and to a sub-mucosal infiltration of fatty tissue, causing chronic cough, dysphonia and swalling disorders (dysphagia). Especially in type 1 MSL, Upper Vena Cava Syndrome has been also diagnosed [17-19]. LT deposition around upper airways has also been related to the development of sleep apnea disorders. A further relevant clinical aspect of MSL is the high prevalence of neurological abnormalities, described since 1937 [20, 21]. Peripheral motor and sensory neuropathies, mainly involving the lower extremities have been demonstrated in MSL subjects by electromyography and nerve conduction study [22-25]. In skeletal muscle nerve (peroneal, sural) biopsies of non diabetic MSL subjects, electron microscopy analysis revealed a significant reduction of both density and minimal diameter of myelinated fibers, with a selective involvement of large fibers and signs of chronic denervation/re-innervation process in muscle [22]. However axonal alterations of sensory fibers were also described [26] and, although rarely, the central nervous system can be also involved (i.e. altered evoked potentials, cerebellar ataxia), configuring the possibility of a multisystem neurological impairment in MSL [27, 28]. Importantly, autonomic neuropathy also occurs MSL patients, causing gustatory sweating, hyperhydrosis at ankles, erectile dysfunction and tachycardia at rest. Evaluation of autonomic cardiovascular reflexes suggests a prevalent involvement of the parasympathetic system [29]. Cardiac autonomic neuropathy is considered almost in part responsible for the higher incidence of sudden death of MSL patients. Recently, a case of cardiac failure due to autonomic neuropathy with cardiac adrenergic denervation was detected by ^{123}I-metaiodobenzylguanidine

scintigraphy in a MSL patient without coronaropathy [30], supporting the hypothesis of a causing role of MSL-related autonomic disorder.

Since the presence of severe peripheral nervous system involvement even in non-drinkers MSL subjects, the lack of a correlation between alcohol intake and the motor and sensory conduction velocities suggests that MSL neuropathies are a specific feature of the disease, even if the elevated alcohol intake could represent a trigger for nerve damage.

Since MSL is as adipose tissue (AT) disorder, questions arise about its association with glycemic and lipid impairment. Although some single cases have been reported of MSL diabetic patients, the disease seems metabolically healthy [5, 11, 31-33]. The lipid profile of MSL is characterized by a peculiar, pronounced elevation of plasma high density lipoprotein (HDL) cholesterol, namely HDL2 cholesterol sub-fraction and Apo A-1 values [34], that may confer cardiovascular protection. The low incidence of coronary artery disease, observed in MSL patients even in long-term follow-up [12], could be a further demonstration of the antiatherogenic and cardioprotective function of elevated levels of the HDL, HDL2 cholesterol fractions and Apo A-1, possibly related to the elevate intake of polyphenols from red wine [35, 36].

Recently, AT Lipoprotein-lipase activity (AT-LPL) has been evaluated in 15 MSL patients [5]. A significantly higher AT-LPL activity was found in MSL patients and a significant correlation of HDL and HDL2 levels with AT-LPL activity was also demonstrated. It is known that peripheral clearance of triglyceride-rich lipoproteins is regulated by the AT-LPL system. In summary, the lipoprotein pattern of MSL patients is consistent with a newly recognized type of hyper-α-lipoproteinemia.

The occurrence of hyperuricemia has been frequently observed in MSL patients. In two MSL female patients of the same family, a marked increase in the whole-body miscible pool and in daily turnover of uric acid has been reported [37] and also in a large MSL cohort the mean values of plasma uric acid were slightly but significantly higher in MSL patients than in age, sex and body weight matched controls. However, it is likely that the elevated alcohol intake of these patients explains uric acid alterations [5].

Body composition has also been studied in MSL patients. Dual Energy X-ray Absorptiometry (DEXA) analysis reveals, as expected, that fat mass FM is significantly increased in MSL affected regions but reduced in distal segments of lower limbs compared to age, sex and BMI matched healthy controls as well as free fat mass FFM resulted decreased [5, 38]. When adjusted for FFM, the resting energy expenditure (REE), evaluated by an open-circuit indirect calorimeter, was significantly higher in MSL patients than in controls. FFM atrophy could be almost in part explained by peripheral neuropathy and the elevated alcohol intake.

Therefore, although MSL could be defined benign in the context of overgrowth/neoplastic disorders lacking the capacity of metastatic spreading, morbidity burden is relevant, profoundly impairing patient quality of life.

Pathogenesis of Multiple Symmetric Lipomatosis

The mechanisms involved in LT formation are still controversial, existing many hypotheses about the origin of lipomatous cells.

Since familial cases of MSL were described, usually affecting younger patients, efforts have been made to unravel the genetic causative alteration. Evaluating the pedigree of affected subjects, MSL could be considered an autosomic dominant inherited disease [39, 40], but also recessive inheritance has been presumed [41]. The discordance among the different studies underlies the genetic variability of this disease and, on the other hand, the possibility that different forms of lipomatosis have been unified under the same generic definition of Multiple Symmetric Lipomatosis, based on phenotypic presentation and not on pathogenesis.

Familiar cases of MSL must be distinguished from Familial Multiple Lipomatosis (FML, OMIM % 151900), generally characterized by encapsulated, well circumscribed lipomas. In FML, cytogenetic analysis reveals in cases of multiple lipomas rearrangements and abnormalities of Chromosome 12 [42, 43]. Comparing multiple lipomas with isolated lipomas and myxoid sarcoma the breakpoint in benign lipomas, including multiple lipomatosis, is situated at 12q15, more distally than in myxoid liposarcoma (12q13.3) [44]. In a severe form of pediatric multiple lipomatosis, characterized by extreme somatic overgrowth and macrocephaly, a chromosomal inversion was found to truncate High Mobility Group AT-Hook 2 (HMGA2), that encodes an architectural factor associated with the development of many benign mesenchymal tumors and that maps to the 12q14.3 breakpoint [45]. Identification of the deletion, amplification, and rearrangement of HMGA2 in myxoid liposarcoma suggests a role of high mobility proteins in the regulation of adipogenesis and mesenchymal differentiation.

Besides the alterations that arise the dysfunctions in lipomatous cells, the question about which kind of cell gives rise to LT is open. Some features of MSL, as the anatomical localization and the high vascularisation of LT, suggest that it could derive from brown adipose tissue (BAT). As increasing evidence demonstrated, BAT persists even in adulthood most frequently at inter-scapular, peri-renal and cervical levels, in the proximal segments of the upper and lower limbs and around the aorta and carotids [46-48]. Therefore, one of the most accredited hypothesis believes that brown precursor cells fail to completely differentiate, proliferating and accumulating abnormally lipids, thus forming the expanding LT. Some authors showed that MSL-derived cells display morphological characteristics of brown adipocytes and express the uncoupling protein 1 UCP1 mRNA, the master BAT specific marker, but, *in vitro,* the β-adrenergic stimulation fails to induce the thermogenic program in MSL derived cell cultures [49, 50]. The defect seems proximal to cyclic AMP formation because theophylline, a potent phosphodiesterase inhibitor, induces a prompt and significant decrease in intracellular ATP in lipomatous cells. Further *in vitro* studies demonstrated a defective noradrenalin-mediated induction of inducible nitric oxide synthase iNOS in LT derived cells[51]. Since nitric oxide NO is known to block proliferation, allowing the cell to enter the

differentiation program, a defect in NO induction was postulated as mechanism of proliferation and impaired brown differentiation of lipomatous cells; β3-adrenergic receptor gene expression alterations or genetic mutations were excluded in lipomatous cells compared to normal adipocytes, while large mitochondrial DNA (mtDNA) deletion were found, possibly contributing to altered lipid accumulation during differentiation of lipomatous cells [51].

Several other authors reported on mitochondrial dysfunctions and multiple deletions of mtDNA associated with MSL: a defective mitochondrial respiration could lead to a reduced fatty acid uptake and oxidation with resulting in an abnormal lipid accumulation. The myoclonic epilepsy ragged red fibers (MERRF) syndrome, caused by A8344G or G8363A tRNA-lysine gene point mutation in mtDNA, has been described in association with MSL in 15-25% of patients [52-54]. Very recently, the concomitant presence of MERRF mutation and m.14484T>C mutation in MT-ND6 (Mitochondrially Encoded NADH:Ubiquinone Oxidoreductase Core Subunit 6) gene, causative of Leber hereditary optic neuropathy phenotype (LHON), has also been described in a patient carrying Madelung disease, myoclonus and ataxic gait disorder [27]. Gene expression analysis of LT compared to healthy SAT in three subjects bearing A8344G or G8363A tRNA-lysine gene mutations showed that LT expressed *UCP1* while normal AT did not; *peroxisome proliferator activated receptor γ coactivator 1α* (*PGC1α*) mRNA was unaltered, *peroxisome proliferator activated receptor γ* (*PPARγ*) was downregulated as well as *preadipocyte factor 1* (*Pref1*), a marker of preadipocytes [55]. In LT of these subjects, however, cytochrome C oxidase gene expression was normal.

Whole exome sequencing analysis demonstrated also *Mitofusin 2* (*MFN2*) mutations in patients affected by MSL associated with neuropathy: while heterozygous mutations of MFN2 is known to cause Charcot Marie Tooth disease (CMT), the homozygous mutation p.R707W has been demonstrated in two unrelated MSL families [56]. Cell based experiments confirm that p.R707W mutation functionally affects mitochondrial biology, reducing cell capacity to tubulate mitochondria and promoting their aggregation.

Since mitochondriopathies imply skeletal muscle alterations, researches aimed to analyze possible muscle involvement in MSL. In muscle biopsies of MSL patients, central hyporeactive areas, hyper-reactive angulated fibers and subsarcolemmal rims of mitochondria and lipid storage defects have been observed [22, 57]. Respiratory chain enzymes activity in these samples showed a significant decrease of cytochrome-c oxidase, succinic dehydrogenase and citrate synthetase activity, with a consequent reduced ATP production but these alterations were not always associated with the presence of mtDNA mutations. Other authors described a defect in mitochondrial respiratory chain with a decrease in oxygen consumption in intact lymphocytes in 9 MSL patients [58], supporting the idea of MSL as mitochondrial disease. Although not all patients carry a mtDNA abnormalities, mitochondrial alterations could also derive from mutation in native DNA coding factors that regulate mitochondrial functions, since ti seems that 95% of mt dysfunction is caused by nuclear DNA [59].

The only recognized environmental factor linked with MSL is alcohol intake, but its molecular role has not been identified so far. Resveratrol, contained in the red wine, acting on sirtuin1 (SIRT1) could in part explained the metabolically healthy phenotype of MSL[60] and the relative protection against coronary artery diseases.

An interesting observation, that open new insight in the molecular causative mechanism of MSL, is the description of the phenotype of *PTEN*^{Myf5cKO} mouse, a selective knock out of phosphatase and tensin homolog (PTEN) in Myf5 lineage [61]. This model recapitulates the fat mass distribution of MSL with enlargement of interscapular WAT and reduction of inguinal and epididymal depots, limb muscle atrophy. Since PTEN acts as a potent inhibitor of the insulin cascade (see below), these data suggest a possible role of insulin signaling hyperactivation in MSL pathogenesis.

Experimental studies on lipomatous tissue and lipomatous adipocytes

Morphometric studies describing LT compared to normal SAT raveal contrasting data. Some reports described median adipocyte area significantly lower in LT than in normal SAT, suggesting a hyperplastic mechanism of LT expansion [51, 62, 63], while others, even as single case reports, described in LT larger adipocytes [64]. LT results a high vascularized tissue with a slightly higher fibrotic component and a tendency to infiltrate muscle across fascio-muscular and vasculo-nervous planes[65].

From *in vitro* studies on LT-derived adipoyte cultures, a defect in noradrenergic-stimulated lipolysis of LT has been postulated [49]; but controversial data are present in literature since Nielsen and colleagues demonstrated *in vivo* even a greater adrenergic dependent lipolysis and a higher fatty acid uptake in deltoid LT compared to normal SAT in type 2 MSL subjects [66].

In Seventies, first studies with MSL isolated pre-adipocytes described a faster culture growth and ultra-structural investigation showed numerous nuclear pockets and cytoplasmic microfilaments, not observed in adipocytes derived from healthy AT, suggesting a cancer-like behavior of the disease [67]. Later on, the comparison of MSL derived preadipocytes with both human preadipocytes and rat brown preadipocytes suggested a close similarity of LT with BAT, corroborating a brown origin [51, 63]. LT derived preadipocytes appear to show a higher proliferative activity compared to normal adipose precursors cells [62], contributing to the idea of a predominant growth by hyperplasia. Interestingly in the same work, an upregulation of several tumor suppressors (p53 signaling pathway) has been found, suggesting a cellular rescue mechanism toward uncontrolled proliferation in lipomatous cells that could explain the relative benign behavior of LT.

Very recently, Zhaohui's group compared gene expression profile of LT derived from three unrelated MSL patients (with history of alcohol abuse) and healthy AT from three age and sex matched control males by gene ontology enrichment (GO), Kyoto Encyclopedia of Genes and Genomes (KEGG) and protein-protein interaction (PPI) network analysis [68]. In LT critical regulatory genes of adipogenesis resulted upregulated

in comparison with normal AT, such as *PPARγ*, *Leptin*, *C/EBPα* and *C/EBPβ*; also *Homeobox C8*, a white specific marker, is overexpressed in LT, whereas JUN and FOS gene family were downregulated, in agreement with the demonstration that, when upregulated these factors are able to inhibit adipogenesis [69, 70]. In contrast with previous reports, this work did not find any differential expression of UCP1 or p53 pathway related genes, confirming that MSL pathogenesis is far to be clearly elucidated.

Recent evidence postulated also a role of miRNA in the etiology of MSL. Among the analyzed 754 human miRnas in LT of three MSL patients and of three matched controls (in each patient biopsies were harvested from the right upper abdominal quadrant) 18 were upregulated in MSL and in particular, miR-125a-3p and miR-483-5p were demonstrated to promote *in vitro* adipogenesis by PPARγ induction and modulating Ras homolog family member A (RhoA)/Rho-associated kinase (ROCK)/ERK1 [71]: it is known that RhoA/ROCK/ERK1 inhibits adipogenesis and is a target of miR-125a-3p [72] [73]. Interestingly, when transplanted in nude mice, preadipocytes transfected with miR-125a-3p and miR-483-5p were able to form larger AT pad in comparison to control, corroborating a possible role of these pro-adipogenic miRna in MSL pathogenesis.

Therapy

In the management of MSL patients the first measure is alcohol withdrawal. In a large cohort of subjects on long term follow up, a spontaneous reduction of the fat mass size was obtained exclusively in those patients who suspended or reduced the alcohol intake [12]. However, surgical approach is the first choice since no effective medical treatment is available so far. Two options could be offered to the patients: lipectomy and/or liposuction. Lipectomy represented the safest option because of better control of bleeding; the neck and the supra-clavear region require a careful toilette, due to the disclocation and infiltration of surrounding muscles, nerves and vessels by LT. Possible complications are lesions of a branch of the brachial plexus or section of the lymphatic duct; due to massive blood loss of the high vascularized LT post-procedure anemia often occurs. Traditional or ultrasound assisted liposuction are considered less invasive, limited scarring and allow to treat multiple areas [74]. For shoulders, deltoid area and proximal segments of the limbs, liposuction seems to be the first choice[75]. Combined lipectomy and liposuction is also possible specially to treat neck and head lipomas [76].

Esthetic and functional results are satisfactory in the majority of the patients, although relapses frequently occur, requiring recurrent intervention. A significant improvement of the dermatological life quality index (DLQI) after surgery has been reported [77]. The recurrence rate of surgical fat excision is 63% while 95% of liposuction [11].

Different medical approach have been investigated without success. Annedotic use of fenofibrate, (200 mg/day) in a MSL patient limited the progression of LT growth, but this remains a single observation not supported by rigorous studies [78]. Contrasting opinions are reported about the efficacy of repeated intra-

tumoral injections of phosphatidylcholine [79, 80]. Unsuccessful administration of oral salbutamol was reported[81].

OTHER TYPES OF ADIPOSE TISSUE OVERGROWTH

The differential diagnosis of MSL takes into account the other rare forms of lipomatosis and soft tissue overgrowth. The PI3K-related overgrowth spectrum (PROS) comprehends a range of overgrowth syndromes associated with somatic mosaic activating *PIK3CA* mutations that leads to a pathological activation of AKT/mTOR pathway: CLOVES syndrome (congenital lipomatous asymmetric overgrowth of the trunk, lymphatic, capillary, venous, and combined-type vascular malformations, epidermal nevi, skeletal and spinal anomalies); hemihyperplasia multiple lipomatosis (HHML); megalencephaly-capillary malformation (MCAP) syndrome; dysplatic megalencephaly (DMEG); Fibroadipose Hyperplasia (FH) and Klippel-Trenaunay syndrome, characterized by "port-wine stains," lymphatic anomalies, arteriovenous malformations in association with variable overgrowth of soft tissue and bone [82]. The mosaic gain of function mutation in *PIK3CA* gene leads to pathological AKT/mTOR pathway activation and is responsible of the clinical manifestations. Finally involving the AKT pathway, Phosphatase and Tensin Homologue (PTEN, see below insulin signaling) hamartoma tumor syndromes (PHTS, OMIM +601728) are a spectrum of disease due to PTEN gene inactivating mutations (Cowden syndrome; Bannayan-Riley-Ruvalcaba syndrome) whose clinical features are the consequences of abnormal overgrowth (adipose tissue, skeletal, muscle, brain, vascular, or lymphatic), skin abnormalities and have the potential risk of tumorigenesis. [83].

Dercum disease (OMIM % 103200) is a very rare syndrome with different phenotypes whose genetic cause has not been found yet: a generalized diffuse form, with diffusely widespread painful AT without clear lipomas, a generalized nodular form with general pain in AT and intense pain in and around multiple lipomas, and localized nodular form, with pain in and around multiple lipomas; juxtaarticular form with solitary deposits of excess fat. Krabbe disease (OMIM # 245200), also known as globoid cell leukodystrophy, is a recessive inherited lysosomal disorder caused by homozygous or compound heterozygous mutation in the galactosylceramidase gene (GALC) and is characterized by central and peripheral nervous system alterations and little multiple subcutaneous lipomas. Encephalocraniocutaneous lipomatosis (ECCL, OMIM # 613001) or Haberland syndrome, characterized by brain, spinal cord and subcutaneous asymmetric involvement by lipomas; it has been proposed that the cause is a postzygotic somatic activating mutation in the FGF receptor 1 (FGFR1) gene. Other overgrowth syndromes, most often causing asymmetrical body overgrowth, are related to AKT gene mutations: Proteus syndrome (OMIM #176920), due to an activating AKT1 gene mutation (see below in insulin signaling) and characterized by dysregulated AT (lipomas, lipohypoplasia, fatty expansion) and bone, skin, vascular abnormalities; Megalencephaly polymicrogyria polydactyly hydrocephalus 2 (MPPH2) syndrome (OMIM #615937), caused by activating AKT3 mutations;

Lipodystrophy syndrome-hypoglycemia (OMIM # 240900) whose underlying alteration is an activating AKT2 mutation [83].

THE DIFFERENT COLORS OF ADIPOSE TISSUE AND ADIPOSE DERIVED STEM CELLS

The concept of AT as a static tissue for fatty acids storage has been deeply reconsidered: indeed, it is involved in important dynamical processes as endocrine organ and hormonal source and moreover as thermogenic regulator which makes it one of the key players involved in body energy balance. The evolution of the concept of AT as an active organ originated also from the description of three different adipose cell subtypes with selective functions and specific involvement in pathology: white and brown adipocytes and the more recently described beige cells [84]. White adipocytes are of large cells with unilocular lipid droplets and few mitochondria, while brown cells are smaller with multilocular lipid droplets, densely packed mitochondria and highly vascularized and innervated (sympathetic nervous system). Their functions differ from each other, being the white cell a main energy storage/release, hormone producer and thereby a hunger/satiety balance regulator, whereas the brown adipocyte provides the non-shivering thermogenesis through the uncoupling protein1 (UCP1) expression, contributing to the regulation of body temperature and energy homeostasis. White AT (WAT) and BAT origin from different lineages during developmental growth. It is widely accepted that BAT and skeletal muscle are closely related during development [85]: fate mapping studies demonstrated that the myogenic factor 5 (Myf5) positive cells, specific for the myogenic lineage, give also rise to brown adipocytes, being PR domain zinc finger protein 16 (PRDM16) the transcription factor that controls the brown/muscle switch [86]. On the other hand, platelet derived growth factor receptor α (PDGFR α) positive and Myf5 negative cells are committed towards the white adipogenic lineage[87].

Beige adipocytes represent a third intermediate population with phenotypic plasticity that are recruited within white depots in response to appropriate stimuli as cold exposure or adrenergic stimulation: on demand, they are able to switch from white to brown phenotype, acquiring a multilocular UCP1-expressing features, activating the thermogenic program, significantly contributing to adaptive thermogenesis [88]. For this reason, research is currently focusing on the study of beige cell behaviour, having promising therapeutic implications in metabolic diseases, such as obesity and diabetes. Regarding the origin of beige adipocytes, the debate is still open and different hypothesis have been drown. Some authors support the notion that beige cells arise from *de novo* differentiation of adipogenic precursor cells [89, 90] in response to cold or adrenergic stimulation. On the other hand, several data support the idea of a direct conversion of mature white adipocytes in beige cells, a process called transdifferentiation [91-94]. Interestingly beige adipocytes, formed during cold exposure, could lose UCP1 expression and the multilocular shape after warming but upon another cold exposition they are able to regain the thermogenic components, underlying the phenotypic flexibility of beige cells in response to environmental request. Another

important issue regards the identity of the beige precursor cell. Interestingly SAT (inguinal AT in mice) and visceral (epididymal) AT (VAT) seem to have different mechanisms of beige induction [89]: in VAT a PDGFRα+ bipotent precursor cell has been identified for white and beige adipocytes dependently from external conditions: upon high fat diet the PDGFRα+ cells give rise to white adipocytes to buffer calorie excess while, under cold exposure or β-adrenergic agonists, the same population origins multilocular UCP1+ adipocytes. Within inguinal AT, different populations of precursors, such as mural cells (defined as PDGFRβ+ smooth muscle actin SMA+ cells) and smooth muscle cells (identified as myosin heavy chain 11 MYH11+SMA+ cells) can differentiate into beige adipocytes [85].

BAT is well represented in rodents and infants, whereas its more recent description in human adults occurred through 18-fluorodeoxyglucose positron emission tomography (FDG PET) studies since BAT is highly metabolically active: it was identified as intercepting areas located in interscapular, perirenal, cervical, periaortic and carotid regions [46]. If these "brown areas" described in humans represent true constitutive brown or beige fat, this is still matter of debate. In healthy subjects, biopsies collected from true BAT regions, identified by FDG-PET or NMR, showed a gene expression profile comparable to murine beige tissue [84, 95], suggesting that human BAT is likely to be beige. In addition, human BAT displays a beige-fat like histology, containing islets of multilocular UCP1 positive cells interspersed among classical white adipocytes. In contrast with these results, the molecular analysis of different region of human neck AT suggests the presence of both classical brown and beige cells [96]. However, it is worth noting that in this study biopsies were harvested during surgery for thyroid diseases that could have influenced AT gene expression pattern. An interesting example of brown/beige AT in humans is represented by AT depots in Pheochromocytoma: in these patients the pathological secretion of catecholamines induces a strong and evident browning of WAT demonstrated in perirenal and omental AT, with the development of large areas of multilocular UCP1 positive adipocytes [97, 98].

Besides adrenergic and PPARγ agonists, beige islands in WAT were shown to appear in response to other molecules as well: bile acids, fibroblast growth factor 21 (FGF21), atrial and ventricular natriuretic peptides (ANP, BNP), bone morphogenetic protein (BMP4 and 7) are able to induce beige differentiation through several mechanisms ([88]). The "browning" of WAT represents a new therapeutic target in obesity treatment, leading to UCP1 hyperexpression and thereby to heat production and energy dissipation. The identification of all those factors involved in this process could represent a revolutionary step in obesity management.

Many studies have focused on gene expression analysis to distinguish white, brown and beige cells[85], especially to identify early markers that predict one specific commitment to potentially induce the thermogenic program as therapeutic intervention for weight loss (Figure 2). Although species-specific differences are present, gene for Leptin (LEP), homeobox C9 and C8 (with currently unknown function in WAT), retinoblastoma protein 1 (Rb1), that interacts with CCAAT/enhancer binding protein (C/EBP) family

in the adipogenic process, resistin (RETN) are considered white specific markers [99]. Although the better and most specific brown marker is UCP1, shared also by the beige cell together with cell death inducing DFFA like effector A (CIDEA), other genes are believed to characterize brown cells: zinc finger in the cerebellum 1 (ZIC1), miR206 [100], epithelial V-like antigen 1 (EVA1 or Mpzl2), LIM homeobox protein 8 (LHX8), fatty acyl chain elongase 3 ELOVL3, that seems to play a fundamental role in early BAT activation upon cold exposure [101]. An even more challenging aspect is the identification of beige specific factors for the distinction with brown cells. The most accepted genes, derived from both animal and human studies, are Cbp/P300 Interacting Transactivator With Glu/Asp Rich Carboxy-Terminal Domain 1 (CITED1), Transmembrane Protein 26 (TMEM26), T-box1 (TBX1) and cluster of differentiation 137 CD137 (also known as TNFRSF9), considered as a beige precursor surface marker.

Type	Location	Developmental origins or precursor type	Common markers		Brown and beige versus white markers		Brown versus beige markers	
			Adipocyte	Pread.*	Adipocyte	Pread.	Adipocyte	Pread.
Brown	Interscapular, cervical, axillary and perirenal	• *MYF5*⁺ *PAX7*⁺ *EN1*⁺ cells in dermomyotome	• *ADIPOQ* • *FABP4* • *PPARG* • *C/EBPIIB*	• *PDGFRA* • *LY6A* • *CD34* • *PREF1* • *CD29*	• *UCP1* • *DIO2* • *CIDEA* • *PPARGC1A* • *PPARA* • *COX7A1* • *COX8B* • *PRDM16* • *EBF2*	• *EBF2*	• *LHX8* • *ZIC1* • *EVA1* • *PDK4* • *EPSTI1*	
Beige	WAT depots (more prominent in inguinal than in epididymal)	Inguinal WAT • *EBF2*⁺ *PDGFRA*⁺ cells • *ACTA2*⁺ smooth muscle cells • *MYH11*⁺ smooth muscle cells • *PDGFRB*⁺ mural cells, epididymal WAT • Bipotent *PDGFRA*⁺ precursor					• *TBX1* • *CITED1* • *SHOX2* • *CD137* • *TMEM26* • *PAT2** • *P2RX5**	• *CD137**
White	Subcutaneous and visceral	• *WT1*⁺ mesothelial (visceral)			• *LEP* • *RETN* • *AGT*	• *WT1* (visceral fat)		

Figure 2. White, brown and beige specific markers are summarized distinguishing those expressed by precursor cells (Pread.) and mature adipocytes (adipocyte). Common genes and factors that allow the distinction between white versus beige and brown versus beige are reported (from[85]).

A huge body of literature has been written about the characterization of adipose precursor cells within WAT depots to understand the biology of AT expansion and therefore its pathological implications. The concept of Mesenchymal Stem Cell, introduced in the late sixties by isolation from bone marrow (BM-MSC), laid the groundwork for the definition of adipose stem cells (ASCs) in 2000 [102, 103]; as stem cells ASCs show both self-renewal and multilineage differentiation properties. Human ASCs are obtained from stromal vascular fraction (SVF), a heterogeneous cell population isolated from AT by enzymatic digestion, centrifugation and removal of the mature adipocytes fraction. Freshly isolated SVF from AT specifically expresses higher levels of CD34 compared to other mesenchymal tissues as bone marrow [104, 105]. The *ex vivo* expression of CD34 on ASCs is rapidly downregulated *in vitro* during culture expansion with a concomitant increase in other mesenchymal markers expression: CD13 (APN), CD73 (L-VAP-2), CD90 (Thy-1), CD105 (endoglin). Also CD271 is described to be expressed by the SVF and represents an additional

marker used to characterize a subpopulation of MSCs in bone marrow. Morphologically ASCs display a peculiar triangle shape and a low proliferation rate (doubling time=20-40 hours); after further culture passages, from an initial fibroblast-like shape they gradually expand on the plastic surface area, rearranging their cytoskeleton with characteristic F-actin and vimentin intermediate filaments (stress fibers) disposition. Under appropriate stimuli ASCs are induced to differentiate towards the adipogenic lineage. Many *in vitro* models are used to study the adipogenic process, such as 3T3L1, 3T3-F442A murine cell line, embryonic cells and primary cultures derived from AT of animals and humans. Adipogenesis (revised in [106]) is characterized by a first phase called determination, where the commitment of a pluripotent stem cell to the adipocyte lineage takes place, and a second phase termed terminal differentiation, divided into mitotic clonal expansion, induction and maturation of preadipocytes. In the determination of cell fate, a central role is believed to be played by the Wnt signaling: in MSCs the non-canonical cascade (Wnt5b) promotes adipogenesis. On the contrary, canonical Wnt signaling (i.e. Wnt10b), through the frizzled receptor and LDL related protein coreceptor, serves as negative regulator of adipogenesis through the chicken ovalbumin upstream promoter transcription factor II (COUP-TFII). The activation of canonical Wnt pathway allows the stabilization and translocation of β-catenin into the nucleus, subsequently β-catenin coactivates the lymphoid enhancer-binding factor/T cell specific transcription factor (LEF/TCF) family that induces Wnt gene targets, including c-myc and Cyclin D1. The final result is the inhibition of different proadipogenic transcription factors. Hedgehog (Hh) and Retinoblastoma protein (Rb) signaling are implied in adipocyte commitment: they seem to exert an inhibitory effect on adipogenesis with a poor known mechanism. Terminal differentiation can be induced *in vitro* by different cocktails containing insulin, corticosteroids and cAMP inducers; after 16-20 hours preadipocytes synchronously re-enter the cell cycle, undergoing at least one or two rounds of mitosis (mitotic clonal expansion) before growth arrest. From the fibroblast-like morphology cells turn to a round shape and start to store lipids as multiple growing droplets. Terminal differentiation is accompanied by a marked increase of *de novo* lipogenesis, β_2- β_3 receptor expression and a progressive acquisition of insulin sensitivity due to upregulation of insulin receptor and GLUT4. During induction (early stage of terminal differentiation, until day 3-4 from the beginning of differentiation) a cascade of transcription factors takes place starting from phosphorylation of CREB by PKA, that upregulates C/EBPβ gene, and activation of C/EBPβ by mitogen-activated protein kinase (MAPK) and glycogen synthase 3 β (GSK3β). The active form of C/EBPβ, together with C/EBPδ, then induces C/EBPα and PPARγ, the master regulator of adipogenesis, being both essential and sufficient for this process, leading to adipocyte gene expression. Another fundamental factor that contributes to induce the adipogenic program is the sterol regulatory element binding protein 1c (SREBP1c), that controls lipogenic genes expression. Differentiating cells start to synthesize specific enzymes related to lipid metabolism (ATP citrate lyase, malic enzyme, glycerol-3-phosphate acyltransferase, fatty acid synthase); adipokines (i.e. leptin, adiponectin), adipocyte

specific fatty acid-binding protein FAT/CD36, perilipin, a lipid droplet associated protein, and fatty acid binding protein (FABP4 also known as aP2).

OBESITY: THE MOST COMMON ADIPOSE TISSUE DISORDER

Obesity is spreading as an epidemic disease and it is considered a major public health concern since it associates with many chronic comorbidities including type 2 diabetes (T2DM), cardiovascular diseases and several types of cancer. As chronic disease, obesity impacts deeply on our society, involving not only a sanitary issue, correlating with a high morbidity and mortality, but also economic and social aspects. In 2014 the WHO estimated that 1,9 people worldwide, aged 18 and over, were overweight; among them 600 million were obese. The European data from the WHO world health statistics report of 2015 reported an obesity prevalence among adults of 21,5% in males and 24,5% in females (World Health Organization: World Health Statistics 2015. Geneva, WHO, 2015, pp101–111. www.who.int/gho/publications/world_health_statistics/2015/en/). Considering the burden of this epidemic and chronic disease associated with severe complications, the elucidation of obesity pathogenic factors and the development of therapeutic strategies, has represented a crucial step. Among therapeutic interventions, although lifestyle changes and, to a less extent, pharmacotherapy represent hypothetically the first, fundamental recommendation, bariatric surgery has dramatically raised in the last years [107]. Indeed, bariatric surgery was shown to induce not just a significant weight loss in the major part of patients, but also to associate with a global metabolic improvement in terms of comorbidities remission. The new coined concept of metabolic surgery refers precisely to this effect, observed even in those patients who obtain poorer results in terms of weight loss [108]. In 2011 over 340.000 bariatric surgical procedures were performed worldwide with a further, steady increase in the last years [109].

Considering one of the major obesity related complication, it is estimated that about 90% of T2DM is attributable to excess weight [110], but the precise pathogenetic mechanisms linking the two conditions have not been fully elucidated. Converging data suggest that an impaired function of AT could play a pivotal role in T2DM development but the mechanisms underlying AT dysfunction remain to be completely established. Currently, two hypothesis have been proposed about the timing and sequence of hyperinsulinemia, hyperglycemia and insulin resistance on the basis of the most recent data : the classical paradigm believes that the positive energy balance in susceptible individuals, characterized by a chronic elevation of free fatty acids (FFA), characterizing obesity, leads to an accumulation of triglycerides within extra-AT organs, such as liver, skeletal muscle and pancreatic β-cell islets and to a predominant utilization of lipids by muscles with a concomitant inhibition of glucose transporter activity (lipotoxicity). These events inhibit glucose uptake and glycogen synthesis in muscles, contributing to the development of a chronic hyperglycemia that further impairs insulin sensitivity (glucotoxicity). In addition, insulin resistance induces a

higher basal lipolysis and a decreased capacity to store fatty acids, worsening the lipotoxic effect of obesity [111]. In this scenario the vicious cycle insulin resistance-hyperglycemia-hyperinsulinemia-insulin resistance, at the end, could drive to T2DM. However strong data also lead to the idea that hyperinsulinemia might be the primary alteration that occurs in obesity, inducing itself insulin resistance before blood glucose increases (review in [112]). Indeed hyperinsulinemia, induced by increased insulin secretion by pancreatic β cells and/or reduced insulin degradation, is the earliest alteration that could be demonstrated in many animal and human studies while blood glucose had not changed yet. Interestingly it was demonstrated that a high fat diet is able to directly increase insulin secretion by pancreatic β cells in still insulin sensitive animals [113], suggesting a potential and direct role of nutrients in the pathogenesis of insulin resistance and metabolic complication of obesity.

INSULIN SIGNALLING

In AT biology, insulin plays a major role in regulating its growth and function, acting on cell proliferation, differentiation, glucose and lipid metabolism. In this view exploring insulin pathway appears fundamental also in a pathological perspective.

Insulin binding to its receptor IR (Figure 3, [114]) causes autophosphorylation at tyrosin residues located in the cytoplasmatic face and thus recruitment and phosphorylation of the insulin receptor substrate proteins (IRS-1-4), which act as a platform for the activation of two main signaling pathway: the phosphatidylinositol 3-kinase (PI3K)-AKT/protein kinase B (PKB), that mediates most of the metabolic actions of insulin and the Ras-mitogen-activated protein kinase (MAPK), which cooperates with PI3K pathway to control cell growth and differentiation [115]. P85/p110 PI3K generates the phosphatidylinositol 3,4,5-trisphosphate (PIP_3), which induces the translocation to the plasma membrane of 3-phosphoinositide-dependent kinase 1 (PDK1) and the Ser/Thr protein kinase Akt/PKB, allowing the PDK1 mediated phosphorylation at Thr308 of the activation loop of Akt catalytic domain. Once further phosphorylated at Ser473 by mTORC2 (the mammalian target of rapamycin complex 2), Akt is then able to phosphorylate a range of substrates that orchestrate a complex metabolic program, leading to cell glucose uptake, increased glycogen and protein synthesis, and inhibition of gluconeogenesis and lipolysis [116]. Upon Akt mediated phosphorylation at Ser9, Glycogen Synthase Kinase 3 (GSK3) is inactivated, causing, in parallel with protein phosphatase-1 (PP1) activation, the dephosphorylation of glycogen synthase (GS), promoting glycogen synthesis [117, 118]. The other fundamental target of Akt is Tre-2 BUB2 CDC16 Domain Family Member 4 (TBC1D4), also known as RabGTPase activating protein AS160 (Akt substrate of 160 KDa), exerting an inhibitory phosphorylation that favors the GTP-loaded state of Rab, involved in the cytoskeletal re-organization for GLUT4 translocation from intracellular compartments to the plasma membrane [119, 120]. In contrast to acute insulin stimulation, prolonged action causes GLUT4 depletion, mainly by accelerated lysosomal degradation [121, 122]. AKT also regulates the expression of gluconeogenic enzymes by controlling the

activity of the winged helix or forkhead (FOX) class of transcription factors. For instance, it induces the sequestration in the cytoplasm of Forkhead Box O1 or FOXO1 (by phosphorylation at Ser256) on binding to 14-3-3 proteins: FOXO1 is known to activate gluconeogenic genes in liver [123] and inhibit adipogenesis [124]. The other fundamental metabolic effect of insulin is exerted on lipid metabolism, particularly important in epatocytes and adipocytes. In fat cells, insulin leads to the activation of phosphodiesterase 3B (PDE3B) which inhibits protein kinase A (PKA) through the degradation of cAMP, affecting the complex machinery (adipocyte lipids droplets and enzymes) for triglyceride hydrolysis [125] and stimulating lipogenesis to store nutrients. Initially, it was believed that phosphorylation and activation of PDE3B mediated by AKT was necessary for insulin inhibition on lipolysis. However, recent evidence weaken this concept, demonstrating that inhibition of AKT is not sufficient to abrogate insulin action on lipolysis, suggesting the existence of an AKT independent pathway, probably linked to the level of β adrenergic stimulation [126]. The exact mechanism of insulin inhibition on lipid metabolism is still unknown and how this pathway is impaired in obesity is a crucial aspect in term of therapeutic targets and of understanding diabetes development. In epatocytes, where insulin pathway, that regulates glucose and lipid homeostasis, is divergent downstream of AKT, AKT activation of mTORC1 promotes the sterol regulatory element binding protein 1c (SREBP1c) that enhance *de novo* lipogenesis (DNL), essential step for very low density lipoproteins (VLDL) packaging [127].

Akt1, Akt2 and Akt3, are homologous isoforms that share the same structural organization: a pleckstrin-homology (PH) domain, which is located at N-terminal and is required for binding to phospholipids, and a catalytic domain at C-terminal, which becomes active on phosphorylation (P) of two residues (Tyr308 and Ser473 for AKT1, Tyr309 and Ser474 for AKT2, and either Tyr305 alone or Tyr305 and Ser472 for AKT3). They are expressed in a tissue-dependent manner: AT and in general insulin target tissues (i.e. liver) mainly express Akt2 [128] and, at lesser extent, Akt1, both involved in the regulation of insulin-mediated metabolic pathways [129]. A siRNA-based approach in 3T3-L1 adipocytes has highlighted the important role of AKT2 on insulin responsiveness in adipocytes[130]. Akt2 knockout mice [131] and patients carrying Akt2 loss-of-function mutations [132] develop severe insulin resistance (IR) and T2DM. Mutations that activate Akt2 have been described to determine a left-side overgrowth (asymmetric) and severe hypoglycemia [133], suggesting a central role for Akt signaling in tissue development and in human insulin sensitivity. AKT3 is predominantly expressed in the nervous system, being involved in neural development [134]. Negative regulators of AKT node of insulin network include the phosphatase and tensin homologue (PTEN) that mediates the degradation of PIP_3 at 3'position: *Pten* deletion in animal models was shown to improve insulin sensitivity [135].

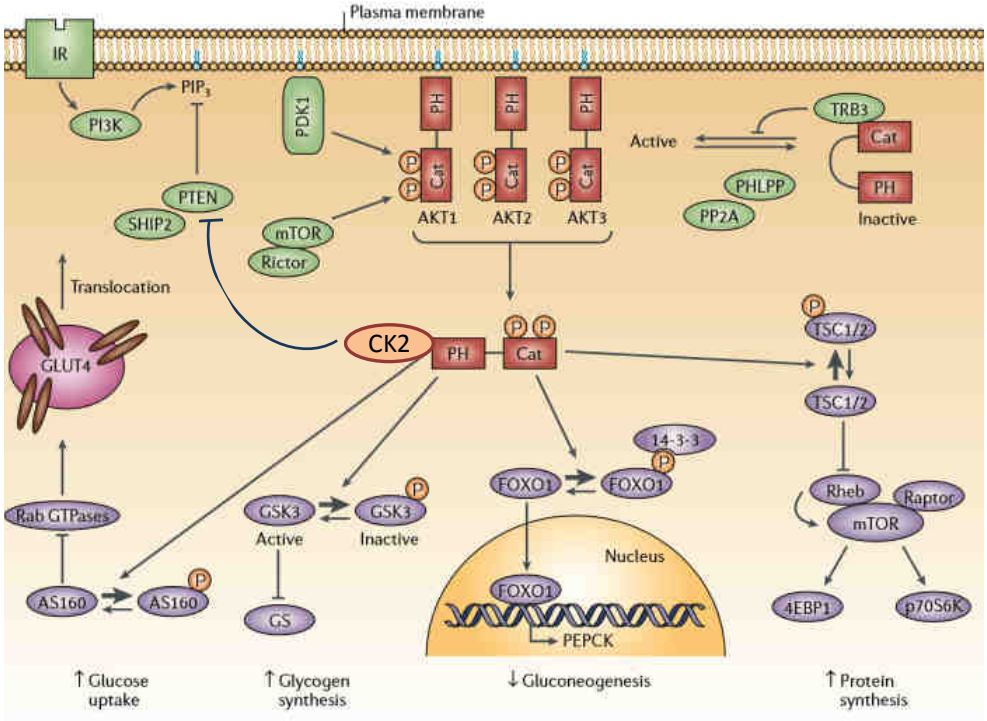

Figure 3. **Schematic overview of insulin signaling**. The bind of insulin to Insulin Receptor (IR) triggers receptor autophosphorylation that generates docking sites for insulin receptor substrate proteins (IRS-1–IRS4). IRS proteins in turn trigger the activation of a wide array of signal transducing proteins: phosphatidylinositol 3-kinase (PI3K) produces phosphatidylinositol3,4,5-triphosphate (PIP3) that recruits phosphoinositide-dependent kinase-1 (PDK1) and AKT (isoform 1, 2, 3) through the pleckstrin domain PH), AKT is phosphorylated on the catalytic domain (Cat) by phosphoinositide-dependent kinase 1 (PDK1) and mTORC2, (the complex between the mammalian target of rapamycin (mTOR) and the rapamycin-insensitive companion of mTOR (rictor)). Activated AKT phsphorylates many downstream substrates, leading to glucose uptake, glycogen and protein synthesis. The phosphatase and tensin homologue (PTEN) represents a negative regulator of insulin pathway, dephosphorylating PIP3, while Protein kinase 2 CK2 directly sustains insulin pathway acting on AKT and indirectly inhibiting PTEN.
Arrows represent positive, activating functions while T-lines represent inhibitory functions. TRB3: Tribbles-3; SHIP2: Src-homology-2 domain-containing inositol phosphatase-2; PHLPP: PH-domain leucine-rich-repeat protein phosphatase; PP2A: phosphatase-2A; AS160: AKT substrate of 160 kDa; GSK3: glycogen synthase kinase type 3; GS: glycogen synthase, GLUT4: glucose transporter 4; FOXO1: Forkhead Box O1; PEPCK: phosphoenolpyruvate carboxykinase TSC1/2: tuberous sclerosis complex-1 and -2; Rheb: small GTPase Ras homologue enriched in brain, that together with mTOR and Raptor forms mTORC1; 4EBP1: 4E-binding protein 1; p70S6K: p70 ribosomal protein S6 kinase.. Adapted from [114].

Since overfeeding and obesity cause the development of IR, understanding how insulin signaling is impaired by these conditions has become a crucial aspect in metabolic research. In liver, the proposed first event that impairs insulin action in lowering blood glucose level is the loss of insulin inhibition on FOXO1, that in turn upregulates the key enzymes for gluconeogenesis and increases the conversion of substrates to glucose [136]: the mechanism underlying altered FOXO1 regulation in obesity is still an open question. Although obesity related hyperinsulinemia is not able to overcome FOXO1 insensitivity, it remains sufficient to activate and, maybe, upregulates mTORC1 that in liver promote *de novo* lipogenesis for VLDLs assembly,

thus contributing to the detrimental metabolic status in overfeeding [127, 137]. In skeletal muscle insulin resistance, one of the alterations seems to reside in an impaired GLUT4 translocation to the cell surface, reducing tissue glucose uptake from circulation [138]. In this context AT plays a pivotal role participating to a vicious loop of metabolic derangement with the other insulin target organs. Recent studies in mice suggest that hyperglycemia and thus reactive hyperinsulinemia caused by the uncoupling FOXO1 from insulin regulation could impair insulin inhibition on adipocyte lipolysis: increased release of adipocyte FFAs and other substrates further promote unrestrained liver gluconeogenesis [139]. In support of this concept, adipocyte lipase ATGL lacking mice present a lower hepatic gluconeogenesis and insulin resistance under HFD [140]. From a molecular point of view, insulin resistance has been clearly demonstrated in human monogenic mutations of insulin receptor, PI3K and AKT genes [141] and an impaired function and/or regulation of these factors have been postulated also for common obesity. For example, an altered AKT phosphorylation has been demonstrated in response to ceramides in obesity [142]. However other components of insulin pathway or other molecular pathways could be involved in insulin resistance development: in mice with ectopic expression of PDGFR in skeletal muscle and fed with HFD, impaired glucose uptake is not accompanied by a decrease of AKT phosphorylation nor TBC1D4 [143], suggesting the role of an alternative pathway in insulin resistance. In addition, after 7 days of HFD, wild type mice already show a marked glucose intolerance without changes in insulin-induced AKT phosphorylation in liver, AT and skeletal muscle [144].

Among AKT upstream factors that could affect insulin signaling, we have to mention also modifications in extracellular matrix in AT and in the other insulin target tissues as liver and muscle [145]; interestingly a fragment of collagen VI (endotrophin) has described to exert detrimental metabolic effect in AT. Finally, reduced capillary recruitment that could limit tissue insulin and glucose delivery and, in general, alterations in AT microvascularization have been proposed as fundamental mechanisms of AT dysfunctions and metabolic complications of obesity.

CK2 STRUCTURE AND FUNCTIONS

Protein (casein) kinase CK2 is known as a pivotal positive regulator of insulin signaling. It was firstly isolated in 1954 from rat liver when it was called casein kinase thanks to its capacity to phosphorylate casein *in vitro*. However, casein is not a physiological target and the first CK2 endogenous substrates was identified only 30 years later its discovery [146] and currently it is widely known that CK2 displays an outstanding pleiotropy, phosphorylating a huge number of protein substrates implicated in several fundamental cell processes as differentiation, signal transduction, proliferation, apoptosis [147]. CK2 is a ubiquitous kinase in eukaryotes, expressed by all tissues and it is localized in the nucleus and cytoplasm. CK2 is a Ser/Thr kinase belonging to CMGC family and is able to use either ATP or GTP as phosphoryl donor, a feature termed dual co-substrate specificity [148].

In most organisms, CK2 is usually present as a tetrameric holoenzyme composed of two catalytic α (44 kDa) and/or α' (38 kDa), coded by two distinct genes (respectively *CSNK2A1* on chromosome 20 and *CSNK2A2* on chromosome 6) and two regulatory (β, 25 kDa coded by *CSNK2B* on chromosome 6) subunits [149]. The catalytic subunits are highly homologous and display *in vitro* a very similar enzymatic activity, although some evidence suggest that they could have different functions *in vivo* [150].

Crystallographic analysis reveals a "butterfly-like" shape of CK2 holoenzyme ([151]; Fig. 4) where β-subunits interact each other through a zinc finger region and with α or α' through an interface that results smaller than other observed in stable proteic complex, suggesting the possibility of an easy subunits association/dissociation that could contribute to CK2 activity regulation. The two catalytic subunits do not interact each other. The C-terminal tail of β-subunit is fundamental for tetramer stability and its phopshorylative activity [152], the β N-terminal tail contains auto-phosphorylative sites (Ser2, Ser3 and probably Ser4, [153, 154], that may probably regulate CK2β stability [155]. In close proximity to N-terminal tail, a acid residues rich sequence (Arg47-Asp55) forms a loop for interaction with polyamines, suggesting the possibility of a regulatory mechanism since polyamines are known to induce *in vitro* CK2 activity [156, 157].

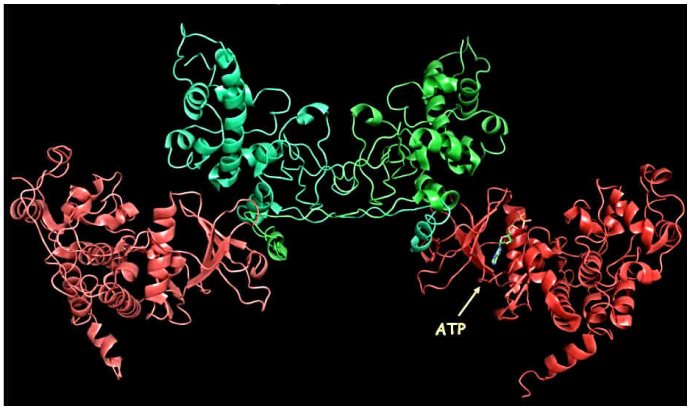

Figure 4. **Crystal structure of CK2 holoenzyme**. CK2 displays a butterfly-like shape in the view perpendicular to the molecular 2-fold axis. α subunits are represented in red while β subunits in green; the arrow indicates ATP binding site (from[151]).

Although CK2α alone is able to phosphorylate *in vitro* many of CK2 substrates, β subunit regulates substrate specificity and protein access to the catalytic domain [158]. Since CK2 acts as an acidophilic kinase, canonical phosphorylation requires one or more acidic residues C-terminal to the phosphor-acceptor site. Accordingly, the most specific determinant is an acid residue at n+3 that determines the minimal consensus sequence for CK2 phosphorylation as S/T–X–X–D/E (S = serin, T = Threonin, D = aspartic acid, E = glutammic acid). While X can be any amino acid, studies have shown that proline, lysine, or arginine at the +1 position and basic residues along n-1 and n+4 are unfavorable. In some instances, phosphorylation by CK2 is

enabled by an acidic determinant in the +1 position instead of the +3 position. Multiple aspartic or glutamic acid residues seem to have an additive effect, and due to this, many known CK2 sites consist of a serine/threonine residue followed by a string of acidic residues [157].

Importantly, CK2 is a constitutive active enzyme since its phosphorylative activity results independent from second messengers or phopshorylative events. This feature has raised questions about how it can be a regulatory factor in intricately controlled cellular pathways and it is currently under debate which mechanisms are able to regulate its expression and activity, [159]. Mining of proteomic databases and network computational assembly suggest a fine interplay between CK2 activity and other post-translational modulations, considering the prevalence of post-translational modifications that reside within CK2 substrates in close proximity to CK2 phosphorylation site [160]. In this view the reciprocal regulation of CK2 phosphorylation and these other modifications in CK2 substrates could be one plausible mechanism to explain how CK2 activity could be tightly tuned in fundamental and intricate cell processes. In the effort to understand how CK2 expression is modulated, gene expression studies suggest that CK2 regulates its transcription by phosphorylation of other transcription factors, excluding the existence of direct feedback inhibition [161].

Apart from canonical, also hierarchical phosphorylation by CK2 appears fundamental in its regulatory function on its substates, contributing to explain the paradox with its constitutively activity [162]. Recent evidence shows that CK2 hierarchical phosphorylation motifs, requiring either multiple phosphoserine residues or a mix of canonical and hierarchical determinants with a precise spacing, can be as enzymatically favorable as canonical phosphorylation and are significantly enrich in proteins controlling many specific cellular processes, reinforcing the idea that CK2 may act in concert with other kinases in regulating signaling pathways.

CK2 has been described to regulate carbohydrate and fatty acids metabolism [163] sustains insulin signaling both directly and indirectly. At a molecular level, CK2 phosphorylates Akt1 at Ser129 potentiating its activity by maintaining a high extent of Thr308 phosphorylation [164, 165]. Furthermore, CK2 indirectly enhances insulin pathway phosphorylating and thus inhibiting PTEN [166], a phosphatase acting as the main negative regulator of PI3K/Akt signaling by dephosphorylating PIP_3 [167]. PTEN can be phosphorylated by CK2 at Ser-370 and Ser385 (C-terminal), consequently PTEN cleavage by caspase 3 results inhibited, stabilizing the inactive form of the protein. In mice lacking one copy of *Pten*, phosphorylation and activation of PI3K/Akt pathway is associated with increased insulin sensitivity [168]. Patients with PTEN loss-of-function mutations show a constitutive insulin sensitivity and obesity, enhancing insulin signaling in both muscle and liver tissues [169].

Finally, CK2 directly controls insulin effect mediating the regulation of GLUT4 traffic towards lysosome. Upon prolonged insulin stimulation CK2 phosphorylates and negatively acts on retromer complex function,

a key component of the endosomal protein sorting machinery, promoting GLUT4 sorting to the degradative pathway [170].

Recent evidence highlights that CK2 down-regulates insulin release in pancreatic β-cells [171], interacting with pancreatic duodenal homeodomain transcription factor PDX-1 [172] and inhibiting muscarin-3-receptor M3R signaling [173]. Interestingly, in type 2 diabetes, analysis of human microarray revealed a small but significant increase in CK2α gene expression in human β-cells compared to non diabetic donors (Gene Expression Omnibus database no. GSE20966), suggesting a possible contribution of CK2 to impaired β cell function and consequently in glucose homeostasis in T2D [174]. In turn, glucose level is implied in CK2 regulation, modifying its subcellular localization, since *in vitro* high glucose concentration leads to the translocation of CK2 subunits from cytoplasm to nucleus in pancreatic β-cell line MIN6, supporting the idea of a fine and reciprocal control of CK2 and glucose metabolism [172].

CK2 in adipose tissue and metabolic disorders

Adipogenesis is one of the key process occurring in adipose tissue expansion both physiological, as during growth, and pathological as obesity. The role of CK2, that regulates cell differentiation and proliferation as mentioned above, has been investigated in adipogenic process in the last years. During adipogenesis CK2 was found to decrease in its protein level and in its kinase activity [175, 176]. Inhibition of CK2 kinase activity at the beginning of the differentiation process prevented differentiation affecting the mitotic clonal expansion of preadipocytes, whereas, at later time points CK2 inhibition had no effect on the differentiation process, indicating that CK2 may only play an early role in adipogenesis, principally impairing proliferation [176-178]. Supporting this hypothesis, it has been recently demonstrated that sirtuin 6 SIRT6, a nicotinamide adenine dinucleotide NAD+ dependent protein deacetylase, is necessary for the mitotic clonal expansion of 3T3L1 preadipocytes, the earlier step in the adipogenic process, and that SIRT6 promotes CK2α' translocation to the nucleus inhibiting Kinesin Family Member KIF5C, whose precise role in adipogenesis is unknown yet [179]. Moreover, Montenarh group confirms that pharmacological CK2 inhibition impairs 3T3L1 preadipocyte clonal expansion, accordingly to CK2 role in cell proliferation, and adipogenesis, reducing the expression of C/EBPα and PPARγ2 through the induction of miR-27a and miR-27b [177]. CK2 has also been linked to beige cell biology, strengthening its role in energy balance and metabolic homeostasis. Shinoda and colleagues demonstrated in mice that pharmacological inhibition of CK2 of only 7 days leads to an evident browning of WAT and is able to improve diet induced obesity and insulin resistance [180].

Another direct link of CK2 to cell energy homeostasis is provided by the observation that CK2 activity and protein expression are elevated under hypoxic conditions. CK2 regulates the hypoxia inducible transcription factor-1α (HIF-1α) activity either directly [181-183] or by the phosphorylation of the Von Hippel Lindau VHL protein [184] and increasing evidence are linking CK2 activity to angiogenesis. In endometriosis, where

endometriosic tissue depends on angiogenesis to growth, CK2 inhibition suppresses vascularization in developing lesions [185]. Vascular endothelial growth factor (VEGF), one of the major proangiogenic factor, may be one target of CK2 in regulating this process, since CK2 is able to inhibit the Prolin rich homeo domain protein PRH that negatively regulates VEGF signaling pathway [186-188]. Furthermore, other growth factors involved in angiogenesis have been linked to CK2: in smooth muscle cells under hypoxic conditions, PDGF has been described to upregulate CK2α' expression and activity, leading to CREB inhibition that is the key event for smooth muscle cells proliferation and artery remodeling [189]. In the retina the CK2-mediated phosphorylated form of pigment epithelium derived factor (PEDF) is described to have an important anti-angiogenic activity [190]; in endothelial cells transforming growth factor-β (TGF-β) transducing signaling implies among the other, the activin like kinase 1 (Alk-1) whose activity could be enhanced by interaction with CK2β, leading to the inhibition of endothelial cell migration [191].

Adiponectin is one of the major hormone secreted by mature adipocytes beside leptin. By co-immunoprecipitation and co-localization studies both CK2β and α have been demonstrated to directly interact with Adiponectin Receptor 1 (AdipoR1) N-terminus tail, providing evidence that CK2 could be an important factor in adiponectin pathway [192, 193], suggesting a possible crosstalk between adiponectin and insulin signaling pathways via CK2.

Increasing evidence support CK2 involvement in fatty acids metabolism, strengthening the hypothesis that CK2 could play an important role in AT biology and pathophysiology. Ceramide synthases CERS2-6 have been recently identified as CK2 target, modifying their activity and thus the distribution and levels of sphingolipids [194]. Hyperactivation of CERS by phosphorylation may worsen diseases in which the levels of sphingolipid species are elevated. For example, CERS2 and CERS6 have been associated with weight gain and insulin resistance [195, 196]. Moreover, CK2 has been demonstrated to interact with sirtuin family. As mentioned above CK2α' could be regulated by SIRT6 [179], that has a pivotal function in lipid metabolism and is able to protect against metabolic alterations caused by diet induced obesity [197]. Accordingly, hepatic *Sirt6* KO mice leads to fatty liver formation due to enhanced glycolysis and triglyceride synthesis [198]. The other member SIRT1 also functions as a master regulator of hepatic lipid metabolism [199], counteracting NAFLD and obesity related alterations as low grade inflammation [200, 201]: SIRT1 activators are described to improve insulin sensitivity and NAFLD in obese animals [60, 202] and conversely liver specific deletion of SIRT1 affects fat oxidation and promotes inflammation [203]. Interestingly, through proteomic LC-MS/MS analysis of SIRT1 liver over-expressed mice fed with high fat diet and CK2 inhibition studies, it was demonstrated that in obese animals SIRT1 is aberrantly phosphorylated at Ser164 by CK2, impairing its nuclear translocation and deacetylase activity that consequently affects fatty acid oxidation and increases liver lipid accumulation [204].

CK2 has also been demonstrated to participate in kidney inflammatory process occurring in T2D. It was recently demonstrated that CK2α is upregulated in kidneys of mouse model of diabetes, mediating the diabetic renal inflammatory fibrosis via NF-kB pathway [205].

CK2 is involved in several fundamental cell processes

CK2 is known to participate to cell cycle regulation, thus promoting cell growth and proliferation. CK2 inhibitory studies reveal that it is requested for G0/G1, G1/S and G2/M transitions, interacting with mitotic spindle and centrosomes, phosphorylating many factors involved in cell cycle regulation such as Cyclin Dependent Kinase 1 CDK1 (also known as $p34^{cdc2}$), CDC34 (cell division cycle 34), topoisomerase II [154, 206, 207]. Obviously linked to cell survival, CK2 exerts a fundamental role in apoptosis, strengthening its implication in cancer development. It regulates both death receptor mediated [208] and DNA damage induced apoptosis [209]. CK2 is proposed to promote cell survival competing with caspases action: for example, as aforementioned, the phosphorylation of PTEN, considered an oncosuppressor, by CK2 at caspase 3 site stabilizes its inactive form and thus promotes pro-survival AKT signaling [210]. Given the role in cell proliferation and survival, it is not surprising that most of studies on CK2 derive from cancer research. CK2 protein is abnormally overexpressed in a wide variety of tumors compared to normal tissues/cells [211, 212], including lung, breast, prostate, kidney, colorectal, hematologic cancers, where it plays a global role of anti-apoptotic and pro-survival agent [213, 214], operating as a cancer driver [149]. The oncogenic potential of CK2 differs from that of other onco-kinases, generated by gain of function mutation conferring constitutive/unscheduled activity: CK2 is constitutively active by itself, and no gain of function CK2 mutations are known to be responsible for neoplastic transformation. Thus, the rising concept is that elevated CK2 level makes the cellular environment more favorable to malignant transformation by the mechanism known as “non-oncogene addiction” [149]. Indeed, many of the effects of abnormally high CK2 are expected to potentiate the cancer phenotype, with special reference to its strong pro-survival and anti-apoptotic efficacy.

CK2 also contributes to cell differentiation process. CK2 phosphorylates the DNA binding protein Ikaros [215], a master regulator of hematopoiesis, especially in the differentiation of thymocytes. Hyperphosphorylation of Ikaros by CK2 leads to its ubiquitin-mediated degradation and thus inhibits the Ikaros-dependent T cell differentiation. In addition, there is some indication that CK2 phosphorylation might regulate Ikaros stability and turnover [216]. Moreover, there is a large body of experimental evidence that CK2 plays a crucial role in self renewal, commitment and blood cell lineage specification by influencing signaling cascades such as the Wnt/β-catenin, the Hedgehog and PI3K/PTEN pathways.

Given its role in malignancies, considerable efforts have been done to develop permeable CK2 inhibitors and hundreds of compounds have been described in recent years [217]. Among ATP/GTP competitor, that represent the most common inhibitory mechanism, the most frequently used are: 4,5,6,7-

tetrabromobenzotriazole or TBB, 4,5,6,7-tetrabromo-1H-benzimidazole or TBI, Quinalizarin (1,2,5,8-tetrahydroxyanthraquinone), Tetrabromocinnamic acid or TBCA, 5,6-Dichlorobenzimidazole riboside or DRB, apigenin (a common flavonoid present in fruits and vegetables), 2-dimethylamino-4,5,6,7-tetrabromo-^{1}*H*-benzimidazole DMAT, emodin (1,3,8-trihydroxy-6-methyl-anthraquinone), and 6,7-dichloro-1,4-dihydro-8-hydroxy-4-[(4-methylphenylamino)methylen]dibenzo[b,d]furan-3(2H)-one named TF. A real breakthrough in CK2 druggability was made by the inhibitor CX-4945, also known as Silmitasertib, that is orally available and entered clinical trials for the treatment of different type of cancers [218] and is currently in Phase II ([219]; "Study of CX-4945 in Combination with Gemcitabine and Cisplatin for Frontline Treatment of Cholangiocarcinoma" NCT02128282). Finally, among the non ATP-competitive compounds, we have to remember hematein [220] and the synthetic peptide CIGB-300, that binds to CK2 targets inducing apoptosis and impairing angiogenesis.

AIM OF THE STUDY

The exact pathophysiology of lipomatous tissue growth in Multiple Symmetric Lipomatosis (MSL) has not been defined yet, as well as all the molecular mechanisms that underlie adipose tissue (AT) expansion and dysfunction in Obesity, the most common AT disorders, are far to be completely understood.

The present work aims to characterize the lipomatous tissue at a morphological, molecular and clonal level, comparing its features with the white subcutaneous AT, harvested from the same MSL patients, and with a human brown AT depot, represented by perirenal fat of a patient affected by catecholamine-secreting tumor (Pheochromocytoma). Since insulin is a master regulator of AT growth and metabolism and protein kinase CK2 acts as an important node of insulin signaling, we focused on a comprehensive analysis of CK2 role in adipocyte glucose homeostasis and in a wide range of expanding/remodeling adipose tissues: in mouse models of obesity, in patients affected by obesity with different degree of glycemic impairment, AT after a significant weight loss and finally in lipomas of MSL patients.

MATERIALS AND METHODS

Materials

[γ^{33}P]ATP was purchased from Perkin-Elmer (Waltham, MA, USA) and 2-[1-3H]deoxyglucose from GE Healthcare (Waukesha, WI, USA). Protease inhibitor cocktail was from Calbiochem (Darmstadt, Germany), while phosphatase inhibitor cocktails were from Sigma-Aldrich (St. Louis, MO, USA). CX-4945 was purchased from AbMole BioScience (Hong Kong, China). The peptide RRRADDSDDDDD and the inhibitor DMAT were kindly provided by Dr. O. Marin (University of Padova, Italy) and Dr. Z. Kazimierczuk (Warsaw Life Sciences University, Poland), respectively. Insulin (Humulin R) was from Eli Lilly (IN, USA), Pantothenate (MP Biomedicals); Rosiglitazone from Art Molecule (Poitiers Cedex, France); 0.025% trypsin/EDTA, Dulbecco's Modified Eagle Medium (DMEM), fetal bovine serum (FBS) from ThermoFisher (Waltham, MA, USA); dexamethasone, iso-butyl-methyl-xantine (IBMX), Triiodo-L-Thyronine (T3), biotin, 4-(2-hydroxyethyl)-1-piperazineethanesulfonic acid (HEPES), dimethyl sulfoxide (DMSO), paraformaldehyde, MTT [3-(4,5-dimethylthiazol-2-yl)2,5-diphenyltetrazolium bromide] and Immobilon-P membranes were from Sigma-Aldrich.

Antibodies

CK2α antisera was prepared as described [221], anti-p-Akt (Ser129) (catalog ab133458), anti-CK2β (catalog ab76025), anti-GLUT4 used for Wb (catalog ab62375) and anti-VAMP2 (catalog ab3347), anti-UCP1 used for IHC (ab10983) antibodies were from Abcam (Cambridge, UK), anti-β-actin (catalog A5441) from Sigma-Aldrich. Antibodies raised against PTEN (catalog sc-7974), Akt1/2/3 (catalog sc-8312), Na^+/K^+-ATPase (catalog sc-28800) and GLUT4 (catalog sc-1606) used for immunolocalization were from Santa Cruz Biotechnology (Santa Cruz, CA, USA), while anti-phospho-PTEN (Ser370) (catalog 07-889) was from Merck Millipore (Darmstadt, Germany). Anti-p-Akt (Thr308) (catalog #13038), anti-p-Akt (Ser473) (catalog #4060), anti-AS160 (catalog #2670), anti-p-AS160 (Thr642) (catalog #4288), anti-p-PRAS40 (Thr246) (catalog #13175), anti-GSK3β (Ser9) (catalog #5558), anti-p-FoxO1 (Ser253) (catalog #9461), anti-FoxO1 (catalog #2880) antibodies were from Cell Signaling Technology (Danvers, MA, USA). 488 donkey anti-goat IgG (H+L) was purchased from ThermoFisher. CD31-FITC and –PE, CD45-FITC, CD34-PerCP-Cy5.5, CD73-APC, CD90-PE, CD271-APC monoclonal mouse anti-human fluorochrome-conjugated antibodies and isotype-matched PE-IgG1, FITC-IgG1, APC-IgG1 and PerCP-Cy5.5-IgG1 monoclonal antibodies were all purchased from BD Biosciences (San Jose, CA, USA).

Subjects

In the present work, patients were enrolled at our Center for the Study and the Integrated Treatment of Obesity (Ce.S.I.T.O.), that works in tight collaboration with the Bariatric Surgery of Padua Hospital in the

management of obese subjects with indication to bariatric surgery according to the guidelines for obesity management in adults [222]. Moreover, in collaboration with Plastic Surgery (Padua Hospital), our Internal Medicine Clinic manages the rare adipose tissue disorder Multiple Symmetric Lipomatosis.

Five patients affected by type 1 MSL who underwent lipectomy for clinical indication at Plastic Surgery of Padua Hospital, were enrolled in the present study, approved by the Ethical Committee of the University of Padua, after written informed consent (Prot. N° 2658P). The range of age was 49-70 years and at least one year of alcohol abstinence was requested as inclusion criteria for the enrollment. Lipomatous tissue (LT), when possible from multiple site, and a biopsy of SAT in MSL-spared site were collected from the same patient during surgical lipectomy; in two patients (2891 and 3002) samples of both LT and SAT were collected twice during two separate intervention, indicated by ordinal numbers. LT samples derived from neck, cervical region (patients 2884, 2891 I and II, 3002 I, 5091) and from upper arms (patients 3002 I, 3002 II, 3030, 5091), whereas SAT mostly derived from abdominal biopsies, in patient 3002 during the first intervention (3002 I) from the lumbar region and during the second collection from the lower limb (3002 II). Perirenal AT was also harvested from a patient affected by Pheochromocytoma during adrenalectomy. This represented a reliable positive control of human brown/beige AT due to adrenergic hypersecretion, that could be harvested in a relative simple manner. In fact other brown AT in humans are found in children or in depots that are rather impossible to reach with a selective biopsy.

For each patient at the time of each surgery, anthropometric parameters (weight, height) were collected and body mass index (BMI) was computed [Weight in kilograms/(height in meters)^2]; a photographic documentation was performed in order to assess the sites and extension of the disease. All enrolled subjects were males, as expected from the M:F ratio of type 1 MSL; only one patient (ID 3030) resulted affected by type 2 diabetes and had no history of alcohol abuse; BMI ranged from 22.5 and 33 kg/m^2: one subject resulted normal weight (2884), three overweight (2891, 3030, 5091) while patient 3002 was overweight during the first intervention and resulted affected by I degree obesity at the time of the subsequent surgery. Clinical data and the sites of LT and SAT collection are summarized in Table 1.

ID	Sex	Age	MSL type	LT site	SAT	T2D	BMI	Alcohol
2884	M	58	1	Neck, left and right cervical region	Abdominal	NO	22.5	yes
2891 I	M	62	1	Neck	Abdominal	NO	26.6	yes
2891 II	M	63	1	Neck, cervical region	Abdominal	NO	26.5	yes
3002 I	M	64	1	Neck, left upper arm	Lumbar region	NO	29.7	yes
3002 II	M	67	1	Right upper arm	Lower limb	NO	33	yes
3030	M	49	1	Upper arm	Abdominal	YES	29.4	no
5091	M	70	1	Neck, left upper arm	Abdominal	NO	28.3	yes

Table 1. Clinical data and anatomical localization of the collected samples of lipomatous (LT) and subcutaneous adipose tissue (SAT). Each patient was identified by an identification number (ID), I and II refers to sample collected during a first or a second surgery; in patients 2891 and 3002, a further SAT biopsy was harvested during the second lipectomy. Sex (M=male) and age (years) at the time of surgery are indicated.

To explore CK2 role in obesity, AT samples (SAT and VAT) were collected from 27 (17F/10M, age 48.2 ± 12.2 years) obese patients (BMI > 38 Kg/m^2) during bariatric surgery, divided in subgroups on the basis of glycemic profile, according to American Diabetes Association, Standards of Medical Care in diabetes-2016 (Diabetes Care 2016;39(Suppl. 1):S1–S2|DOI: 10.2337/dc16-S001), HOMA index and antidiabetic therapy (Table 2). Weight, height as well as waist circumference (at midpoint between the lower margin of rib cage and the top of iliac crest) were measured in overnight fasted obese patients. Blood samples were used for the biochemical determinations, performed with standard diagnostic kit according to WHO First International Reference Standard: glucose (Glucose HK Gen.3, Roche Diagnostic, USA), insulin, IL6, TNF-α (IMMULITE 2000 Immunoassay Insulin, IL-6 and TNF-α (Siemens Healthcare GmbH, Germany), hs-CRP (CardioPhase, High Sensitivity C-Reactive Protein, Siemens, Healthcare) and Leptin (Leptin-RIA – CT, Mediagnost, Germany). HOMA was calculated and used as IR index [223]. Obese normoglycemic (OB/N, n=12) obese prediabetic (OB/preT2D, n=7) and obese diabetic (OB/T2D; n=8) were compared. No statistical differences were observed in the 3 groups among mean values of weight (124.1±12.1; 125.0±17.7; 127.0±21.2), BMI (44.45±3.16; 46.44±8.46; 44.62±5.60) and Leptin level (36.6±16.3; 36.2±15.6; 38.0±12.3). OB/T2D group displayed a mean value of age (57±5 vs 41±11, p=0.0006) and waist (139.6±9.9 vs 124.5±9.6, p=0.004) higher than OB group; OB/preT2D group had an intermediate mean age (51±14) and waist (133.9±9.3) not significantly different from the other groups. The 3 groups differed significantly in fasting blood glucose level (4.9±0.6; 5.9±0.7; 7.9±2.2; $p<0.05$) as expected by the selection criteria used. Regarding systemic inflammation markers, no statistical differences were obtained, but in OB, OB/preT2D and OB/T2D groups an increase trend was observed for IL-6 (3.0±1.8; 2.8±1.4; 3.7±2.9), TNF-α (7.8±1.3; 7.7±2.0; 9.5±2.4) and hs-CRP (5.37±5.68; 7.44±7.02; 11.5±9.5) levels. OB and the OB/preT2D groups were further divided in 2 subgroups on the basis of the insulin resistance degree estimated by HOMA index (HOMA low = HOMA<3 and HOMA high = HOMA>3). Considering all patients with low HOMA (n=10) vs patients with high HOMA or diabetes (T2D) (n=17), independently from their glucose profile, they did not significantly differ in age, weight, BMI and Leptin level, but showed a statistical different mean value of waist (125.8±7.7 vs 134.7±12.1, p=0.03), fasting blood glucose (4.9±0.6 vs 6.7±1.9 p=0.002), hs-CRP level (3.61±3.07 vs 9.84±8.32 p=0.02) and, as expected for the selection criteria used, blood fasting insulin (8.0±4.1 vs 26.2±14.0, p=0.0003) and HOMA index (1.70±0.86 vs 7.51±5.03 p=0.0008).

From General Surgery Unit and Plastic Surgery of Padova Hospital that collaborate with our Center, 11 (8F/3M, age 47.8 ± 14.2 years) nondiabetic, normal-weight subjects (18.5 < BMI < 24.9 kg/m^2) were enrolled as control group and both SAT and VAT samples were harvested during abdominal surgery as laparoscopic cholecystectomy (n=5) and fundoplication (n=3) or SAT alone during plastic surgery (ps) for minor abdominal wall defects (n=3).

Group	ID	Sex	Age	Glycemic profile	DM2 therapy	Weight	BMI	Waist	Glucose	Ins	HOMA	IL6	TNFα	usCRP	Leptin
OB	2432	F	47	N		111.0	42.8	114	5.0	12.0	2.67	1.9	9.1	2.08	64.0
	2740	F	41	preT2D		156.0	54.0	149	6.2	20.0	5.51	1.9	6.8	7.61	55.7
	2476	F	41	N		118.0	46.7	119	5.2	2.0	0.46	7.1	8.5	8.47	43.0
	2980	M	46	N		143.0	50.1	135	4.8	5.0	1.07	1.9	5.5	7.12	20.0
OB/H low	2352	M	67	N		123.0	43.1	131	3.7	10.2	1.68	2.5	6.9	0.49	17.0
	3939	M	50	N		126.0	38.5	123	4.7	3.0	0.63	5.8	8.1	2.30	nd
	3595	F	40	N		106.0	38	118	5.1	13.0	2.95	2.0	8.4	0.98	29.0
	3970	F	22	N		128.0	48.2	135	4.3	14.0	2.68	2.1	5.8	>10	50.0
OB/H high	3086	F	37	N		128.0	45.9	110	5.1	19.0	4.31	1.9	7.0	4.19	36.0
	2491	M	37	N		148.7	46.4	125	4.9	19.0	4.14	1.9	9.0	1.32	14.0
	2492	F	36	N		120.0	44.6	117	4.7	27.0	5.64	1.9	7.1	7.59	35.0
	3726	F	41	N		117.0	45.1	126	5.6	22.0	5.48	3.1	9.8	>10	36.0
	3502*	F	33	N		120.0	44.1	142	5.3	39.0	9.19	4.5	8.2	19.20	58.0
OB/preT2DH low	3794	F	59	preT2D		100.0	41.6	124	5.8	7.0	1.80	2.0	nd	3.81	41.0
	4044	F	65	preT2D		124.0	59.8	135	5.0	7.0	1.56	5.8	9.2	>10	50.0
	3921	F	31	preT2D		120.0	38.7	125	4.9	7.0	1.52	2.0	8.9	>10	16.0
OB/preT2DH high	3951	M	37	preT2D		116.0	39.2	128	5.9	27.0	7.08	2.9	4.0	2.29	16.0
	3843	M	63	preT2D		121.0	40.4	133	6.9	51.0	15.64	2.0	8.2	4.01	33.0
	3585	F	57	preT2D		138.0	51.3	143	6.6	18.0	5.28	3.0	8.9	19.5	42.0
OB/T2D	2862	F	64	T2D	Ins	130.0	45.5	142	8.6	nd	nd	1.9	10.5	3.15	43.0
	2597	F	54	T2D	Met+SU	92.0	38.3	123	5.1	2.0	0.45	10.0	12.0	2.18	32.0
	2267	M	58	T2D	Met+Ins	147.0	53.4	145	12.0	nd	nd	2.8	7.5	10.10	19.0
	3256	M	54	T2D	Ins	160.0	49.9	157	nd	nd	nd	6.1	10.8	30.20	59.0
OB/T2D Met	2698	F	56	T2D	Met	115.0	43.3	132	6.8	14.0	4.23	2.4	7.1	19.60	39.0
	2540	M	56	T2D	Met	122.0	39.8	140	8.8	38.8	15.18	1.9	8.6	8.41	26.0
	2650	F	49	T2D	Met	136.0	48.2	136	6.2	19.0	5.24	2.4	6.6	13.20	43.0
	3110	M	62	T2D	Met	114.0	38.5	142	7.7	51.0	17.45	2.0	13.1	4.83	43.0

Table 2. Anthropometric, metabolic and inflammatory parameters in the 27 studied obese patients. Each patient was identified by an identification number (ID). Sex (F=female, M=male) and age (years) are indicated. Patients were classified as normoglycemic (N), prediabetic (preT2D) or type 2 diabetic (T2D) (Glycemic profile). In OB/T2D, diabetes was managed with insulin therapy (Ins), sulfonylureas (SU), metformin (Met) or their associations (Met+SU, Met+Ins). Weight (kg), body mass index (BMI, Kg/m^2) and waist (cm) are obtained by clinical anthropometric evaluation. Fasting blood glucose (mmol/L), insulin (mU/l) and HOMA (=fasting glucose x fasting insulin/22.5) are reported as metabolic characterization. Inflammatory profile was assessed measuring blood levels of IL-6 (ng/L), TNF-α (ng/L) and hs-CRP (=high-sensitivity C-reactive Protein, mg/L); blood level of the adipokine Leptin (µg/L) was quantified.
OB=obese OB/H low=obese normoglycemic with HOMA <3 OB/H high=obese normoglycemic with HOMA>3 OB/preT2D/H low=obese prediabetic with HOMA<3 OB/preT2D/H high=obese prediabetic with HOMA>3 OB/T2D=obese diabetic OB/T2D Met=obese diabetic subject treated with metformin.

Among the subjects followed up by our Center during weight loss program, we were able to enroll in the present study 12 obese patients who had achieved relevant weight loss (≥ 50% of excess WL) and had indication for an abdominal surgery. Three patients underwent laparoscopic cholecystectomy (n=3) that provided both SAT and VAT specimens, while the other 9 individuals underwent abdominoplasty for abdominal wall laxity, that provided SAT samples. As reported in Table 3, in these patients, weight loss was obtained by previous bariatric surgery (n=9) or by lifestyle modification (n=3).

The whole study on AT biopsies was approved by Ethical Committee of the University of Padua (Prot. N° 2892P) and patients signed a written informed consent before enrollment.

Group	ID	Sex	Age	Glycemic profile	Surgery	Weight loss intervention	Weight PRE	Weight POST	Delta Weight	BMI pre	BMI post	% EWL
OB/WL	3406	F	40	N	Cholecystectomy	SG	106.0	77.0	-29.0	38.93	28.28	76.4
	2370	F	39	N	Cholecystectomy	SG	124.7	75.0	-49.7	51.90	31.22	76.9
	2377	F	58	N	Cholecystectomy	SG	175.0	99.0	-76.0	63.51	35.93	71.6
OB/WL ps	2664	F	33	nd	Abdominoplasty	GB	176.0	113.0	-63.0	57.47	36.90	63.4
	2441	F	67	T2D	Abdominoplasty	diet	120.0	98.0	-22.0	45.17	36.89	41.1
	748	M	56	N	Abdominoplasty	GB	125.0	53.0	-72.0	41.29	23.78	107.5
	3519	F	34	N	Abdominoplasty	GB	114.0	84.0	-30.0	40.39	29.76	69.1
	2785	F	47	ex-T2D	Abdominoplasty	SG	101.0	68.5	-32.5	38.96	26.43	89.8
	2087	F	58	N	Abdominoplasty	SG	102.0	70.0	-32.0	38.87	26.67	87.9
	4098	F	38	N	Abdominoplasty	diet	90.0	58.0	-32.0	36.51	23.53	112.8
	4208	F	27	N	Abdominoplasty	diet	125.0	76.0	-49.0	40.82	24.82	101.2
	3132	F	50	N	Abdominoplasty	SG	101.0	60.6	-40.4	37.55	22.53	119.7

Table 3. Clinical characteristics of obese patients after weight loss. Each patient was identified by an identification number (ID). Sex (F=female, M=male) and age (years) are indicated. Patients were classified as normoglycemic (N), prediabetic (preT2D) or diabetic (T2D), as reported in Table 2 (Glycemic Profile). Ex-T2D indicates diabetes regression after weight loss. SAT and VAT biopsies were collected during cholecystectomy, while only SAT biopsies during plastic surgery (abdominoplasty). Weight loss (WL) was obtained by bariatric surgery (SG=sleeve gastrectomy, GB= gastric banding) or caloric restriction (diet). Weight (kg) and body mass index (BMI, Kg/m2) before (PRE) and after (POST) WL-intervention were reported as well as weight differences (delta). The percent of excess weight loss (% EWL= [(preoperative weight-current weight)/ preoperative weight-ideal weight]x100) was used to confirm the degree of WL and the efficacy of WL-intervention. After WL-intervention all patients reduced significantly their weight (121.6±27.6 vs 79.3±16.5 $p<0.001$) and their BMI (44.28±8.69 vs 28.89±5.28 $p<0.0001$) with a mean value of 84.8% EWL.

Animal care handling

Animal procedures were approved by the Animal Committee at Padua University (O.P.B.A.) (Permit Number: 56/2013). Mice were purchased from Charles River Laboratories Italia (Lecco, Italy) and the standard diet (4% fat, Crispy Pellets Omnivores) was from Versele-Laga (Deinze, Belgium).

C57BL6/J (B6 n=12), B6.V-LEP OB/J (ob/ob, n=5), BKS.CG-M+/+ LEPRDB/J (db/db, n=5) and controls B6.V-LEP OB/J +/? (?ob/+, n=5), BKS.CG-M DB/+ (db/+, n=5) male mice were fed with standard diet (4% fat) in a temperature and humidity controlled setting with a 12 h light/dark cycle. Animals were starved for 6 hours before experiments. Where indicated B6 mice were injected intraperitoneally (ip) with saline solution of CX-4945 (20 mg/kg) 2 hours before stimulation with insulin (1 U/kg, ip); after further 30 minutes, animals were sacrificed by CO_2 euthanasia to collect and freeze tissues (visceral/epididymal AT, indicated as VAT-E, subcutaneous/inguinal AT indicated as SAT, brown BAT, red and white quadriceps, indicated respectively as RQ and WQ, liver). ob/ob, db/db and relative controls were starved for 6 hours and sacrificed by CO2 euthanasia to collect and immediately freeze in liquid nitrogen the indicated tissues (VAT-E, SAT, BAT, WQ, liver).

Mouse 3T3-L1 cell cultures

Mouse 3T3-L1 preadipocyte cell line (ECACC Culture Collection, Public Health England, Salisbury, UK, cat n° 86052701) was maintained in standard medium (DMEM high glucose (4.5 g/L), 2 mM glutamine, 150 U/ml

streptomycin, 200 U/ml penicillin and 10% FBS). For *in vitro* adipogenic differentiation $1X10^5$ 3T3-L1 cells/well (24 wells plate) or $5X10^5$ cells/well (6 wells plate) were seeded in standard medium and two days post confluence, medium was changed with adipogenic medium (AM), prepared with standard medium added with 2 µM insulin, 1 µM dexamethasone and 0.5 mM IBMX for 3 days and without IBMX for further 9 days of adipogenic differentiation. Medium was changed every 3 days. Mature adipocytes were maintained in standard medium for 2 days before further assays.

Tissue collection

After sampling, tissues were partly frozen in liquid nitrogen and stored at -80°C before further assays, formalin fixed for histological/immunohistochemical analysis. From LT and paired SAT of MSL and SAT of WL/ps patients (ID 3519, 3525), SVF was extracted to obtain human adipocyte primary cultures and to performed further *in vitro* assay.

Histological and immunohistochemical analysis

LT and SAT sections were fixed in 4% buffered formaldehyde (Diapath S.p.A, Bergamo, Italy), paraffin-embedded, cut into 4 µm thick sections and stained with standard hematoxylin-eosin (H/E). AT sections were observed with a Leica DM LB2 light microscope, at least 20 fields at 20X magnification for each specimen were observed to determine adipocyte morphology (mature univacuolated cells for white AT versus multivacuolar cells for brown AT). Digital images of at least 10 fields per slide were captured with a Leica DFGC450 digital camera to calculate adipocyte size as the median adipocyte area of a minimum of 160 random adipocytes for LT and SAT, manually measured using LAS Software (Leica Microsystems Inc, Deerfield, IL, USA). Immunohistochemical staining was performed using the standard protocol F (Bond-maX; Leica, Newcastle Upon Tyne, UK). Sections were pre-treated using heat mediated antigen retrieval with sodium citrate buffer (pH 6) for 30 minutes. Specimens were then incubated with anti-UCP1 antibody (1:250 dilution) for 15 minutes at room temperature and detected using an HRP conjugated compact polymer system. The staining was visualized with 3,3'-diaminobenzidine (DAB) and the slides were counterstained with Mayer's haematoxylin. Sections were then dehydrated, cleared, mounted and observed with a Leica DM LB2 light microscope to assess the presence/absence of UCP1 positive cells.

Stromal vascular fraction extraction

LT and AT biopsies were thoroughly minced with scissors and digested for 1 hour in Collagenase type II solution (1 mg/ml) (Sigma-Aldrich) on a shaking water bath at 37°C. Undigested tissue was removed by filtering through a sterile 100 µm pore Cell Strainer (BD Falcon, BD Bioscience) and centrifugated (350xg 10 minutes) to separate the floating mature adipocyte layer from SVF pellet. Cells were resuspended and incubated for 5 minutes at room temperature in erythrocyte lysis buffer (NH_4Cl 1.5 M, $KHCO_3$ 100mM,

EDTA 1.3 mM) as previously described by Sanna et al. (2009). After neutralizing with human standard medium (hSM), containing DMEM/F12 (1:1) with L-glutamine, 10% FBS, 150 U/ml streptomycin, 200 U/ml penicillin, 1 mM HEPES, cells were centrifugated and resuspended in the appropriate volume of hSM. Total cell number was assessed by staining with Trypan Blue and counting of viable cells in Neubauer Chamber before further use.

For LT and paired SAT samples of MSL patients, $1X10^6$ freshly isolated cells were pelleted by centrifugation and immediately frozen for protein extraction or lysed with RLT buffer (Qiagen) and frozen for RNA extraction.

***Ex vivo* flow cytometry analysis of stromal vascular fraction**

For paired samples of LT and SAT of MSL patients, $1X10^5$ freshly isolated cells (*ex vivo*) were washed with cold FACS buffer (2% bovine serum albumin BSA in phosphate buffered saline PBS 1X), collected by centrifugation (350 xg, 8 min) and simultaneously incubated in the dark for 10 min at room temperature with monoclonal mouse anti-human fluorochrome-conjugated antibodies in different combinations (CD31-FITC and –PE, CD45-FITC, CD34-PerCP-Cy5.5, CD73-APC, CD90-PE, CD271-APC). After washing with FACS buffer, labeled cells were collected by centrifugation (350xg, 10 min), resuspended in 200 µl of FACS buffer per sample and acquired (30000 events/sample) by a FACSCanto™ Flow Cytometer (BD Biosciences). Data acquisition and analysis were performed using the BD FACSDiva™ software. Regions and gates were set with the aid of a negative control, isotype-matched PE-IgG1, FITC-IgG1, APC-IgG1 and PerCP-Cy5.5-IgG1 monoclonal antibodies. This method allows to determine *ex vivo* the percentage of cells in the SVF that co-expresses different surface markers avoiding bias due to plastic adhesion and culture conditions.

***In vitro* morphology and adipogenic differentiation of human preadipocytes**

For the morphological observation of LT and SAT derived ASCs contained in SVFs, $4X10^5$ freshly isolated preadipocytes were seeded in duplicates in 24well plates in hSM (p0) and observed after 2 days with a Leica DM IL LED inverted microscope equipped with camera. To obtain preadipocytes at subsequent culture passages (p1, p2, p3), cells were detached with 0.025% trypsin/EDTA for 3 minutes whose action was then blocked with an appropriate volume of hSM; $4X10^5$ cells were than seeded in 24well plates and after further 2 days optical microscopy observation was repeated.

To evaluate *in vitro* adipogenic differentiation, SVF cells freshly isolated from LT and SAT biopsies (p0) were seeded in 96-well (10^5 cells per well), 24 ($0.5x10^6$) or 6 well ($1.5x10^6$) plate. $0.5x10^6$ ASCs at p1, p2 or p3, obtained as described above, were seeded in duplicates in 24well plates to evaluate the effect of preliminary culture passages on adipogenesis of LT derived ACSs in comparison with paired SAT precursor cells. At cell confluence, hSM was replaced with adipogenic medium (AM), containing 66 nM insulin, 100 nM dexamethasone, 1 nM T3, 33 µM biotin, 17 µM pantothenate, and added with 0.25 mM IBMX and 10

µM Rosiglitazone, a known PPARγ agonist, to fully induce adipogenic differentiation. After 3 days (induction phase), AM added with IBMX and Rosiglitazone was replaced with AM alone and changed every 3 days. At day 12, representative images of *in vitro* differentiated cells were taken with Leica DM IL LED inverted microscope equipped with camera and then cultures were lysed using RLT buffer for RNA extraction.
Finally, to elicit brown/beige phenotype, at day 12 of differentiation, cultures were maintained in hSM for 48 hours and then treated for 4 hours with 10 µM Forskolin, an activator of adenyl cyclase that mimics adrenergic stimulation before cell lysis for RNA extraction.

Cell viability assay

$3x10^4$ 3T3-L1 cells were seeded in 96-well plates, differentiated using AM as described before, and then treated with 2.5 or 10 µM CX-4945 for 24 hours in presence or absence of FSB. 10^4 human SVF cells were plated in 96-well plates and analysed in the undifferentiated state (h-preadipocytes) or after *in vitro* differentiation (h-adipocytes), as previously described, upon 1, 2.5 or 10 µM CX-4945 (dissolved in DMSO) treatment for 48 hours; treated cultures were compared with DMSO treated controls. At the end of treatments, we evaluated cell viability using the colorimetric MTT assay, based on mitochondrial integrity. MTT is metabolized into formazan whose concentration is proportional to viable cell number. MTT solution in PBS was added to each well (0.4 mg/ml) for 3 hours at 37°C. Medium was removed and the formazan precipitate was dissolved in DMSO. OD, that resulted proportional to viable cell number, was measured at 550 nm with a reference at 620 nm, using a Victor3™ spectrometer (PerkinElmer); 6 replicates of each sample were assayed and each experiment was performed 2 times.

Cell cycle length estimation and proliferation assay

From patient 2884 affected by MSL, 10^4 freshly isolated ASCs from neck and cervical LT and corresponding SAT were seeded in 96-well plates in triplicates in DMEMF12 and 10% FBS. At time 0, after 48 and 72 hours from seeding, cell number was determined using CellTiter-Glo® Luminescent Cell Viability Assay (Promega Corporation, Madison, WI, USA) according to kit instruction. This method determines the number of viable cells based on ATP production: the luminescent signal is generated by the ATP-dependent reaction catalyzed by the Ultra-Glo™ Recombinant Luciferase on Luciferin, contained in the CellTiter® Reagent, with an intensity proportional to ATP quantity. The day of the assay, plate was equilibrated to room temperature for 30 minutes and 1:1 volume of CellTiter-Glo® reagent was added to each well, mixed for 2 minutes to induce cell lysis and after 10 minutes luminescent signal was recorded using Victor3™ microplate reader (PerkinElmer).
In MSL patient 3002 II, LT and SAT-derived SVFs (10^4 cells) were seeded in triplicates in 10% FBS SM in 96-well microtiter plates. At time 0, after 24 and 48 hours from cell plate attachment, cell number was determined using CyQUANT® Direct Cell Proliferation Assay Kit (Invitrogen), according to manufacture

instructions. This assay is based on a cell permeant DNA binding fluorescent dye, combined with a background suppression reagent, resulting independent from the metabolic features of cells (i.e. ATP production). Fluorescence intensity is proportional to DNA amount and thus to cell number. At the indicated time point, 2:1 volume of Cyquant Reagent was added to each well and after 60 minutes of incubation at 37°C and fluorescence was read at 480/535 nm using FluoStar Optima microplate reader (BMG Labtech, Orterberg, Germany).

In both methods, doubling time was calculated with the following equation: $g = Th \times \log2/\log(N_{Th}/N_{0h})$ where g indicates the doubling time during the logarithmic growth phase, N_{Th} the estimated number of cells after 24 or 48 hours of culture, N_{0h} the number of cells at time 0.

Clonal analysis of stromal vascular fraction by limiting dilution analysis

LT (neck and cervical samples) and SAT derived SVFs from patient 2891 I, extracted as described above, were differently diluted and seeded in hSM in order to obtain 1000, 100, 30, 10, 3, 1 cell/well or one cell every 3 wells (indicated for simplicity as 0.3 cell/well) of 96-well plate. Subsequently, positive wells for cell proliferation were counted by a Leica DM IL LED inverted microscope and the percentage of positive wells was determined in respect of expected value. To evaluate the adipogenic potential of proliferated clones, at cell confluence, wells were differentiated by adding adipogenic medium, as described above, and then differentiated wells were scored for the presence of adipocytes, estimating the percentage of mature adipocytes by double blind observation with a Leica DM IL LED inverted microscope. The number of differentiated wells were also counted, considering as adipogenic a clone with an adipogenic differentiation equal or greater than 20% and the fraction of adipogenic clones of the total number of observed clones was calculated.

RNA extraction and RT-Real time PCR

In MSL samples, total RNA was extracted using Rneasy Mini (for cell RNA extraction) or Lipid (for tissues) Kits (Qiagen Inc, CA, USA) according to supplier instructions. RNA content was quantified using NanoDrop technology (Fisher Scientific SAS, Illkirch Cedex, France) and quality-checked using an Agilent 2100 Bioanalyzer (Agilent Technologies, PaloAlto, USA). RNA samples were then treated with Dnase Treatment & Removal Reagents (Ambion, Inc, Austin, TX, USA) and reverse-transcribed for 1 h at 37° C with 150 ng random primers, 0.5 mM dNTPs, 20 units of RNAsin Ribonuclease Inhibitor and 200 units of M-MLV RT (Promega, Madison, WI, USA). Oligonucleotide sequences and amplification conditions are reported in the Table 4. Real Time PCR was carried out with Platinum® SYBR® Green qPCR SuperMix-UDG (ThermoFisher) on a DNA Engine Opticon™ 2 Continuous Fluorescence Detection System (MJ Research, MA, USA). Duplicate samples (5 ng of cDNA) were normalized by *18S* rRNA content and reported as ratio.

GENE	FORWARD (5'-3') REVERSE (5'-3')	ANNEALING (°C)	PRIMERS (F/R nM)	AMPLICON (BP)
PPARG	ACCCAGAAAGCGATTCCTTCA AGTGGTCTTCCATTACGGAGAGATC	60	900/900	87
LEPTIN	GTGCGGATTCTTGTGGCTTT GGAATGAAGTCCAAACCGGTG	63	100/100	174
UCP1	CTACGACACGGTCCAGGAGT AGTGGCAGTATTCATTGGGC	60	300/300	110
CIDEA	ACGTGAAGGCCACCATGTATGA TGCCCAGATAGATGAGAAACTGTCC	62	300/300	141
ELOVL3	CCTTGCAATCTTCAGTATCCTGG GATGAAGTTGATGAAGCACACG	60	300/300	146
EVA1	CAGTTCGACGACAATGGGACAT AGAGAAGCGTACAGTGTGCACGA	60	300/300	108
ZIC1	AGCCCTTCAAGTGCGAGTTT TGGACCTTCATGTGTTTGCG	60	300/300	672
CD137	CGACCCTGGACAAACTGTTCTTT AAGGAGATGATCTGCGGAGAGTGT	63	300/300	170
VEGFA	TCACCATGCAGATTATGCGGA TGTTGTGCTGTAGGAAGCTCA	58	300/300	75
KDR	CCGTTAAGCGGGCCAATGGA TTCAGCCGGTCTCTGGGGAA	60	300/300	142
FLT1	CGCCGGAAGTTGTATGGTTAAAA AGCCACGAGTCAAATAGCGAG	58	300/300	72
ERG1	TGCTCAACCATCTCCTTCCA TGGGTTTGCTCTTCCGCTCT	60	300/300	260
18S	CGGCTACCACATCCAAGGAA GCTGGAATTACCGCGGCT	60	100/100	186

Table 4. Primer sequences and PCR conditions for *PPARγ2* (Peroxisome proliferator activated receptor γ 2); *LEPTIN*; *UCP1* (uncoupling protein 1); *CIDEA* (cell death inducing DFFA like effector A); *ELOVL3* (Fatty Acyl Chain Elongase 3); *EVA1* (Epithelial V-like antigen 1); *ZIC1* (Zinc Fingers in the Cerebellum 1); *CD137* (cluster of differentiation 137); and endothelial factors, as *VEGFA (*vascular endothelial growth factor A), *KDR (*Kinase Insert Domain Receptor), *FLT1* (Fms-Like Tyrosine Kinase 1), *ERG1* (E26 transformation-specific related gene 1).

Protein extraction and quantification

Tissues were minced, covered by a cold (+4°C) lysis buffer containing 50 mM HEPES, pH 7.5, 150 mM NaCl, 10% glycerol, 5 mM Triton-X-100 and homogenized with dounce homogenizer for 20 min. Cells were lysed by suspension (1h at 4^{o}C) in the lysis buffer containing 20 mM Tris-HCl (pH 7.5) 1% Triton X-100, 10% glycerol, 1 mM EDTA and 150 mM NaCl, containing protease and phosphatase inhibitor cocktails. After centrifugation (16 000g for 15 min) protein concentration was determined in the supernatants by Bradford method. Briefly, Bradford method is a colorimetric assay that allows to determine with a good sensitivity protein concentration in a range 1-5 mg/ml. Each sample was appropriately diluted with H2O to a final volume of 100 uL and added with 900 µL of Bradford reagent (0.003% p/v Coomassie blu G250, 5% H_3PO_4; 10% p/v ethanol). Spectrophotometric reading was performed at 595 nm. and protein quantification was determined by interpolation of sample absorbance with a standard curve, prepared using serial decreasing dilution of bovine serum albumin (BSA).

CK2 kinase activity assay

Protein lysates (2µg) were incubated for 10 min at 30^{o} C in 25 μl of a phosphorylation medium containing 50 mM Tris-HCl (pH 7.5), 100 mM NaCl, 12 mM $MgCl_2$, 400 μM synthetic peptide-substrate

RRRADDSDDDDD and 20 µM [γ^{33}P]ATP (1000 -3000 cpm/pmol). Assays were stopped by absorption onto phosphocellulose p81 filters (Whatmann). Filters were washed four times in 75 mM phosphoric acid and analyzed by a Scintillation Counter (PerkinElmer). CK2 activity, that is proportional to radioactivity, was expressed as CPM/mg of protein.

Western blot analysis

Protein lysates were separated by SDS-PAGE (sodium dodecyl sulphate-polyacrylamide gel electrophoresis). Each sample was added with Laemmli sample buffer (0.6 M Tris-HCl pH 7.8, 2% p/v SDS, 20% v/v glycerol and 5 mM 2-mercaptoethanol). 11% polyacrylamide gels were 8 x 10 x 1 cm and composed by a stacking part at pH 6.8 and running gel at pH 8.8. The running was performed at 25-30 mA for 60 min. Proteins were then blotted on PVDF (Polyvinylidene fluoride) membranes (P-Immobilon Millipore) following manufacturer instruction and using TE 22 Mini Tank transfer unit (GE Healthcare) with 60V voltage for 90-120 min. Transfer buffer was composed by 10 mM CAPS-NaOH (3-cicloesil amino-1-propanesulfonic acid) pH 10, 3 mM DTT and 1% v/v methanol. Membrans were then rinsed with TBS buffer (50 nM Tris-HCl pH 7.5, 50 mM NaCl) and incubated overnight with primary antibodies, diluted in TBS 1% p/v BSA (Sigma-Aldrich). After removal of primary antibodies, membranes were rinsed with TBS three times for 5', then incubated with the specific secondary antibodies (TBS with 1% BSA p/v) for 30 minutes and rinsed again with TBS. Signal was developed using an enhanced chemiluminescent detection system ECL (Amersham Biosciences, Little Chalfont, United Kingdom). Immunostained bands were quantified by means of a Kodak-Image-Station 4000MM-PRO and analysis with Carestream Molecular Imaging software (New-Haven, CT).

Glucose uptake assay

After overnight serum starvation, 3T3L1 and human mature adipocytes (n=4) were pre-treated with DMSO (control), 2.5 µM CX-4945 or 20 µM DMAT and then stimulated with increasing insulin concentrations (0, 1, 10, 100 or 1000 nM) for 30 min at 37°C, 5% CO_2. 1.5 µCi of 2-Deoxy-D-^{3}H-glucose per ml were added at 2-Deoxy-D-glucose 50 µM solution to incubate cells for 15 min, or indicated timing, at 37°C. The test was terminated by ice treatment to block the glucose entry; adipocytes were lysed with NaOH 0.5 M and radioactivity measured by Scintillation counter (PerkinElmer, Waltham, MA, USA). An aliquot of each lysed well was collected to quantify protein concentration with Micro BCA Assay Kit (ThermoFisher) for normalization. This colorimetric based method allows the determination with a good sensitivity of protein concentration in a range 0.5-2 µg/mL, resulted reliable for diluted sample. Samples were analyzed in microplates in duplicates and spectrophotometric reading was performed at 560 nm with iMark Microplate Absorbance reader (Bio Rad, Hercules, CA, USA).

Subcellular fractionation by differential centrifugation

To evaluate the effect of CK2 inhibition on GLUT4 trafficking, plasma membrane (PM) and low density microsomes (LDM) were obtained from *in vitro* differentiated 3T3L1 adipocytes pre-treated with DMSO or 2.5 µM CX-4945 for 1 hour and then stimulated or not with 100 mM Insulin for 30 minutes. The fractionation of PM and LDM was obtained by a differential centrifugation method previously described by [224]. 3T3-L1 mature adipocytes were washed and re-suspended in HES buffer (20 mM HEPES, pH 7.4, 1 mM EDTA, and 255 mM sucrose containing protease/phosphatase inhibitor cocktails). Cell lysates were prepared by shearing the cells through a 22-gauge needle 10 times and centrifugation at 19,000g for 20 min at 4 °C. The pellet, containing the PM-rich fraction, was re-suspended in HES buffer and layered onto a 1.12 M sucrose cushion for centrifugation at 100,000g for 60 min. The PM layer was removed from the sucrose cushion, centrifuged again at 40,000g for 20 min and the resulting pellet was resuspended in lysis buffer. The supernatant obtained after the first centrifugation of lysates was further centrifuged at 41,000g for 20 min and then at 100,000g for 75 min to obtain the LDM pellet, which was re-suspended in lysis buffer. Lysates from PM and LDM were than analyzed by Western Blot.

Immunolocalization of GLUT4 transporter by confocal microscopy

3T3L1 and human mature adipocytes were pre-treated with DMSO (control), 2.5 µM CX-4945 or 20 µM DMAT and then stimulated with 100 nM insulin for 30 min at 37°C. Cells were then fixed in 4% paraformaldehyde, incubated with anti-GLUT4 antibody 1:50 for 2 hr at RT, washed twice in PBS 1x and then incubated with a 488 donkey anti-goat IgG (H+L, 1:200). Cells were counterstained with Draq5 (Abcam) and viewed using a DMI 6000 microscope (Leica Microsystem, Hilden, Germany). Images were taken and analyzed using SP8 software (Leica) to analyze insulin-stimulated GLUT4 translocation in presence or absence of CK2 inhibitors.

Statistical analysis

Results are presented as mean ± SEM or as median, 25^{th} and 75^{th} percentile. Statistical analysis was performed using unpaired Student's t (two-tailed) for normal distributed variables or Mann-Whitney non-parametric test for skewed data. All p values were two-sided and differences were considered significant at $p < 0.05$. Statistical analysis was performed using Sigmaplot 13.0 software. Analysis of limiting dilution data was performed using a Web application made available by the Walter and Eliza Hall Institute of Medical Research, Melbourne, Australia, http://bioinf.wehi.edu.au/software/elda/ [225]. This software test departures from the single hit Poisson model using a generalized linear model.

RESULTS

LIPOMATOUS TISSUE CHARACTERIZATION

Morphological analysis reveals white features of lipomatous tissue

A careful examination of subcutaneous (SAT) and lipomatous tissue (LT) morphology were performed by optical microscopy and samples were compared with the positive control of human brown/beige AT represented by the perirenal AT of a patient affected by Pheochromocytoma (Pheo). In fact, as discussed in Introduction, in humans brown tissue is present in childhood and maintained also in adult age but depots are usually not available for biopsies. Conversely, patients affected by Pheochromocytoma must undergo adrenalectomy that allows the collection of AT.

By H&E staining (Fig. 1A) and IHC for UCP1 (Fig. 1B), LT, as well as SAT, contained only mature univacuolated UCP1-negative adipocytes, while in Pheo islands of small, multilocular UCP1 positive cells are interspersed between white adipocytes (Fig. 1 A, B). Moreover, adipocytes of all analyzed LT samples have a slightly smaller area in comparison with SAT cells, as shown in Figure 2 (median area: LT vs SAT 4423 vs 5446 μm^2). Nevertheless, LT cells show a high variability within depots and among different patients: patient 3030 exhibited a higher adipocyte are in LT of arm than its paired subcutaneous adipocytes, whereas in subject 3002 II, arm-LT contained smaller cells. Variability was also found among different depots of the same patient: for example, in patient 5091, LT from arm contains larger adipocytes than its paired SAT, while LT from neck presented the opposite behavior. LT from neck and cervical area, that form the most known lipoma of MSL, Madelung collar, presented smaller cells than SAT in all patients.

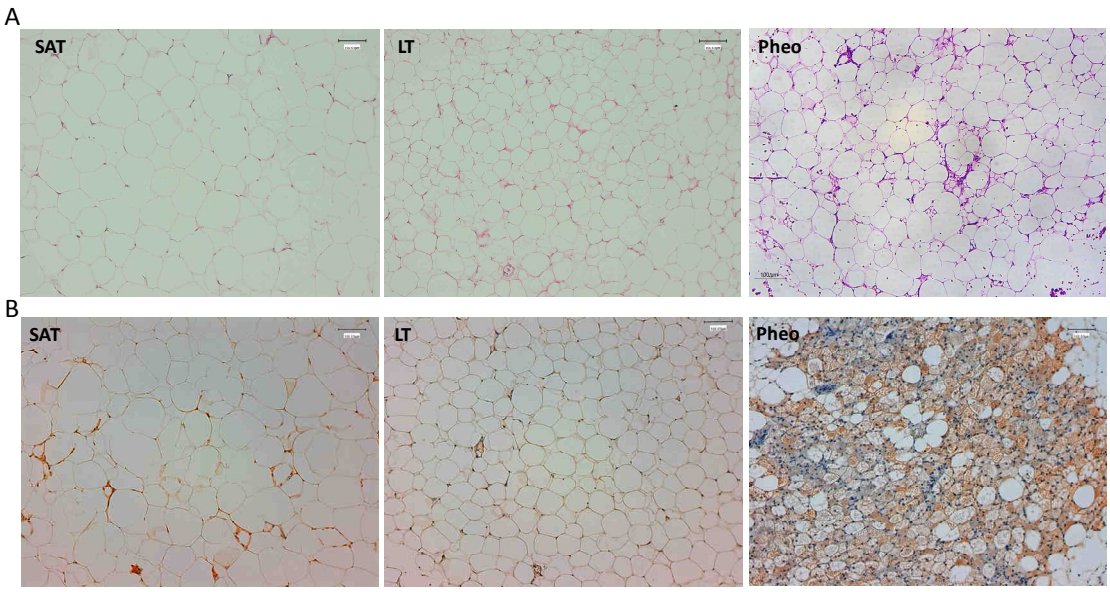

Figure 1. Representative images obtained by optical microscopy from patient 2884 of H/E (**A**) and IHC staining with anti-UCP1 antibody (**B**) of SAT (subcutaneous adipose tissue), LT (lipomatous tissue) and Pheo (perirenal adipose tissue of a patient affected by Pheochromocytoma). Magnification 10X.

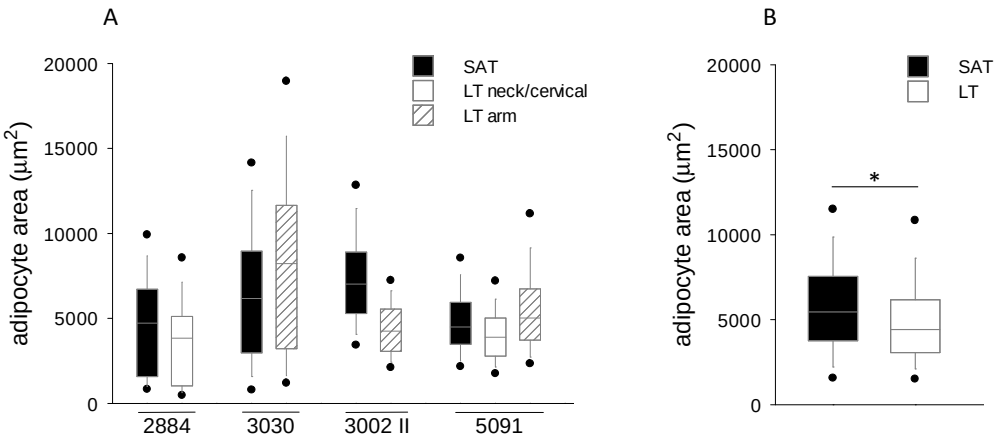

Figure 2. **A.** Adipocyte area (µm^2) of LT (lipomatous tissue), harvested from different anatomical sites, and paired SAT (subcutaneous adipose tissue) are presented for each analyzed patient indicated by ID number (2884, 3030, 3002 II and 5091), as in Table 1 (Materials and Methods); **B.** Median adipocyte area of all LT specimens is compared with SAT. Data are represented as median, 5th, 95th (circles) percentile (n=4 patients); *p<0.05.

Lipomatous tissue and its adipose stem cells exhibit a white gene expression signature

We performed gene expression profile by RT-PCR of white, brown and beige markers in LT, compared with SAT and Pheo (Fig. 3). LT and SAT express the classical white adipose markers (*PPARG2*, *LEPTIN*) at comparable levels, although a trend towards a higher expression of both markers by LT could be appreciated. Importantly, the most specific brown AT marker, *UCP1*, was negligible in both tissues in comparison with Pheo, that clearly upregulates *UCP1*, in agreement with IHC analysis shown in Figure 1B. We then analyzed other brown/beige specific markers: epithelial V-like antigen 1 (*EVA1*), Zinc finger in the cerebellum 1 (*ZIC1*) are described to distinguish BAT from beige, Cell death inducing DFFA like effector A (*CIDEA*) that is shared by both brown and beige cells [85], and the Fatty acid elongase 3 (*ELOVL3*), considered a brown marker but its role in beige adipocytes is not clear. Given the high variability of data, we did not highlight statistically significative differences among the depots for these markers. However, it is worth noting that *ZIC1* and *EVA1* presented opposite trend between SAT and LT, being ZIC1 basically higher in LT and EVA1 in SAT, and that Pheo did not overexpress these markers, as in case of *UCP1*. *ELOVL3* presented a higher trend of expression in LT in comparison with both SAT and Pheo. Taken together, these findings suggested that reliable molecular markers to distinguish white, beige and brown need further investigations

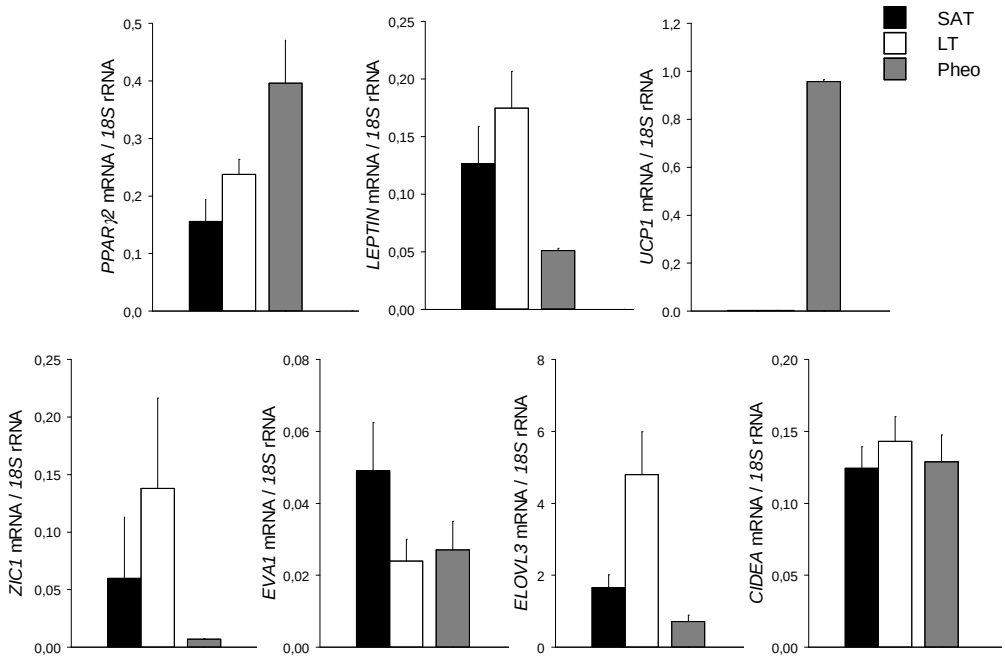

Figure 3. Gene expression quantification by RT-PCR of *PPARG2*, *LEPTIN*, *UCP1*, *ZIC1*, *EVA1*, *ELOVL3*, *CIDEA* in SAT (black bars), LT (white bars) and Pheo (grey bars). RNA was extracted from whole tissue. Data (ratio of arbitrary units) are reported as mean values ± SEM; mRNA of indicated genes was normalized to *18S* rRNA content; n = 5 patients (2884, 2891 I, 2891 II, 3002 I, 3030).

To further evaluate the molecular features of MSL, gene expression analysis was performed *ex vivo* in freshly isolated stromal vascular fraction (SVF), that is mostly represented by ASCs. Performing RT-PCR without previous *in vitro* expansion of the SVF avoids bias due to gene expression modulation induced by culture conditions. LT-derived SVF displayed a similar expression of *PPARG2* and *LEPTIN* in comparison with SAT-derived SVF and, importantly, negligible level of *UCP1*, that is clearly expressed in Pheo-derived SVF, in agreement with its brown/beige commitment (Fig. 4). Since CD137 is considered a marker of beige preadipocytes, it has been evaluated only in SVF, showing that LT-derived SVF express a substantially lower level of this marker in comparison with SAT derived cells, although not reaching a statistically significant difference. Even SVF from AT near Pheochromocytoma presented lower level of *CD137* mRNA than SAT. The other brown/beige markers (*ZIC1*, *EVA1*, *ELOVL3*, *CIDEA*) did not appear statistically different in LT and SAT, but, *ZIC1* and *EVA1* presented the same trend than shown in whole tissues: *ZIC1* and *ELOVL3* were slightly higher in LT derived SVF, *EVA1* in SAT derived precursor cells while *CIDEA* resulted similarly expressed. Interestingly, the gene profile of SVF from AT near Pheochromocytoma is characterized by a relatively higher expression of *EVA1* and *CIDEA* compared with LT and SAT.

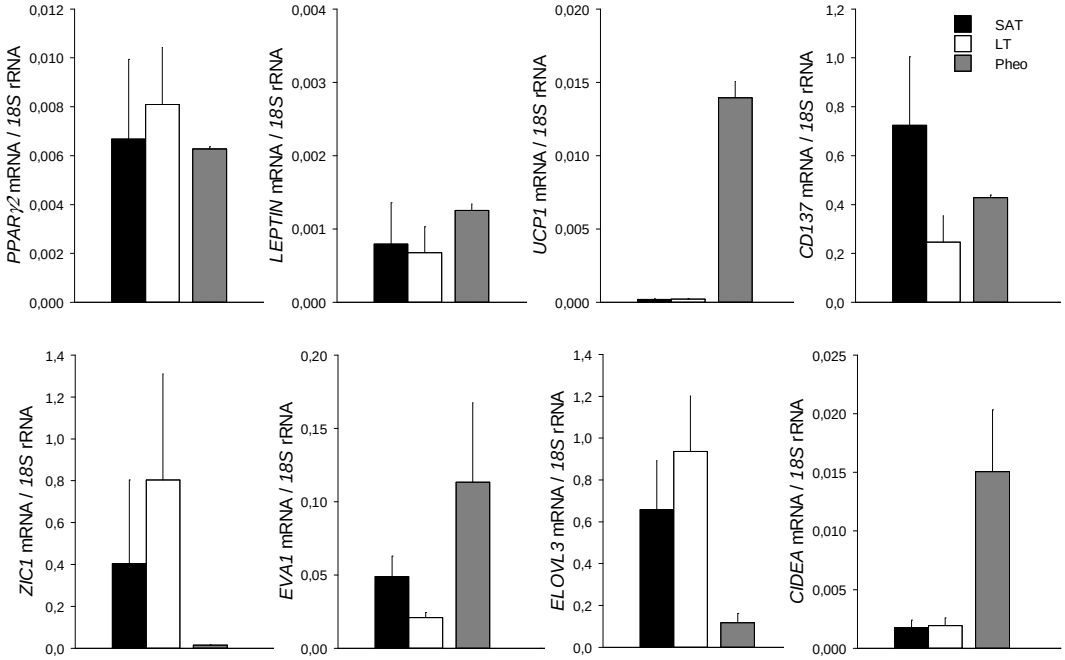

Figure 4. Gene expression analysis of freshly isolated stromal vascular fraction from SAT, LT and AT near Pheochromocytoma (Pheo). *PPARγ2*, *LEPTIN*, *UCP1*, *CD137*, *ZIC1*, *EVA1*, *ELOVL3*, *CIDEA*, mRNA was quantified by RT-PCR and is normalized by *18S* rRNA content. Data (ratio of arbitrary units) are reported as mean values ± SEM; n = 5 (2884, 2891 I, 2891 II, 3002 I, 3030).

Observations during surgery reported that LT carries a higher bleeding in comparison with healthy adipose tissue and it is considered a high vascularized tissue. In this view, the most important ETS (E26 transformation-specific family) endothelial factors [226] were evaluated in both whole tissues and freshly isolated SVF in LT and SAT as markers of angiogenetic potential (Fig. 5). Gene expression of both early, *ERG1* (ETS related gene 1) and late, as *VEGF-A* (vascular endothelial growth factor A), *KDR* (Kinase Insert Domain Receptor or VEGF Receptor 2) and FLT1 (Fms-Like Tyrosine Kinase 1 or VEGF Receptor 1) ETS factors did not reveal differences of LT in comparison with SAT. However, it is to underline that SVF from LT displayed a trend towards a higher expression than SAT, in contrast to what shown in whole tissue where SAT appeared to have the higher VEGF-A mRNA amount.

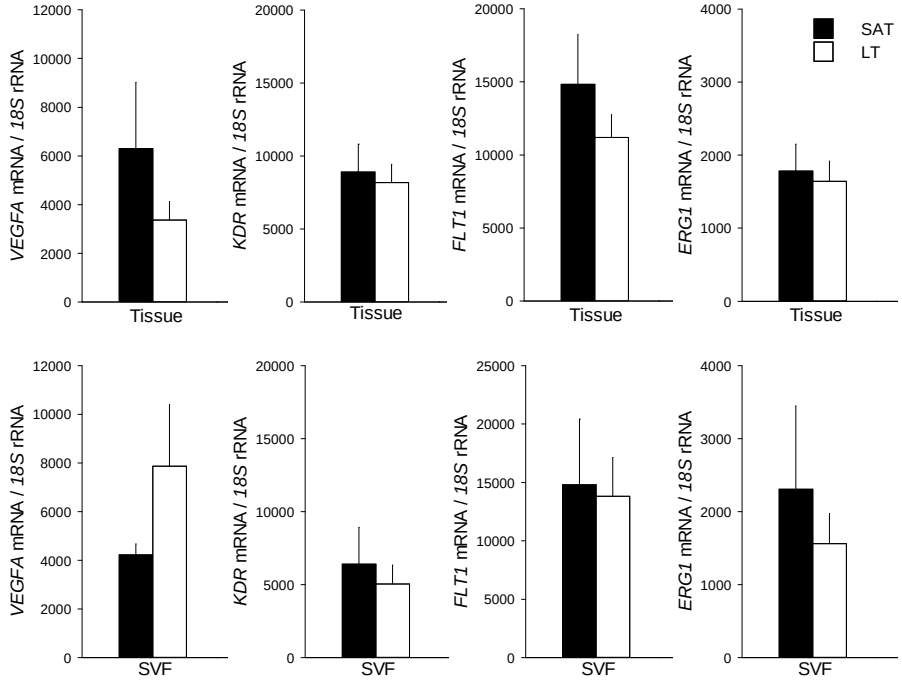

Figure 5. Gene expression analysis in whole tissue (histograms above) and freshly isolated SVF (histograms below) of SAT and LT. *VEGFA* (vascular endothelial growth factor A), *KDR* (Kinase Insert Domain Receptor), *FLT1* (Fms-Like Tyrosine Kinase 1), *ERG1* (ETS related gene 1) mRNA was quantified by RT-PCR and is normalized by *18S* rRNA content. Data (ratio of arbitrary units AU) are reported as mean values ± SEM; n = 5 (2884, 2891 I, 2891 II, 3002 I, 3030).

Adipose stem cells characterization: quantification, proliferation and adipogenic potential

LT-derived SVFs were characterized *ex vivo* quantifying the ASCs subpopulation by flow cytometry analysis as CD45-CD31-CD34+ cells and compared with SAT-derived SFVs from the same patients in anatomical region free of disease (see also Table 1). Freshly extracted SVFs were analyzed through a forward/side scatter morphological gate to exclude cellular fragments, aggregates and immune cells. Interestingly, LT harvested from neck/cervical region (Madelung collar) resulted significantly enriched in CD45-CD31-CD34+ cells in comparison with paired SAT (Fig. 6; LT vs SAT: 74,25 ± 1,17 % vs 60,6 ± 4,67 %, $p < 0.05$), while LT from axillary/upper arm did not show the same behavior (LT vs SAT: 59,58 ± 3,35 % vs 54,8 ± 2,04 %), presenting an ASCs number comparable with SAT.

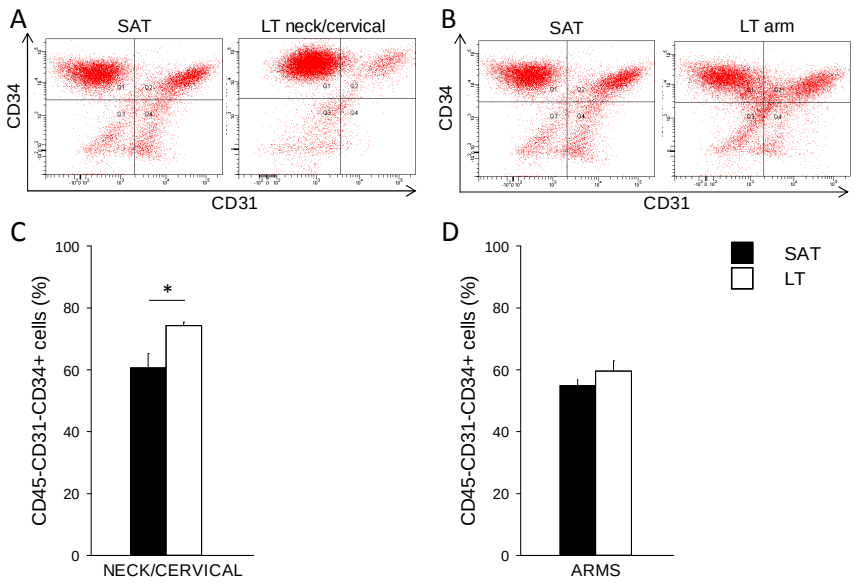

Figure 6. Representative flow cytometric dot plots (**A**, **B**) for surface markers CD34 vs CD31, determining the percentage of adipose stem cells ASCs (CD45-CD31-CD34+) within total stromal vascular fraction (SVF) from patient 3002 I where both neck/cervical and arm lipomatous tissue (LT) were collected. In the graphs (**C**, **D**), quantification (%) of neck/cervical (**C**) or arm (**D**) LT and the corresponding SAT-derived ASCs is reported as mean values ± SEM. In **C**, data are derived from neck/cervical region of 2884, 2891 I, 3002 I neck, 5091 and the paired SAT; in **D** from arm area of 3002 I, 3002 II, 3030, 5091 and the paired SAT; *p<0.05.

ASCs phenotype was further characterized in the immunological gate (Fig. 7), evaluating mesenchymal surface markers (CD90, CD73 and CD271). Although not statistically different, CD90 seems to show a lower expression in LT-derived ASCs, especially in neck/cervical lipomas, while in the same LT depot, CD271 displays a trend towards a higher expression in comparison with the corresponding SAT derived ASCs. CD73 was similarly well expressed by LT and SAT derived ASCs, independently from lipoma localization. We also evaluated ACSs expression of the pericyte marker CD146, that had a similarly low expression (in neck/cervical LT vs SAT: 0.45 ± 0.18 vs 0.525 ± 0.099 %; arm LT vs SAT: 0.525 ± 0.17 vs 0.38 ± 0.15; data not shown).

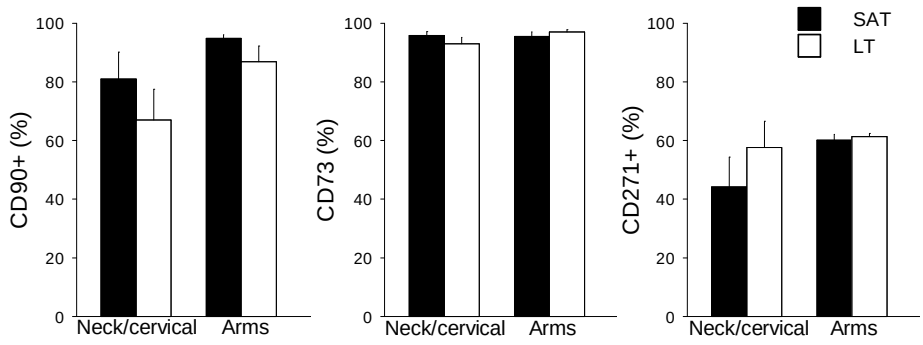

Figure 7. Percentage of CD45-CD31-CD34+ cells expressing the mesenchymal markers CD90, CD73 and CD271 in LT from neck/cervical region (n = 4) or from upper arm (n = 4), represented by white bars, and their paired SAT (black bars). Data are presented as mean values (%) ± SEM.

LT derived-ASCs were then compared with SAT derived preadipocytes in their behavior during in vitro culture. Cell morphology was evaluated by optical microscopy observation at subsequent culture passages (from p0 to p2) in human standard medium (hSM) and LT and SAT derived ASCs did not show any morphological differences: adipose precursor cells from both tissues displayed the peculiar fibroblast like shape, appearing as flat, spindle cells (Fig. 8A). Moreover, since the contribution of hyperplasia or hypertrophy has not been established yet in growing LT, proliferation analysis was performed. Proliferative capacity was assessed by ATP-based assay in patient 2884 in two samples of LT (neck and cervical) and in the corresponding SAT, while in LT derived from upper arm and SAT of patient 3002 II, a DNA-based assay, that is independent from the cell metabolic features, was performed. Interestingly, in both experiments, LT derived ASCs possessed a doubling time slightly but significantly lower than SAT precursors (Fig. 8B), independently from lipoma localization.

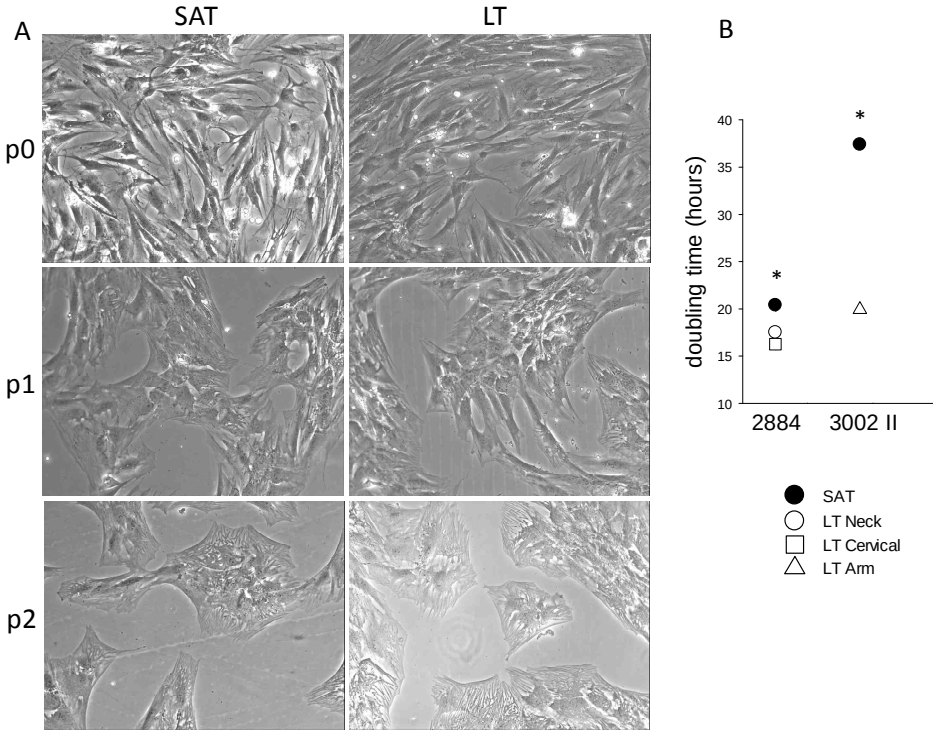

Figure 8. Representative images (**A**) obtained by optical microscope of *in vitro* cultured ASCs isolated from SAT and LT (neck) from patient 2884 at different passages in culture (p0, p1, p2), magnification 10X. **B.** Doubling time was derived in SAT (black circles) and neck/cervical and arm LT (white symbols) of patients 2884, by ATP-based cell proliferation assay, and 3002 II, by DNA-based method. Data (hours) are reported as mean values ± SEM, * $p < 0.05$ SAT vs LT.

Tissue-derived ASCs were then differentiated *in vitro* with adipogenic medium (AM) and adipogenesis was evaluated by optical microscopy at day 12. Preadipocytes from LT disclosed a greater adipogenic potential than SAT-derived SVF (Fig. 9); in addition, LT-derived precursor cells maintained their adipogenic potential

even after preliminary passages in culture (p0-p3), that usually reduce the adipogenic potential of stromal vascular fraction.

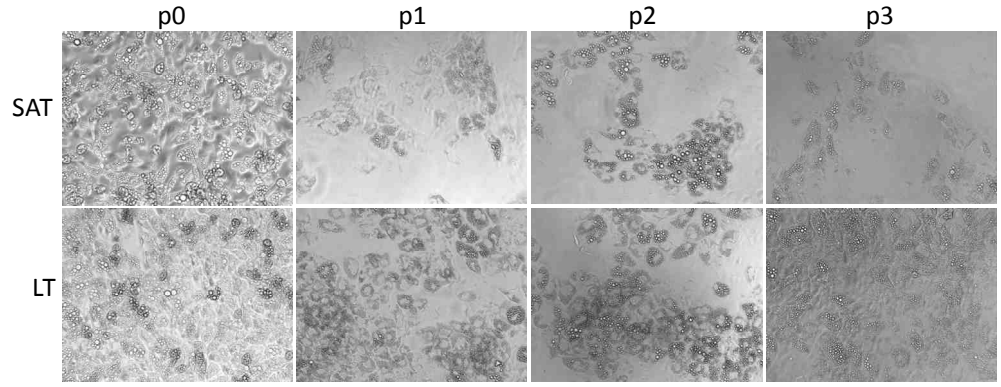

Figure 9. Representative images at optical microscope of *in vitro* adipogenesis from SAT and LT-derived ASCs of patient 2884. P0 – p3 refer to preliminary passages in culture of SVF before induction with adipogenic medium (AM). Magnification 10X.

Gene expression analysis of mature adipocytes was performed in 3 patients (2884, 2891 I, 3002 I). In comparison with undifferentiated preadipocytes, LT-derived mature cells upregulate the typical white adipocyte markers *PPARG2* and *LEPTIN*: although there is no statistical difference, *LEPTIN* tends to be more expressed in LT than in SAT mature adipocytes. When treated with 10 µM Forskolin (adenylyl cyclase inducer) at the end of differentiation (AM + Forsk), in 2 of 3 patients, LT adipocytes show a lower *UCP1* induction (browning) than SAT cultures (Fig. 10).

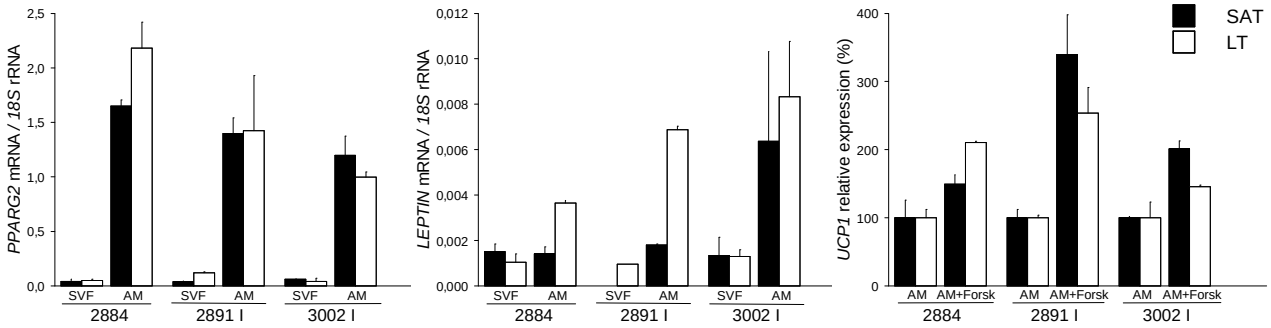

Figure 10. Gene expression of *ex vivo* stromal vascular fraction (SVF) and *in vitro* differentiated adipocytes (AM) from SAT and LT of 3 patients (ID subjects 2884, 2891 I, 3002 I). *PPARγ2* and *LEPTIN* mRNA (ratio of arbitrary unit, AU) are expressed as mean values ± SEM and normalized by *18S* rRNA content; *UCP1* expression upon stimulation with 10 µM Forskolin (AM + Forsk) is reported as percentage (%) respect to control (AM), not treated with Forkolin.

LT derived SVF display a greater clonogenic and adipogenic potential than SAT derived cells

We further analyzed SVF, obtained from neck/cervical LT and SAT of patient 2891 I, by clonal analysis performing a limiting dilution assay. For each dilution (1000, 100, 30, 10, 3, 1, 0.3 cells/well) wells, where

cell proliferation could be detected at microscopy observation, was considered positive and the percentage (%) of positive wells was calculated in respect of the expected value. At low dilution (1000, 100, 30 cells/well), all seeded wells resulted positive since the relative low number of SFV cells isolated from LT and SAT were able to proliferate. Conversely, in condition of high cell dilution (3, 1 cells/well or one cell every 3 wells), LT-derived precursors gave rise to a higher number of positive wells, suggesting a higher clonogenic potential of LT, that is indicative of a greater clonogenic capacity (Fig. 11B). In fact, in LT, seeding 1 cell/well is sufficient to obtain a 60% of positive wells, while in SAT at least 3 cells/well are necessary to reach a similar result.

To explore SVF adipogenic potential at a clonal level, positive wells were then induced to differentiate by addition of AM and wells positive for adipogenic differentiation were quantified and the percentage (%) was calculated in respect of the total grown wells during the limiting dilution assay. Especially for low dilution (1000, 100, 30), LT derived SVF gave rise to a higher number of wells positive for adipogenic differentiation in comparison with SAT (Fig. 11C). The limiting dilution analysis showed that LT resulted significantly enriched of colony forming precursor cells and that this population contained a higher number of adipogenic precursors than SAT. Considering now the efficiency of adipogenesis evaluated by optical microscopy (representative clones are shown in Fig. 11A), adipogenic wells from both LT and SAT presented a high variability in terms of percentage of differentiated cells. At low cell dilution (1000, 100 cells/well), LT adipogenic clones seem to display a greater adipogenic potential, as previously reported in Fig. 9 (Fig. 11D). Conversely, clones obtained by a lower number of SVF cells (30, 10, 3, 0,3/well) maybe lack of the necessary adipogenic stimuli for an optimal differentiation and in this condition no differences could be appreciated between LT and SAT.

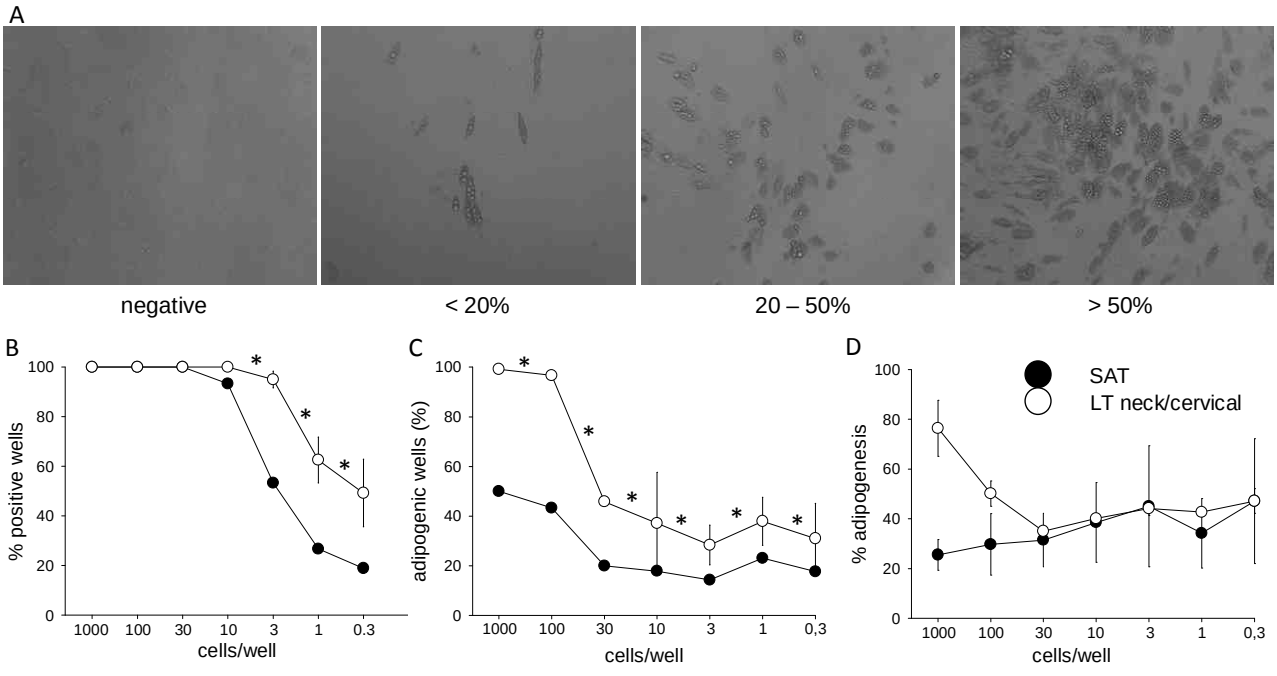

Figure 11. Representative images by optical microscopy (magnification 10X) of LT derived clones with increasing percentage of adipogenic differentiation (**A**). **B**. The percentage of positive wells is reported for SAT (black circles) and neck/cervical LT (mean value of the two deposits ± SEM, white circles) in respect of the number of seeded cells/well. **C.** The percentage of adipogenic wells in respect to positive wells is represented. **D.** The mean percentage of adipogenic differentiation (% adipogenesis), estimated by optical microscopy as exemplified in panel A, of adipogenic wells is compared between SAT and LT. *p< 0.05, LT vs SAT.

PROTEIN KINASE CK2 IN EXPANDING ADIPOSE TISSUE: OBESITY AND MSL

Since insulin signaling is one of the major responsible for AT growth and metabolism and genetic hyperactivation of this pathway leads to a MSL-like phenotype in mice, we focused on the role of protein kinase 2 CK2 in AT. To investigate CK2 involvement in AT, we took advantage from the availability of chemical selective inhibitors for this kinase (see also Introduction), Wb analysis to quantify its expression and of *in vitro* assay to determine its activity, that is known to be proportional to its amount, being independent from phosphorylative event. First *in vitro* and *in vivo* experiments were performed to evaluate CK2 role in AT glucose homeostasis and then its expression and activity was evaluated in mouse model of obesity and diabetes, in patients affected by obesity and in Multiple Symmetric Lipomatosis.

CK2 is involved in insulin-stimulated glucose uptake of 3T3-L1 adipocytes

Preliminary experiments were performed in 3T3L1 and human differentiated adipocytes to confirm that CK2 amount and activity is unaffected by insulin stimulation and that CK2-inhibitors, CX-4945 and DMAT (see Introduction) blocked the kinase activity without modifying its protein-level or causing cytotoxicity. After overnight serum free conditions, DMSO (CTRL), 2.5 μM CX-4945 or 20 μM DMAT were added for 1 hour to 3T3L1 mature adipocytes before 100 mM insulin stimulation for 3 or 30 further minutes. CK2α and β protein level, evaluated by Western blot, was not modified by treatments (Fig. 12A), while CK2 inhibitors were able to efficiently lower kinase activity (Fig. 12B), even at low concentration. Therefore, human preadipocytes, 3T3L1 and human mature adipocytes were treated with 1, 2.5, 10 μM CX-4945 or 10 μM DMAT in presence or absence of FSB for 24 or 48 hours (Fig. 12C, D) and then MTT assay was performed. Cell viability resulted slightly impaired only upon prolonged treatment (48 hours) or, in human preadipocytes, at higher concentration of CX-4945. On the basis of these results, we decided to work with CX-4945, a CK2 inhibitor currently used in cancer clinical trials, using the lowest concentration (2.5 μM) and pre-treatment time (1hour) able to efficiently inhibit CK2 activity, avoiding any cytotoxic effect.

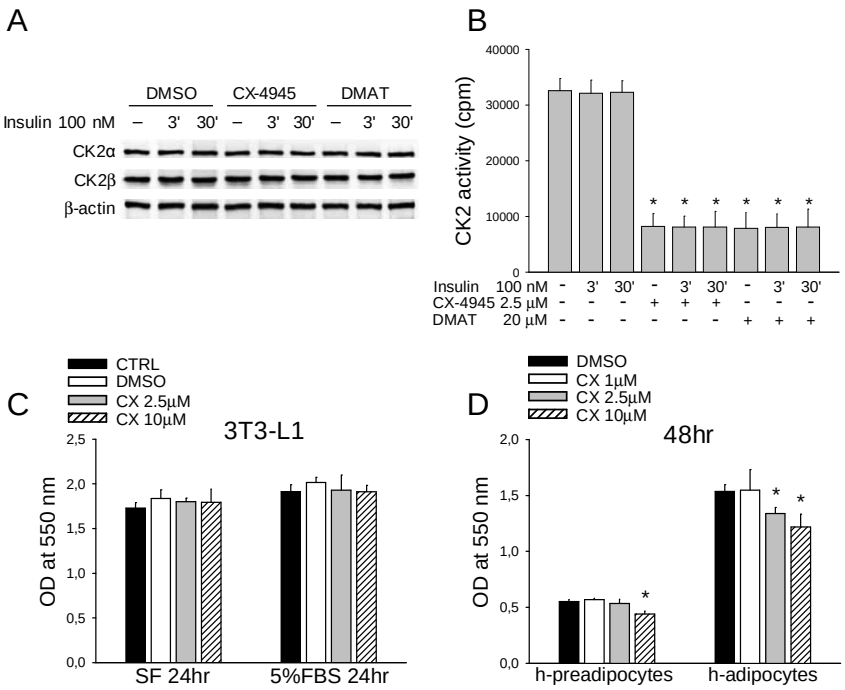

Figure 12. 3T3-L1 adipocytes (n=3) were pre-incubated with vehicle (DMSO), 2.5 µM CX-4945 or 20 µM DMAT for 1hr and then stimulated or not (-) with 100 nM insulin for 3 or 30 min. In **A**, representative panel is shown of 4 separate experiments, where protein extracts (40 µg) were analyzed by Wb with anti-CK2a and anti-CK2b antibodies. Anti-β-actin is shown as loading control. In **B**, cell lysates (2 µg) were tested for CK2 kinase activity (n=4). In **C**, *in vitro* differentiated 3T3-L1 adipocytes (n=6) were untreated (CTRL), treated with DMSO or CX-4945 in serum free culture medium (SF) for 24 hours with or without 5% fetal bovine serum (FBS). In **D**, human (h) pre-adipocytes (n=6), obtained from SAT, and *in vitro* differentiated mature adipocytes were treated for 48 hours with DMSO or CX-4945 in medium with 10% FBS and in SF, respectively. Cell viability was assessed by MTT colorimetric test and absorbance values are reported.
Data are reported as mean values ± SEM; *p<0.05 vs CTRL or DMSO.

To evaluate CK2 involvement in adipocyte glucose homeostasis, different experimental settings were designed. First, 2 Deoxy-D-glucose (2DG)-uptake was assessed in 3T3-L1 adipocytes pre-treated for 1hr with DMSO or 2.5 µM CX-4945 and then stimulated or not (basal uptake) with increasing insulin concentration for 30 min (Fig. 13A). Second, 3T3-L1 adipocytes were pre-treated with DMSO or CX-4945 (CX) for 1hr, stimulated or not with 100 nM insulin for further 30 minutes and 2DG-uptake was quantified in relation with time (Fig. 13B). Finally, 2DG-uptake of 3T3-L1 adipocytes (n=4), pre-treated with DMSO, CX-4945 or DMAT for 1 hour and stimulated with increasing insulin concentrations (0, 10, 100, 1000 nM) for 30 min (Fig. 13C). Importantly, a great and constant reduction of insulin-induced glucose uptake was observed in 3T3-L1 mature adipocytes, pre-treated for 1hr with CX-4945 and then stimulated with increasing insulin doses for 30 min, (Fig. 13A). The inhibitor did not influence the basal glucose uptake nor the time-course of the insulin-stimulated glucose entry (Fig. 13B). Comparing the two inhibitors (Fig. 13C), a less striking decrease in insulin-dependent glucose uptake was obtained by adipocyte treatment with 20 µM DMAT, a less potent CK2 inhibitor structurally unrelated to CX-4945.

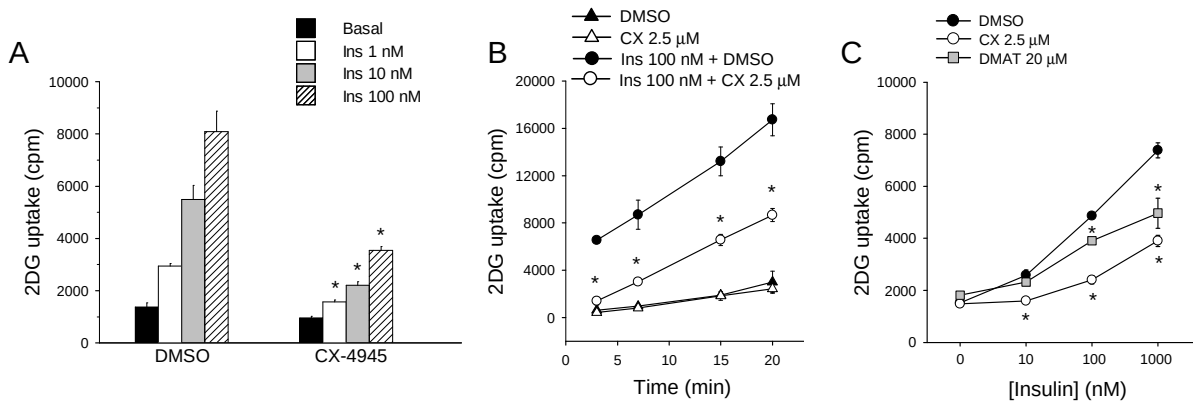

Figure 13. **A**. 2 Deoxy-D-glucose (2DG)-uptake of 3T3-L1 adipocytes (replicates n=4) pre-treated for 1hr with DMSO or 2.5 μM CX-4945 and stimulated or not (Basal) with the indicated insulin concentration for 30 min. **B.** 3T3-L1 adipocytes (n=4) were pre-treated with DMSO or CX-4945 (CX) for 1hr and stimulated or not with insulin for 30 min; 2DG-uptake was quantified at the indicated times. **C**. 2DG-uptake of 3T3-L1 adipocytes (n=4), pre-treated with DMSO, CX-4945 or DMAT for 1hr and stimulated with the indicated insulin concentrations for 30 min. In 2DG uptake assays, total protein content of each sample was quantified and no statistical differences were found among samples. Results are presented as mean ± SEM; *p<0.05 *vs* DMSO treatment.

To highlight the molecular mechanisms underlying glucose-uptake reduction, we examined the effect of CK2 inhibition on the insulin signaling pathway in 3T3-L1 adipocytes by western blot (Wb) analysis with specific phospho-antibodies. For this aim, 3T3-L1 mature adipocytes, pre-treated with DMSO, 2.5 μM CX-4945 or 20 μM DMAT for 1hr, were stimulated or not with insulin for 3 or 30 min. Akt signaling resulted greatly counteracted by both CK2 inhibitors, CX-4945 and DMAT, as indicated by the strong decrease of the constitutive CK2-mediated phosphorylation of Akt1 Ser129 (Fig. 14, lanes 1-3 vs 4-9). In parallel, the insulin-triggered phosphorylation of Akt1/2 Thr308 was almost abrogated and that of Ser473 was strongly hampered by CX-4945 and DMAT. Immunostaining with anti-Akt antibodies, which recognize Akt1/2/3 isoforms, was not modified by cell treatment with inhibitors. Insulin activation of Akt1/2 allowed the phosphorylation of its substrates, including the TBC1D4 (AS160), the most distal insulin-signaling protein linked to GLUT4 translocation (see Introduction), at Thr642, and GSK3β at Ser9 (Fig. 14, lanes X). Consistent with the down-regulation of Akt1/2 activatory sites, CK2 inhibition strongly impaired also the phosphorylation of Akt substrates (Fig. 14, lanes 1-3 vs 4-9), including TBC1D4 (AS160), suggesting that CK2 plays a role in the cellular trafficking of this glucose transporter. Moreover, according with the action of CK2 on PTEN, cell treatment with CX-4945 and DMAT caused a substantial decrease of PTEN CK2-mediated phosphorylation at Ser370 and a parallel reduction of its protein level (Fig. 14, lanes 4-9), suggesting PTEN activation.

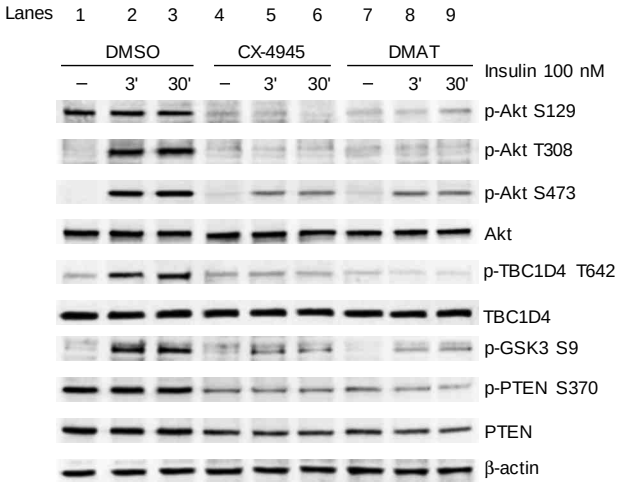

Figure 14. 3T3-L1 adipocytes, pre-treated with DMSO (lanes 1,2,3), 2.5 μM CX-4945 (4,5,6) or 20 μM DMAT (7,8,9) for 1hr, were stimulated or not (-, lanes 1,4,7) with insulin for 3 (lanes 2,5,8) or 30 min (lanes 3,6,9). Protein extracts (40 μg) were analyzed by Wb with the indicated antibodies. β-actin is shown as loading control.

GLUT4 localization was then examined in CX-4945 pretreated and insulin stimulated 3T3-L1 adipocytes. Subcellular distribution of GLUT4 was accomplished by isolating the cell plasma membrane (PM), and the low-density microsomes (LDM) fractions (Fig. 15A). In controls, insulin-stimulation increased GLUT4 level in PM fraction (lane 1 vs 2), lowering its amount in LDM fraction, where intracellular GLUT4 was mainly localized in unstimulated cells (lane 4 vs 5). Consistently, CX-4945 pre-treatment strongly reduced GLUT4 recruitment to PM fraction (lane 2 vs 3) revealing that CK2 mediates the transporter translocation to the plasma membrane. These observations were further confirmed by confocal IF microscopy (Fig. 15B). Under basal conditions, GLUT4 showed an intracellular punctuated staining preferentially around the nucleus, corresponding to the well characterized GLUT4 vesicles. A weak signal appeared at the plasma membrane, where GLUT4 staining greatly increased upon insulin stimulation. CX-4945 Adipocyte pre-treatment altered the insulin-induced GLUT4 distribution in a dose dependent manner, decreasing the PM signal and enhancing GLUT4 intracellular localization.

A

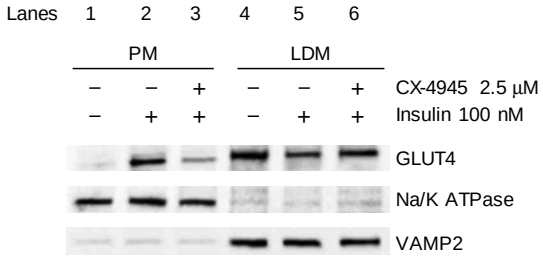

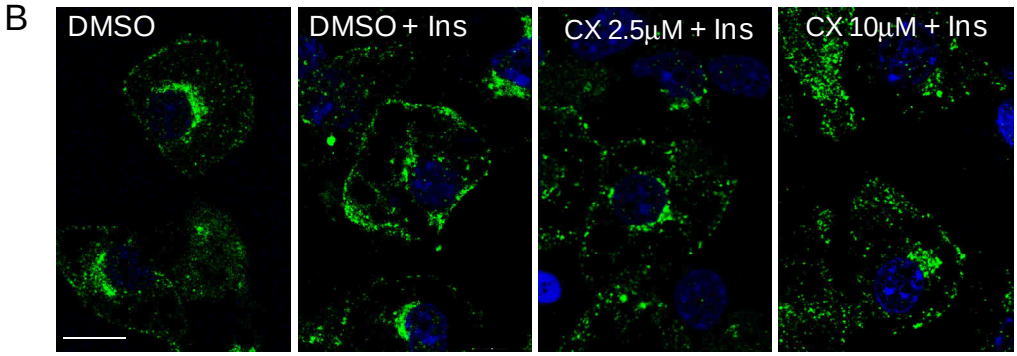

Figure 15. **A**. 3T3-L1 adipocytes, pre-treated with DMSO (lanes 1,2,4,5) or 2,5 μM CX-4945 (lanes 3,6), were unstimulated (lanes 1,4) or stimulated with 100 nM insulin for 30 min (lanes 2,3,5,6). Plasma membrane (PM, 15 μg) and low density microsome (LDM, 10 μg) fractions were isolated and analyzed by Wb (representative panel) with anti-GLUT4, anti-Na/K ATPase (PM marker) and anti-VAMP2 (LDM marker) antibodies. **B**. Representative images of confocal immuno-fluorescence (IF) staining with anti-GLUT4 antibody of 3T3-L1 adipocytes pre-treated with DMSO or CX-4945 at the indicated doses and stimulated or not with 100 nM insulin (Ins) for 30 min. Scale bar=10μm. Green=anti-GLUT4, Blue=Draq5 for nuclei staining. 100x magnification, zoom factor 2. Results are representative of 3 independent experiments.

These results highlight that CK2-inhibition counteracts the insulin-stimulated glucose transport in 3T3-L1 adipocytes, revealing a novel function of CK2 in supporting insulin signaling activation and GLUT4 recruitment to cell surface.

CK2 inhibition reduces insulin-induced glucose uptake and Akt signaling in human primary adipocytes

Human mature adipocytes were differentiated *in vitro* from SAT of patients 3519 and 3625, pre-treated with DMSO, CX-4945 (2,5 μM or 10 μM) or DMAT (10 μM) for 1 hour, stimulated with increasing insulin concentrations (1, 10, 100 nM) for 30 min and assayed in 2DG-uptake (replicates=4). Results obtained in 3T3-L1 cells were confirmed in human adipocyte primary cultures where CX-4945 and DMAT pre-treatment were able to substantially inhibit insulin-stimulated glucose uptake (Fig. 16A). Moreover, also in CX-4945 (2,5 μM) or DMAT (10 μM) pre-treated (for 3 and 30 minutes) and insulin (100 nM)-stimulated human cells (Fig. 16B), Wb analysis demonstrated that CK2-inhibition led to a striking decreased phosphorylation of the Akt1/2 activatory sites Ser129, Thr308 and Ser473 and Akt1/2 substrates TBC1D4 and GSK3β. PTEN protein level was substantially reduced also in human adipocytes, suggesting its activation. Immunolocalization analysis confirmed CX-4945 inhibitory effect on the insulin-induced GLUT4 translocation in human adipocytes, showing a dose-dependent decrease of plasma membrane GLUT4 staining (Fig. 16C).

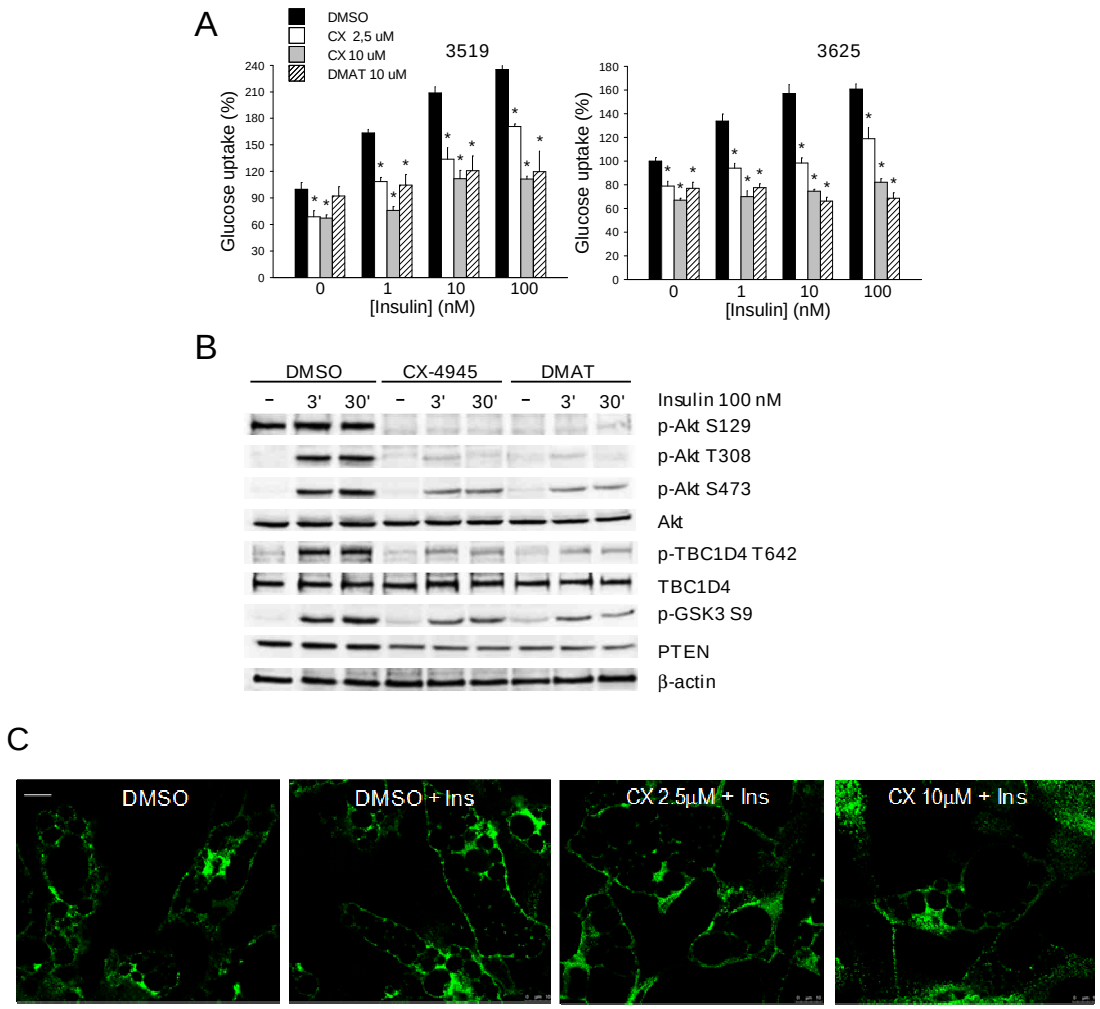

Figure 16. **A**. 2DG-uptake in human primary adipocyte cultures (see text for details), pretreated with CK2 inhibitors at the indicated concentration and then exposed to insulin (1, 10, 100 nM) for 30 min. Data are normalized for total protein content and reported as percentage relative to control adipocytes (DMSO, Ins 0). 3519 and 3625 indicates patient ID numbers whose SAT was processed to isolate the SVF for human primary cultures. Results are presented as mean ± SEM; *p<0.05 vs DMSO. **B.** Human adipocytes, pre-treated for 1hr with DMSO, 2.5 µM CX-4945 or 10µM DMAT, were stimulated or not (-) with insulin as indicated. Cell lysates (40 µg) were analyzed by Wb (representative panel, n=2 patients). (**C**) Confocal immuno-fluorescence staining (representative images, n=2 patients) with anti-GLUT4 antibody of human adipocytes pre-treated with DMSO or CX-4945 and stimulated or not with 100 nM insulin (Ins) for 30 min. Scale bar=10µm. Green=anti-GLUT4. 100x magnification, zoom factor 1.

CK2 acts *in vivo* on insulin signaling in WAT depots, skeletal muscle and liver

CK2 expression and activity were first compared in different mouse tissues, with particular regard to insulin-target tissues. Tissue quantification of CK2 α and β subunit level by Wb and densitometry (Fig. 17A, B) and of CK2 activity (Fig. 17C) highlighted that white skeletal muscle fibers (glycolytic) of quadriceps (WQ) and liver contained the highest quantity of this kinase. A significant lower protein level and activity of CK2 were present in the red skeletal muscle fibers (oxidative) of quadriceps (RQ) and CK2 was even lower in AT depots. In BAT, CK2 was expressed at an intermediate level between WAT depots and skeletal muscle and no significant differences were highlighted between SAT and epididymal VAT (VAT-E).

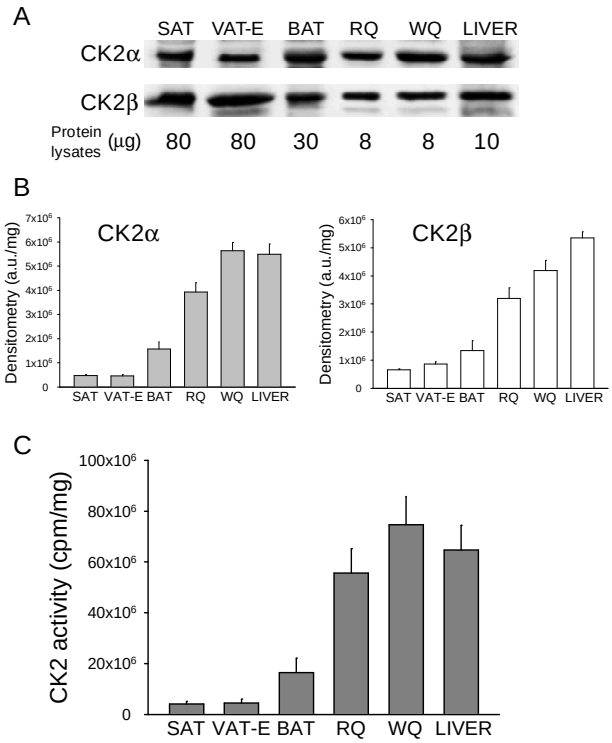

Figure 17. C57BL6/6J (B6) male mice (n=3) of 22 weeks of age were sacrificed to collect the following tissues: subcutaneous (SAT), visceral epididimal (VAT-E) and brown (BAT) adipose tissues, red (RQ) and white quadriceps (WQ), and liver. **A**. The indicated amounts (μg) of tissue proteins were analyzed by Wb with anti-CK2α and anti-CK2β antibodies. **B.** Immunostained bands were quantified by densitometry and expressed as arbitrary units/mg proteins. Results are presented as mean ± SEM. Statistical analysis for CK2α expression: SAT vs BAT p=0.0047; VAT vs BAT p=0.0041; BAT vs RQ p=0.000093; RQ vs WQ p=0.00054; RQ vs LIVER p=0.0016; LIVER vs BAT p=0.000014; statistical analysis CK2β: SAT vs VAT p=0.006; VAT vs BAT p=0.07; SAT vs BAT p=0.03; BAT vs RQ p=0.00036; RQ vs WQ p=0.0098; RQ vs LIVER p=0.00023 ; WQ vs LIVER p=0.0032; LIVER vs BAT p=0.0000064. **C**. CK2 activity was quantified in tissue proteins of mice (n=3) and expressed as 33P-phosphate transferred to the substrate per mg of lysate proteins. Statistical analysis: SAT vs BAT p=0.021; VAT vs BAT p=0.021; BAT vs RQ p=0.00098; RQ vs WQ p=0.042; RQ vs LIVER p=0.23; WQ vs LIVER p=0.23; LIVER vs BAT p=0.00042; WQ vs BAT p=0.0043.

To analyze the effect of CK2 inhibition in insulin-target tissues *in vivo*, B6 mice were acutely treated with a single dose of CX-4945 and, 2 hours after CX-4945 administration, injected with insulin (1 U/kg) intraperitoneally (ip). After further 30 min from insulin stimulation, animals were sacrificed for tissue collection and CK2 activity and Akt-signaling were evaluated in tissue extracts. Insulin-treatment did not affect the basal kinase activity of different tissues, while CX-4945 strikingly inhibited CK2 in VAT-E, SAT and liver (Fig. 18A, C, G). A significant lower activity inhibition was detected in WQ (Fig. 18E). Accordingly, CX-4945 treatment counteracted insulin-trigged Akt1/2 activation in all tissues analyzed as demonstrated by Wb and quantification of Akt Ser473 phosphorylation extent (Fig. 18B, D, F, H). CK2 inhibition caused the expected drop of TCB1D4 phosphorylation in VAT-E, SAT and WQ (Fig. 18 B, D, F), which suggests a reduction in GLUT4 translocation, while in liver it was associated with a substantial decrease of FoxO1 Ser253 phosphorylation (Fig. 18H), indicating a gluconeogenesis activation. Interestingly, insulin activation and CX-4945 inhibition of Akt1/2 signaling were more evident in VAT-E and liver (Fig. 18B, H).

These data show that, in mice, an acute CX-4945 treatment causes a great inhibition of CK2 activity in WAT depots and liver, and a limited effect in skeletal muscle, ensuing a relevant inactivation of the tissue specific insulin-driven pathways.

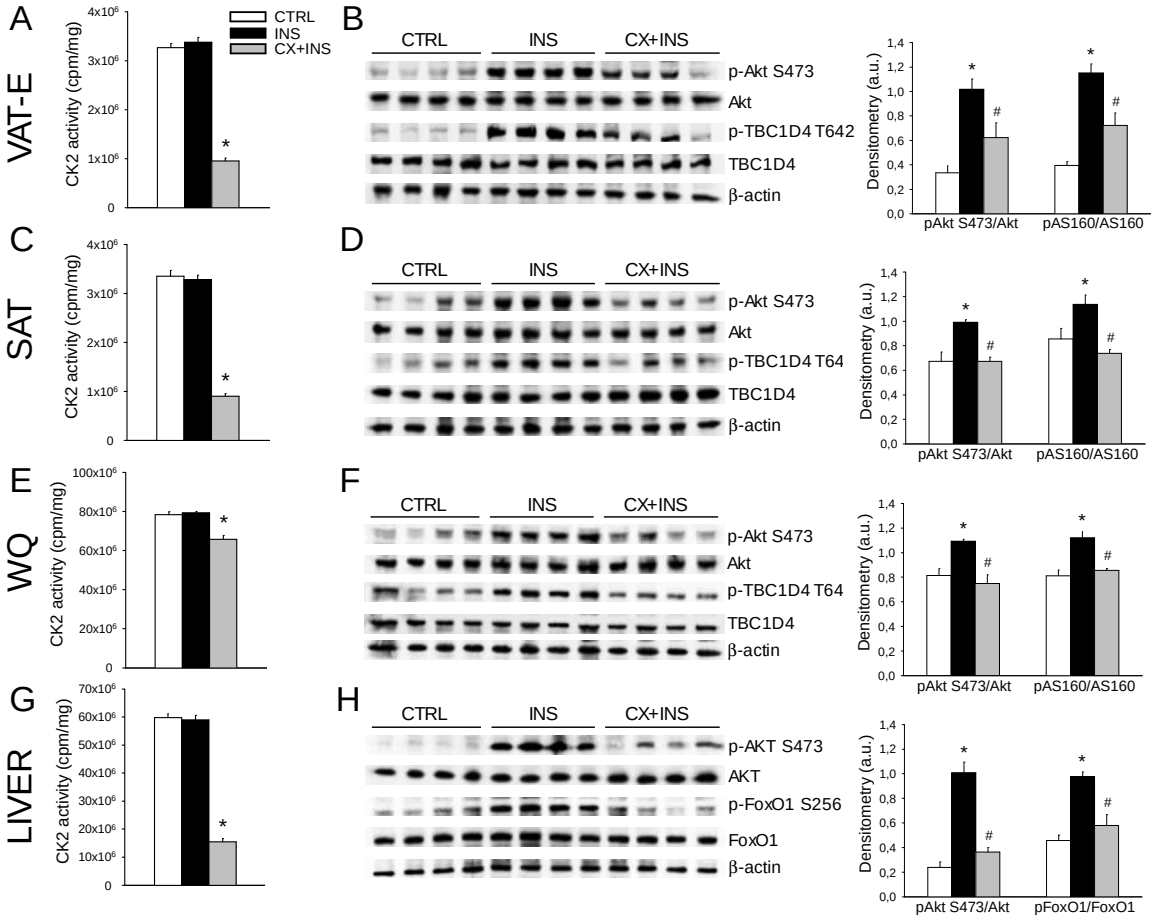

Figure 18. C57BL6/6J (B6) male mice of 22 weeks of age were untreated (CTRL, n=4), ip injected with insulin (INS, n=4) or pretreated with CX-4945 (20 mg/kg in NaCl 0.9%, ip) 2 hour before being stimulated with insulin (CX+INS, n=4). Thirty min after insulin-injection mice were sacrificed and the following tissues were collected and lysed: visceral epididymal, VAT-E, (**A, B**) and subcutaneous, SAT, (**C, D**) adipose tissues, white quadriceps, WQ, (**E, F**) and liver (**G,H**). In **A, C, E** and **G**, CK2 activity was assayed in tissue extracts and expressed as cpm of 33Pi transferred to the substrate/mg proteins. In **B, D, F** and **H,** tissue lysates were analyzed by Wb using 40 µg (VAT-E, SAT), 8 µg (WQ) and 10 µg (liver) of proteins (left panels). Immunostained bands were quantified by densitometry and right panels reported the mean values ± SEM relative to the phosphorylation extent of Akt S473, AS160 (TBC1D4) T642 and FoxO1 S253. Results are presented as mean ± SEM; *p<0.05 vs controls (CTRL); #p<0.05 vs insulin-injected mice (INS).

CK2 is up-regulated in VAT-E and SAT of obese and obese/diabetic mice.

Given the pivotal role of CK2 in insulin signaling of the main insulin target-tissues, the kinase was analyzed in mouse models of obesity (ob/ob) and obesity associated with hyperglycemia (db/db). CK2α and β subunit protein-level and CK2 activity were examined in AT depots, WQ and liver (Fig. 19). In the ob?/+ and db/+ genetic control mouse tissues, CK2 activity was similar to that found in wild type mice (Fig. 19 and 17C). Notably, higher CK2 protein-level and activity were observed in WAT depots (VAT-E and SAT) of ob/ob

and db/db mice compared to relative controls, while the kinase was unchanged in BAT, skeletal muscle and liver. The finding that CK2 up-regulation was similar in mice characterized by obesity or obesity associated with increased blood glucose and insulin, mimicking type 2 diabetes features, suggests that AT expansion could be the main determinant for CK2 alterations that probably mirror an AT intrinsic dysfunction.

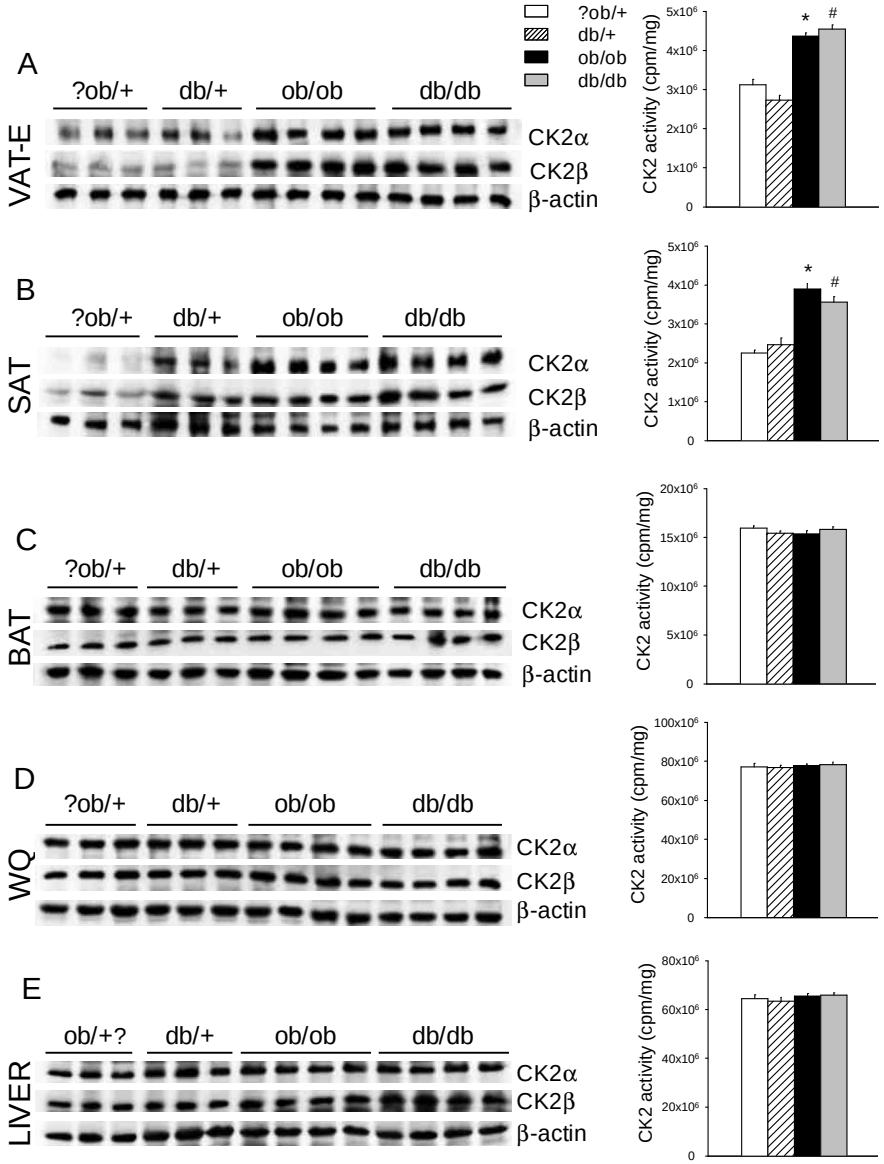

Figure 19. B6.V-LEP OB/J (ob/ob) and B6.V-LEP OB/J +/? (?ob/+) control male mice (13 weeks) and BKS.CG-M+/+ LEPRDB/J (db/db) and BKS.CG-M DB/+ (db/+) control male mice (14 weeks) were sacrificed to collect VAT-E (**A**), SAT (**B**) and BAT (**C**), WQ (**D**) and liver (**E**). CK2α and CK2β protein amount (left panels) were analyzed by Wb using 40 µg (**A,B**), 20 µg (**C**), 8 µg (**D**) and 10 µg (**E**) of tissue extracts. CK2 kinase activity was also detected (right panels) (n=5 per group). *p<0.05 vs ?ob/+; #p<0.05 vs db/+. Results are presented as mean ± SEM.

CK2 during adipose tissue remodeling: normal weight, obesity/diabetes and weight loss

CK2 relevance was then evaluated in human obesity and AT remodeling. 27 obese (OB) and obese/diabetic (OB/T2D) patients were enrolled, who underwent bariatric surgery (Table 2), and their abdominal VAT and SAT were compared with those of 11 normal-weight non-diabetic controls (CTRL). An up-regulation of CK2

protein-level and activity, greater than those found in mouse models, was observed in both VAT (Fig. 20 A-C) and SAT (Fig. 20 D-H) from obese patients. Furthermore, CK2 hyper-activation resulted similar in OB/T2D and in OB subjects. Importantly we analyzed VAT and SAT biopsies of 3 OB patients (3406, 2370, 2377), who underwent an abdominal surgery after substantial weight loss (WL) obtained by bariatric surgery (OB/WL). Notably, these patients showed CK2 expression and activity in both WAT depots comparable to those of normal-weight controls. This observation was confirmed in other 9 SAT biopsies of obese patients, who underwent plastic surgery after relevant weight loss due to bariatric surgery or diet intervention (OB/WLps) (Fig. 20F, G, H). CK2 activity was similar in SAT controls obtained from abdominal (CTRL) or plastic (CTRL/ps) surgery, excluding any bias due to different surgery approach (Fig. 20H). CK2 activity was assayed in VAT extracts from 4 CTRL, 4 OB, 4 OB/T2D, 4 OB/WL and in SAT extracts from 4 CTRL, 3 CTRL/ps, 6 OB, 4 OB/T2D, 5 OB/WL, 10 OB/WLps.

These data prove that CK2 undergoes an anomalous activation in human obesity, independently from the presence of T2DM, and its expression and function completely normalize after AT size reduction and remodeling.

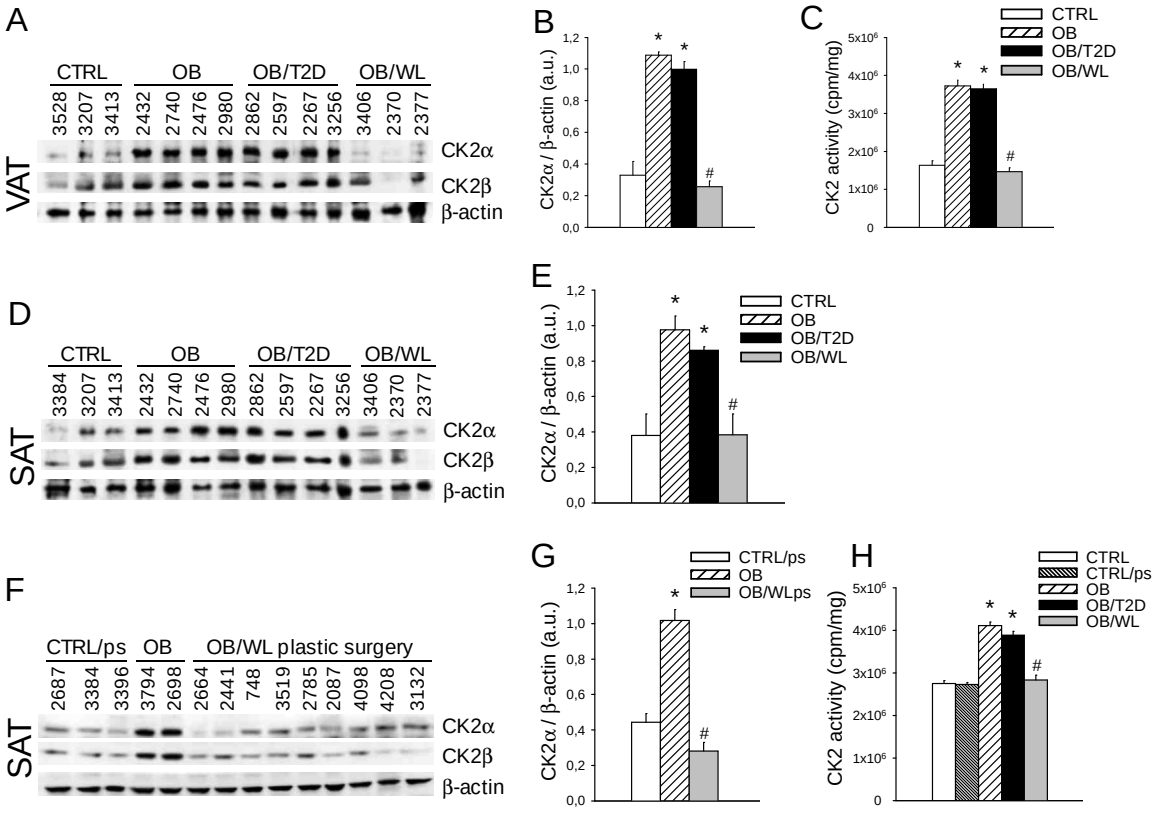

Figure 20. VAT (**A-C**) and SAT (**D-H**) specimens were obtained from normal-weight (CTRL), obese (OB), obese/diabetic (OB/T2D) and obese patients that, after relevant weight loss, underwent abdominal surgery (OB/WL) or plastic surgery (OB/WLps), indicated by the ID number. Tissue extracts (40 μg) were analyzed by Wb (**A,D,F**) and CK2α amount was quantified by densitometry (**B, E, G**). CK2 activity was measured and expressed in cpm/mg of protein extracts (**C**, **H**). Results are presented as mean ± SEM; *p<0.05 vs CTRL or CTRLps; #p<0.05 vs OB and OB/T2D.

CK2 in human obesity and type 2 diabetes: role of glycemic profile and insulin resistance

To further understand if CK2 dysregulation is merely linked to AT expansion or could be influenced also by insulin resistance or overt T2D, we analyzed SAT and VAT from normoglycemic (OB), prediabetic (OB/preT2D) and diabetic (OB/T2D Met) obese patients with different degree of IR, estimated by HOMA index (Table 2). To avoid the potential confounding effect of insulin treatment on CK2, only metformin treated patients were included in OB/T2D Met group. We quantified CK2 protein-level as well as Akt S473 phosphorylation as a marker of peripheral insulin sensitivity in VAT (Fig. 21 A-D) and SAT (Fig. 21 F-I) of patients. By loading the same reference samples in different gels, we could compare several human specimens (Fig. 21). CK2 activity was also evaluated in all samples (Fig. 21 E,L). Up-regulation of CK2 protein-level and activity in VAT and SAT was similar, independently of glycemic status or HOMA index. In VAT Akt protein-level and phosphorylation were substantially higher in obese patients with low insulin resistance (OB/H low) than in control subjects (CTRL) and obese patients with a high HOMA (OB/H high) (Fig. 21 A, D). Moreover, OB/T2D Met patients exhibited a very low level of VAT Akt phosphorylation compared to other subgroups (Fig. 21D).

These data demonstrate that AT CK2 hyper-activation is a peculiar hallmark of obesity and is not influenced by IR or type 2 diabetes presence.

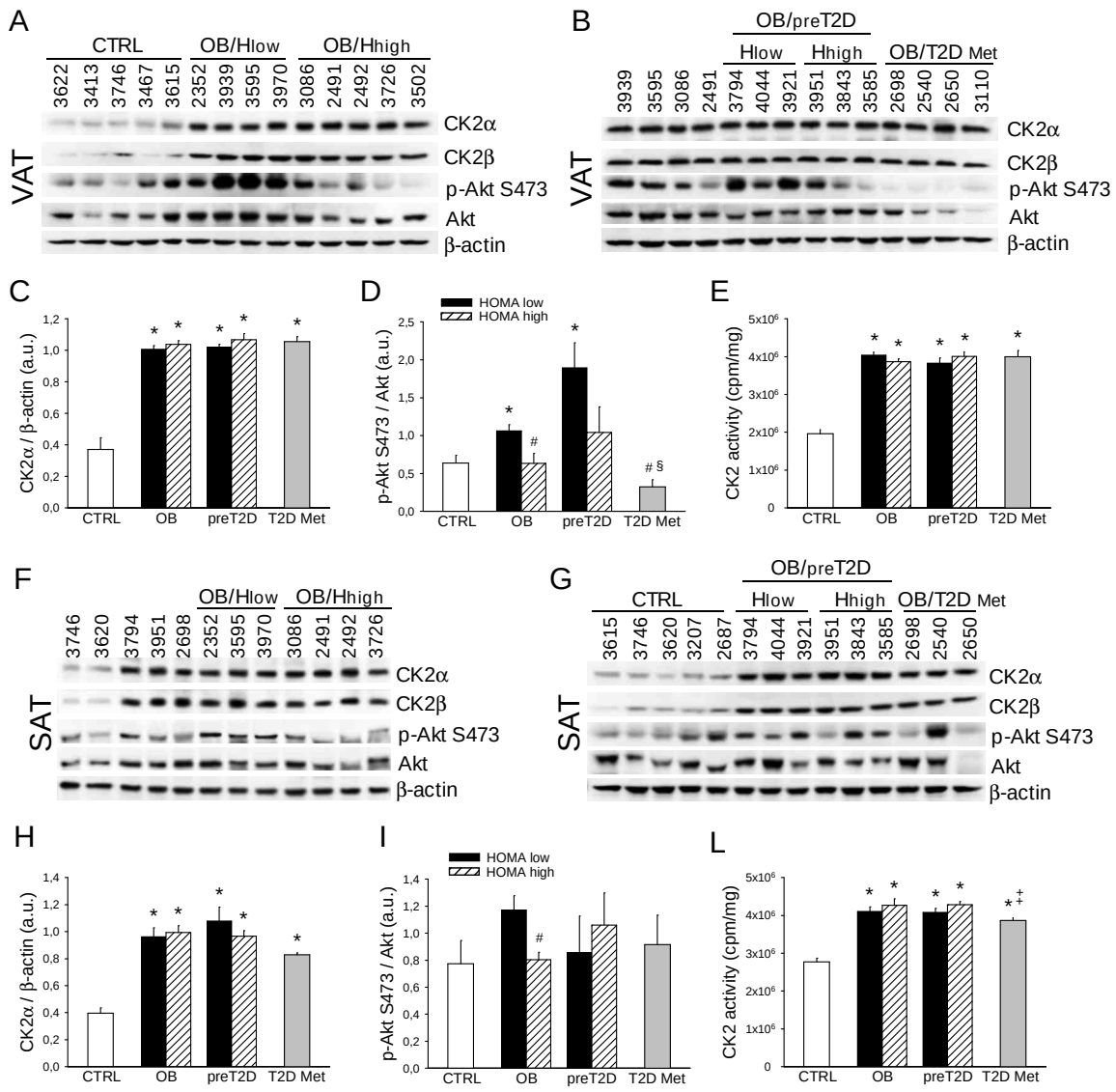

Figure 21. VAT (**A-E**) and SAT (**F-L**) specimens were obtained from normal weight (CTRL), obese (OB) and obese pre-diabetic (OB/preT2D) patients characterized by different HOMA index (H low and H high, see Table 2) and from Metformin-treated obese/diabetic patients (OB/T2D Met), indicated by the ID number. To compare several specimens, tissue extracts 3939, 3595, 3086 and 2491 were analyzed in both panels **A** and **B**, while extracts 3746, 3620, 3794, 3951 and 2698 were analyzed in panels **F** and **G**. Tissue extracts (40 µg) were analyzed by Wb (**A, B, F, G**) and CK2α amount and Akt S473 phosphorylation extent were quantified by densitometry (**C**, **D, H, I**). CK2 activity was assayed in VAT extracts (**E**) of 7 CTRL, 5 OB/H low, 5 OB/H high, 3 OB/preT2D H low, 4 OB/preT2D H high, 4 OB/T2D Met and in SAT extracts (**L**) of 8 CTRL, 4 OB/H low, 5 OB/H high, 3 OB/preT2D H low, 4 OB/preT2D H high, 5 OB/T2D Met.*p<0.05 vs CTRL; #p<0.05 vs OB/H low; § p<0.05 vs OB/preT2D/H low; ‡ p<0.05 vs OB/H high and OB/preT2D/H high. Results are presented as mean ± SEM.

CK2 overexpression is a hallmark also of lipomatous tissue

We then analyze LT from MSL patients to further explore the role of CK2 in AT expansion and to unravel a possible pathogenetic pathway for this rare disease. As demonstrated in human obesity, CK2 expression resulted upregulated in all LT specimens in comparison to healthy SAT of the same patient (Fig. 22A), as

well its activity as shown in Figure 22B. This overexpression resulted independent from the anatomical localization of lipomas.

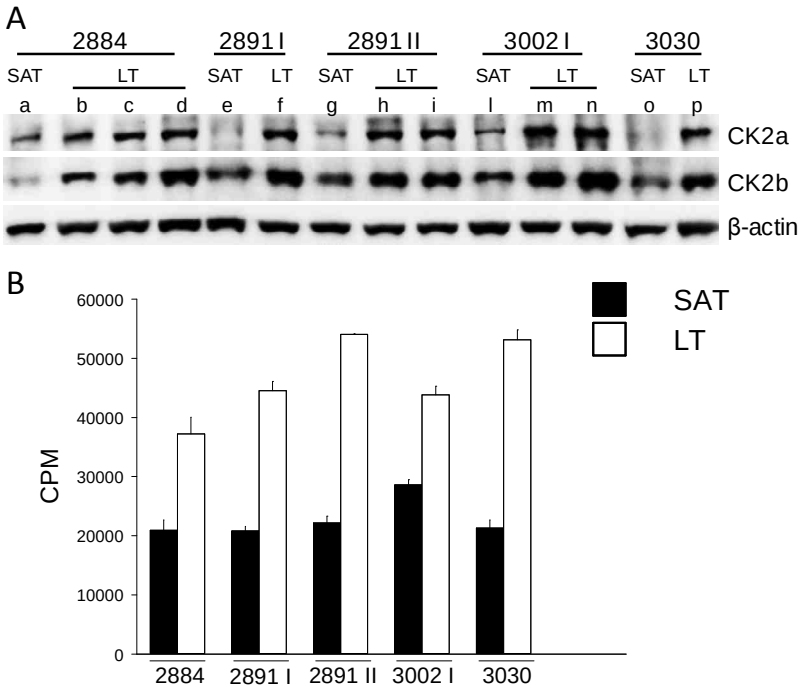

Figure 22. **A**. Tissue extracts (40 µg) from LT and SAT were analyzed by Western blot with the indicated antibodies; β-actin represents the loading control (**A**). In **B**, CK2 activity was assayed in SAT (black bars) and LT (white bars) extracts of the indicated patients and expressed as cpm of 33Pi transferred to the substrate/mg proteins. 2884, 2891 I, 2891 II, 3002 I, 3030 represent the patient ID numbers; letters refer to the specific anatomical localization of samples (see also Table 1 in Material and Methods): b, c, d: respectively samples from neck, left and right cervical LT of 2884; f: neck of 2891 I; h, i: respectively neck and cervical LT of 2891 II; m, n: respectively arm and neck LT of 3002 I; p: arm LT of 3030.

In patient 2891 during the second surgery (2891 II), it was possible to analyze CK2 protein expression not only in the whole tissue but also in freshly isolated LT and SAT-derived SVF, due to sample availability. Interestingly, as shown in Figure 23, CK2 expression seemed more expressed in SVF than in whole tissue in normal SAT. Moreover, CK2 amount resulted slightly higher in SVF from LT (neck/cervical) than in SAT-derived precursor cells, although the differences were mostly evident in tissues. These data suggest that in healthy SAT CK2 could be downregulated in mature adipocytes, a finding supported also by previous works [178], while LT could maintain a high expression of the kinase in both precursors and mature adipocytes. Importantly, CK2 expression resulted unaltered in LT from one intervention and the following surgery.

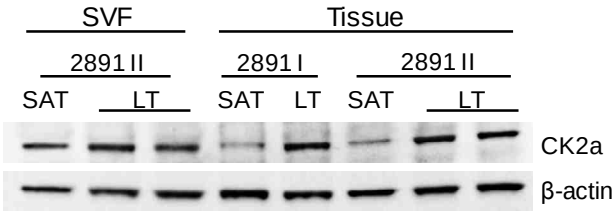

Figure 23. Protein extracts (40 µg) from freshly isolated stromal vascular fraction (SVF) and from lipomatous tissue (LT) and subcutaneous adipose tissue (SAT) were analyzed by Wb with anti-CK2α in patient 2891 I and II surgery; two LT samples, harvested from neck and cervical region of 2891 II, were analyzed. β-actin represents the loading control.

DISCUSSION

Our multidisciplinary Center for the Study and the Integrated Treatment of Obesity (Ce.S.I.T.O.) manages patients affected by obesity by diet/behavioral intervention, medical therapy or bariatric surgery thanks to the different professionals (clinicians, nutritionists, surgeons, psychologists) that have formed a network of collaboration at the clinical and research level. Moreover, our Endocrine-Metabolic Laboratory have acquired important skills in adipose tissue (AT) biology, allowing the realization of translational research projects, also in collaboration with other Laboratories, such as Donella-Deana's group (Department of Biomedical Sciences – University of Padova), in the field of obesity and metabolic diseases. Recently, given our interest on unraveling the mechanisms and the consequences of AT expansion, we have also broadened our scientific focus on other adipose tissue disorders such as Multiple Symmetric Lipomatosis (MSL).

The first part of the present work provides an extensive characterization of lipomatous tissue (LT) of patients affected by MSL. Since it is a rare disease, we were able to enroll five patients, that are all affected by type 1 MSL, whereas patients with type 2 MSL were, at the moment, excluded from the Study to guarantee phenotype homogeneity. Conversely, many previous works, that have conducted evaluations on LT and not only clinical studies on patients, have analyzed single case reports [66], a lower number of patients [179, 227] or have enrolled subjects affected by both type 1 and 2 MSL [49, 51]. Moreover, according to the type and site of lipectomy, our study analyzed LT samples from multiple anatomical sites (neck, cervical region, upper arm), allowing to unravel possible differences related to lipoma localization. Importantly, healthy SAT was harvested from the same MSL patients and during the lipectomy surgery, reducing data variability, whereas in other studies LT was often compared with AT from unrelated matched healthy subjects [68]. Besides of comparing LT with a white AT, another important key factor of this study was also the possibility to compare the pathological tissue with a human brown/beige AT, represented by AT from a patient affected by Pheocromocytoma, being able to set a reliable positive control for brown markers, especially for UCP1.

The main hypothesis about MSL origin states that LT arises from brown adipose precursor cells presenting a defective differentiation. The fundamental data supporting this notion are the similar localization of lipomas with BAT deposits and the expression of UCP1, the most specific marker for brown adipocytes, by lipomatous tissue [5, 50, 67]. Histological and immunohistochemical observation reported in our study reveals that LT appears as a normal, white AT, containing mature, unilocular adipocytes. Importantly, all LT samples do not express UCP1 protein as demonstrated by IHC (Fig. 1B), confirming the white features of LT. Other studies performed histological analysis of LT, reporting similar observation [31, 63], but, at our knowledge, no data are available about UCP1 protein expression in MSL. In agreement with morphology, LT gene expression analysis showed a profile comparable to SAT, presenting similar level of *PPARG2* and *LEPTIN* mRNA (Fig. 3). Recent data have investigated the transcription profile of LT [62, 68], failing to

provide definitive demonstration about the “color”, white or brown, of MSL tissue. Our data show that, as well as SAT, LT and its derived SVF express negligible level of UCP1, concordantly with gene expression analysis performed by Chen and colleagues [68], that did not demonstrate any differences in UCP1 expression between LT and SAT. On the contrary, other studies have shown that LT expresses higher level of UCP1 mRNA in comparison with SAT [51, 62], but differences in experimental settings could explain the contrasting results. In fact, these studies lack of a reliable positive control of human BAT or performed gene expression analysis after several culture passages, that profoundly modify the transcriptomic profile of cells. It is worth noting that both IHC and gene expression of UCP1 have confirmed the brown nature of perirenal AT from Pheo and the brown commitment of its precursor cells, justifying its use as positive control in our experimental settings.

Recently a third type of adipocyte has been described along with white and brown fat cells: since it can acquire a brown like phenotype and thermogenic properties upon appropriate stimuli (cold exposure, adrenergic activation) in the context of white adipose tissue, it was called beige to underline the halfway characteristics between white and brown features [84]. Therefore, in addition to brown specific markers, we also evaluated if LT might express some “beige” factors, that, at our knowledge have been poorly investigated. The analysis of the markers *ZIC1*, *EVA1* and *CIDEA* showed a similar expression of LT in comparison with SAT (Fig. 3), reinforcing the idea that LT presents a gene signature similar to white SAT. LT-derived SVF also presented similar level of the three markers in comparison with SAT precursor cells, while in preadipocytes from the perirenal AT of Pheo, *EVA1* and *CIDEA* resulted higher than both LT and SAT (Fig. 4). Although not evident in whole tissue, gene analysis in freshly isolated SFV, that were not modified by culture conditions, strongly suggest that LT resulted more similar to SAT than Pheo. Moreover, our data showed a lower expression of *CD137*, a recognized marker of beige precursor cells [85], in LT-derived ASCs in comparison with SAT, suggesting that LT does not seem enriched of beige precursors. Interestingly, even Pheo-derived preadipocytes express lower level of CD137 in comparison with SAT derived SVF. Although adipose specific markers to distinguish brown, beige and white adipocytes are still a matter of debates, EVA1 is considered a specific brown marker, not expressed by beige adipocytes, CIDEA is shared by brown/beige and not expressed by white cells, while CD137 characterizes beige precursors. On the basis of this classification, our findings suggest that LT, does not express brown markers, as well as SAT, and, differently from SAT, LT precursor cells present a lower commitment towards beige lineage. Moreover, perirenal AT from Pheocromocytoma, that has been previously described as a beige tissue [98], seems by contrast more similar to a brown tissue. The other marker evaluated in the present study was *ELOVL3* and we found a higher expression in both whole LT and in lipomatous SVF, although in the latter only a trend could be described, not reaching the statistical difference. This gene encodes for an elongase responsible for the elongation of very long chain (C18-C24) saturated and monounsaturated fatty acids and it is usually associated with BAT biology, being early upregulated by adrenergic stimulation, by cold exposure [101, 228]

or PPARγ agonists [228, 229]. Studies in 3T3L1 adipocytes demonstrated that ELOVL3 has also an important function in white AT: preadipocytes upregulate its expression during adipogenic differentiation in a PPARγ-depedent pathway and, in turn, C18:1 and C20:1 very long chain fatty acids (VLCFAs) synthesized by ELOVL3 promote *PPARG* expression [230]. Further studies in vitamin D nuclear receptor (VDR) knockout mice demonstrated that *Elovl3* is regulated through VDR in WAT, especially in SAT, confirming the important role of this factor in white AT lipid metabolism [231]. In this view, the in-depth analysis of lipidomic and, in general, metabolomic profile of LT is certainly a field of interest for future research.

Moreover, our findings suggest that in humans the distinction among white, brown and beige entities by gene expression of molecular markers is far to be completely clarified.

Although mainly qualitative evaluations are available [50, 62, 65], LT is described as a pretty high vascularized tissue in comparison with a normal AT. The gene expression analysis, performed in our study, might support this observation, as LT-derived SVF present a higher *VEGFA* expression, even if data were not statistically significant due to the high variability among patients (Fig. 5). Quantitative evaluation of lipomas microvasculature, such as capillary density, could be an aspect for future research.

Previous data suggest that lipomatous adipocytes arise from brown precursors that fail to normally differentiate and to upregulate UCP1, probably due to a defect of adrenergic pathway proximal to cAMP formation but distal to β-receptors [49, 51]. We also evaluate the *in vitro* differentiation and the browning potential of ASCs in LT and SAT, treating *in vitro* differentiated adipocytes with Forskolin, that directly acts on adenyl cyclase to produce cAMP (Fig. 10). Similarly to the SAT-derived adipocytes, lipomatous fat cells upregulated PPARG2 and LEPTIN gene expression during adipogenesis. Regarding browning potential, it was demonstrated that theophylline [49], that increases cAMP inhibiting phosphodiesterase (PDE), restores the capacity of lipomatous cells to upregulate UCP1. Conversely, in our experimental setting, Forskolin failed to significantly prompt UCP1 expression in LT derived cultures. Importantly, we clearly demonstrated that LT upregulates protein kinase CK2 expression and activity (Fig. 22). Taken these data together, it could be hypothesized that, since AKT/PKB activates PDE, the higher activity of CK2 in lipomatous cells leads to an upregulation of phosphodiesterase activity and thus a higher cAMP degradation, explaining, in the same time, why theophylline, and not Forskolin, is able to induce browning in cell cultures. Nisoli's group have found that the chronic *in vitro* restoring of nitric oxide (NO) pathway in lipomatous cell cultures was able to restore their capacity to upregulate UCP1 in comparison with normal white adipocytes [51]. However, our experimental settings were quite different, evaluating the browning potential at the end of *in vitro* adipogenic differentiation with acute stimulation with Forskolin.

Existing literature does not provide definitive answers about how LT forms and grows in MSL. Many data of the present work reinforce the hypothesis that LT preferentially expands by hyperplasia. First, adipocyte morphometry shows that LT cells are slightly smaller than in SAT (Fig. 2) and the high variability in cell size suggest a recruitment and differentiation of new cells during LT expansion. Second, LT resulted enriched of

CD45-CD31-CD34+ cells, named adipose stem cells (ASCs), as demonstrated by *ex vivo* FACS analysis (Fig. 6). Importantly, flow cytometry performed immediately on freshly isolated SVFs avoids interferences due to plastic adherence and culture conditions, that are known to profoundly modify cell surface marker expression. This technical aspect increases the strength of our results and could explain some differences with previous reports where ASCs were analyzed after passages in culture [62]. Analyzing ASCs in the immunological gate CD45-CD31-CD34+ to identify "qualitative" differences between LT and SAT, they appeared quite similar in surface markers expression of CD90, CD73 and CD271 (Fig. 7). However, in neck/cervical LT-derived ASCs, CD90 and CD271 were expressed by respectively a higher and a lower percentage in comparison with SAT-derived precursors, although not reaching the statistical significance. These data suggest that lipomas in different localizations could display peculiar characteristics: for example, the anatomical site could provide a specific environment and paracrine signals for lipomatous cells that modulate their features. The timing of surgery could also represent an important factor that determine LT characteristics: lipomas could be at different stage of development or previous surgeries on the same site could induce pro-inflammatory, pro-fibrotic and pro-angiogenetic factors that influence the natural history of LT and its precursor cells. LT-derived ASCs have been shown also to have a shorter doubling time, as demonstrated with two different methods and in different LT depots (Fig. 8). The difference found in the calculated doubling time by the ATP and DNA-based methods could be ascribed to the influence by the metabolic state of lipomatous cells. Moreover, in agreement with Tremp and coworkers [227], LT-derived precursor cells displayed a higher clonogenic potential which in our study was assessed by the limiting dilution analysis, an elegant technique to evaluate the frequency of stem cells. Interestingly, together with this proliferative tendency, LT-derived SVF are characterized by a greater adipogenic differentiation in comparison with the corresponding SAT-SVF, as shown by the analysis of adipogenis differentiation obtained in subsequent subcultures (Fig. 9) and confirmed also at a clonal level (Fig. 11D). Proliferation seems strictly coupled with differentiation, that from one side, allows mature adipocyte generation and, from the other, is protective from an uncontrolled growth, as in cancer. Importantly, LT proliferative advantage is compensated by high differentiative potential, concordantly with the relative benign behavior of the disease, where pathological tissue has only a local, "benign" expansion.

In MSL, CK2 protein upregulation was clearly demonstrated in all LT depots, independently from lipomas localization (Fig. 22A). As expected from its constitutive active function, CK2 activity resulted similarly upregulated in all LT specimens in comparison with SAT (Fig. 22B). Our preliminary data showed an overexpression also in freshly isolated SVF from LT, in comparison with SAT-derived SVF, suggesting a possible mechanism for the higher ASCs number and proliferation in MSL (Fig. 23). In LT derived ASCs, overexpressed CK2 might promote insulin signaling in its pro-survival and growth action, while it may give a metabolic advantage in differentiating preadipocytes sustaining their adipogenic potential. This is also supported by very recent observation about CK2 role in adipogenic differentiation. In fact, as discussed in

the Introduction, CK2 seems involved in the clonal expansion stage of the adipogenic process [178, 179], favoring proliferation and contemporarily differentiation of adipose precursor cells. The upregulation of a component of insulin pathway is also concordant with the findings of Guertin's group about the effect of knocking out PTEN in mice. The lack of PTEN, like the overexpression of CK2, results in the activation of insulin signaling, inducing a MSL-like growth of AT in the $PTEN^{-/-}$ mouse[61].

Conflicting data have been reported on the insulin effect on CK2 protein-level and activity in human skeletal muscle, rat liver and cell cultures [148, 163, 175, 232-234]. Our results demonstrate that CK2 amount and activity are unaffected by insulin-treatment in adipocytes (Fig. 12A,B) and in mouse insulin-target tissues after *in vivo* insulin injection (Fig. 18). More importantly, we show that CK2 is required for insulin-induced glucose-uptake, regulating the hormone-signaling at different levels in both murine and human adipocytes (Figs. 13-16). In fact, CK2-inhibitors strongly counteract Akt1/2 activation directly by reducing the phosphorylation extent of Akt1 Ser129 and indirectly by activating PTEN, the main negative regulator of Akt activation. Down-regulation of Akt1/2 activity is associated with strong impairment of the following events: phosphorylation of the Akt-target TBC1D4 (As160), GLUT4-translocation to cell surface and insulin-induced glucose-uptake.

In vivo analysis in insulin-stimulated mice demonstrates that an acute pre-treatment with the CK2-inhibitor CX-4945 is sufficient to strongly counteract the activation of tissue-specific insulin-signaling. Importantly, our results suggest that CK2-inhibition might decrease glucose-uptake in VAT-E, SAT and skeletal muscle and activates gluconeogenesis in liver (Fig. 18).

Since insulin signaling is also a known growth regulator of AT, we decided to explore CK2 in an expanding AT represented by SAT and VAT of mouse models of obesity and diabetes. CK2 analysis showed that both amount and activity of CK2 are substantially higher in WAT (VAT-E and SAT) of ob/ob and db/db mice than of controls, while they are similar in BAT, muscle and liver (Fig. 19). Present results are consistent with a recent report showing that CK2 pathway is preferentially activated in WAT in response to β3 agonist and to high-fat diet (HFD) [180]. These authors also showed that CK2-inhibition by CX-4945-treatment for 40 days protects mice from diet-induced obesity and moderately improves insulin-sensitivity by promoting UCP1 dependent thermogenesis. It has been also demonstrated that prolonged CK2-blockage by CX-4945 reduces the diet-associated hyperglycemia and glucose intolerance in HFD mice [173].

CK2 relevance in obesity was further supported by data obtained in obese patients. We found that VAT and SAT from obese subjects exhibit a strong CK2 up-regulation, independently from the concomitant presence of type 2 diabetes (Figs. 20, 21). We also studied the potential link between CK2 and insulin resistance (IR) by analyzing WAT of obese patients with different HOMA index and glycemic profile (prediabetes and diabetes). It is widely accepted that the early, dynamic phase of obesity is indeed characterized by healthy AT expansion. When adipocytes reach a critical size and macrophages infiltrate AT causing local inflammation and changes in adipokines production, fat tissue fails to adequately respond to insulin. In

parallel, the free fatty acid release increases and contributes to peripheral lipotoxicity inducing IR and favoring diabetes development [235]. Our results demonstrate that WAT CK2 amount and activity observed in the different groups of BMI-matched obese patients are higher than in normal-weight controls, independently of the degree of IR estimated by HOMA index, the early alterations in glycemic profile characterizing a prediabetic condition, the presence of overt T2D or the level of WAT insulin-sensitivity evidenced by Akt1/2 phosphorylation extent (Fig. 21). Constitutive activation of VAT Akt1/2-signaling is indeed present in fasting obese and obese/prediabetic patients with low HOMA index, suggesting that AT preserves its insulin-sensitivity despite the initial alterations in glucose homeostasis in prediabetic subjects. At variance, Akt1/2 phosphorylation is low in obese patients with high HOMA index and almost absent in diabetic patients (Fig. 21).

CK2 up-regulation in WAT of obese patients seems tightly linked to AT growth rather than to IR severity or T2D development. During the early phases of AT expansion, CK2 overexpression might represent an attempt to increase the storage capacity of white adipocytes, maintaining an efficient insulin action for cell growth, high glucose-uptake and lipid synthesis. Nevertheless, if chronic calorie excess persists, this putative regulatory mechanism mediated by CK2, is probably overcome and systemic IR and T2 diabetes could develop despite CK2 upregulation. It is worth noting that, contrarily to acute action, chronic hyperactivation of insulin signaling could lead itself to insulin resistance: for instance, it was demonstrated that chronic insulin stimulation causes GLUT4 depletion by accelerated lysosomal degradation of the transporter [121, 122]. It could not be excluded that in the later stage of obesity CK2 overexpression negatively affects insulin pathway. Moreover, increasing data highlight the presence of AKT-independent pathway of IR [236], that could explain the apparent lack of association between CK2 and glucose impairment of obese patients.

The hypothesis that CK2 up-regulation might be considered as an AT intrinsic dysfunction occurring during obesity is also supported by the finding that CK2 amount and activity revert to normal levels in WAT of obese patients after a relevant weight loss (Fig. 20). CK2 normalization is evident in all patients regardless the type of weight-loss intervention, the presence of metabolic complications and the achievement of normal BMI, demonstrating that fat mass reduction and related AT functional remodeling are associated with a normal CK2 activity. Moreover, the demonstration of CK2 upregulation also in expanding LT of MSL strengthen the hypothesis that CK2 is related to AT growth and structural remodeling rather than its metabolic function.

These data suggest that a proper CK2 down-regulation might be considered an additional tool to counteract human obesity and, for MSL, the unique medical therapy to prevent lipoma expansion and relapse, avoiding recurrent surgery. In addition, the CK2-inhibitor CX-4945, currently used in oncological clinical trials (NCT02128282), could be regarded as an emerging drug targeting AT. In obesity, this therapeutic strategy is also supported by the outcome that CX-4945-treatment reduces the diet-induced obesity in mice

by promoting whole-body energy expenditure [180] and that CK2 is involved in pathways implicated also in adiposopathy as HIF1-driven angiogenesis [218] and NF-kB-mediated inflammation [237]. As for MSL, this work provides the first demonstration of a possible, druggable therapeutic target.

Another important aspect to be considered about the role of CK2 in MSL and obesity is the link with cancer. Some authors described morphological atypies in MSL that suggest a neoplastic nature of the disease [63] and, since it is a overgrowth disorder, it is sometimes considered a benign tumor. On the other hand, CK2 is traditionally a matter of research for oncology, since it acts with a mechanism known as non-oncogene addiction [149, 213, 214]. Finally, also obesity has frequently compared in some features with cancer [238]. Our observation that WAT and LT upregulate CK2 could be considered a similarity with tumor cells. However, both in MSL and in obesity, the contro-regulatory mechanisms (i.e. anti-proliferative), that in cancer are disrupted, are maintained, allowing exclusively the actions of necessary signals for a “controlled” expansion.

In conclusion our data show that LT resembles a normal white AT from a histological and molecular point of view and it seems to grow mainly by hyperplasia, probably sustained by CK2 upregulation. In the meantime, proliferation is accompanied by a higher differentiation potential of lipomatous ASCs that might be an explanation for the benign behavior of MSL. Moreover, our data unveil a new role for CK2 in promoting AT insulin-signaling and influencing glucose homeostasis. We also identified CK2 up-regulation as a hallmark of expanding adipose tissue, both in human obesity and in Multiple Symmetric Lipomatosis, opening a new therapeutic option for common and rare AT disorders.

BIBLIOGRAPHY

1. Brodie, B., *Lectures illustrative of various subjects in pathology and surgery.* Longman: London, 1846: p. 275-276.
2. Madelung, O., *Uber den fetthals (diffuses lipom des halses). .* Archiv Fur Klinische Chirurgie, 1888: p. 106-130.
3. Launois, P. and R. Bensaude, *De l'adeno-lipomatose symmetrique.* Bull Mem Soc Med Hop 1989: p. 1:289.
4. Enzi, G., *Multiple symmetric lipomatosis: an updated clinical report.* Medicine (Baltimore), 1984. **63**(1): p. 56-64.
5. Enzi, G., et al., *Multiple symmetric lipomatosis: a rare disease and its possible links to brown adipose tissue.* Nutr Metab Cardiovasc Dis, 2015. **25**(4): p. 347-53.
6. Gonzalez-Garcia, R., et al., *Benign symmetric lipomatosis (Madelung's disease): case reports and current management.* Aesthetic Plast Surg, 2004. **28**(2): p. 108-12; discussion 113.
7. Busetto, L., et al., *Differential clinical expression of multiple symmetric lipomatosis in men and women.* Int J Obes Relat Metab Disord, 2003. **27**(11): p. 1419-22.
8. Castro-Gago, M., et al., *[Multiple symmetric lipomatosis associated to polyneuropathology, atrophy of the cerebellum and mitochondrial cytopathy].* Rev Neurol, 2003. **36**(11): p. 1026-9.
9. Kratz, C., et al., *Multiple symmetric lipomatosis: an unusual cause of childhood obesity and mental retardation.* Eur J Paediatr Neurol, 2000. **4**(2): p. 63-7.
10. Shetty, C., et al., *Multiple symmetric lipomatosis (MSL) of neck in a child (Madelung's disease): report of a rare presentation.* Dentomaxillofac Radiol, 2007. **36**(1): p. 51-4.
11. Brea-Garcia, B., et al., *Madelung's disease: comorbidities, fatty mass distribution, and response to treatment of 22 patients.* Aesthetic Plast Surg, 2013. **37**(2): p. 409-16.
12. Enzi, G., et al., *Multiple symmetric lipomatosis: clinical aspects and outcome in a long-term longitudinal study.* Int J Obes Relat Metab Disord, 2002. **26**(2): p. 253-61.
13. Laure, B., et al., *Launois-Bensaude syndrome involving the orbits.* J Craniomaxillofac Surg, 2011. **39**(1): p. 21-3.
14. Lopez-Ceres, A., et al., *Benign symmetric lipomatosis of the tongue in Madelung's disease.* J Craniomaxillofac Surg, 2006. **34**(8): p. 489-93.
15. Vargas-Diez, E., et al., *Madelung's disease involving the tongue.* J Am Acad Dermatol, 2000. **42**(3): p. 511-3.
16. Poggi, G., et al., *Scrotal involvement in Madelung disease: clinical, ultrasound and MR findings.* Abdom Imaging, 2006. **31**(4): p. 503-5.
17. Borges, A., et al., *Laryngeal involvement in multiple symmetric lipomatosis: the role of computed tomography in diagnosis.* Am J Otolaryngol, 1997. **18**(2): p. 127-30.
18. Enzi, G., et al., *Computed tomography of deep fat masses in multiple symmetrical lipomatosis.* Radiology, 1982. **144**(1): p. 121-4.
19. Milisavljevic, D., et al., *Severe dyspnea as atypical presenting symptom of Madelung's disease.* Hippokratia, 2010. **14**(2): p. 133-5.
20. Gouriou, E.A., H.; Chevalier, R., *Un cas nouveau de lipomatose symmétrique associée à un double mal perforant plantaire.* Bull Mem Soc Hop Paris, **1937**: p. 39-53.
21. Vivaldo, J.C., *Paralisis general progresivo associada a una lipomatosis difusa simmetrica.* Prensa Med Argent, **1940**: p. 28-135.
22. Coin, A., et al., *Multiple symmetric lipomatosis: evidence for mitochondrial dysfunction.* J Clin Neuromuscul Dis, 2000. **1**(3): p. 124-30.
23. Enzi, G., et al., *Sensory, motor, and autonomic neuropathy in patients with multiple symmetric lipomatosis.* Medicine (Baltimore), 1985. **64**(6): p. 388-93.
24. Pollock, M., et al., *Neuropathy in multiple symmetric lipomatosis. Madelung's disease.* Brain, 1988. **111 (Pt 5)**: p. 1157-71.

25. Teplitsky, V., et al., *Multiple symmetric lipomatosis presenting with polyneuropathy.* Isr J Med Sci, 1995. **31**(11): p. 693-5.
26. Plummer, C., et al., *Multiple Symmetrical Lipomatosis--a mitochondrial disorder of brown fat.* Mitochondrion, 2013. **13**(4): p. 269-76.
27. Lopez-Blanco, R., et al., *Beyond cervical lipomas: myoclonus, gait disorder and multisystem involvement leading to mitochondrial disease.* BMJ Case Rep, 2017. **2017**.
28. Naumann, M., et al., *Neurological multisystem manifestation in multiple symmetric lipomatosis: a clinical and electrophysiological study.* Muscle Nerve, 1995. **18**(7): p. 693-8.
29. Fedele, D., et al., *Impairment of cardiovascular autonomic reflexes in multiple symmetric lipomatosis.* J Auton Nerv Syst, 1984. **11**(2): p. 181-8.
30. Fonseca, V.R., et al., *Cardiac noradrenergic denervation in a patient with multiple symmetric lipomatosis.* Cardiology, 2012. **121**(3): p. 160-3.
31. Chen, K., et al., *Multiple symmetric lipomatosis: substantial subcutaneous adipose tissue accumulation did not induce glucose and lipid metabolism dysfunction.* Ann Nutr Metab, 2010. **57**(1): p. 68-73.
32. Gu, W., et al., *The endocrine and metabolic evaluation of benign symmetrical lipomatosis: a case report and literature review.* Neuro Endocrinol Lett, 2010. **31**(4): p. 446-50.
33. Haap, M., et al., *Multiple symmetric lipomatosis: a paradigm of metabolically innocent obesity?* Diabetes Care, 2004. **27**(3): p. 794-5.
34. Enzi, G., et al., *Metabolic abnormalities in multiple symmetric lipomatosis: elevated lipoprotein lipase activity in adipose tissue with hyperalphalipoproteinemia.* J Lipid Res, 1983. **24**(5): p. 566-74.
35. Kim, M.K., et al., *Harmful and beneficial relationships between alcohol consumption and subclinical atherosclerosis.* Nutr Metab Cardiovasc Dis, 2014. **24**(7): p. 767-76.
36. Medina-Remon, A., et al., *Effects of total dietary polyphenols on plasma nitric oxide and blood pressure in a high cardiovascular risk cohort. The PREDIMED randomized trial.* Nutr Metab Cardiovasc Dis, 2015. **25**(1): p. 60-7.
37. Greene, M.L., et al., *Benign symmetric lipomatosis (Launois-Bensaude adenolipomatosis) with gout and hyperlipoproteinemia.* Am J Med, 1970. **48**(2): p. 239-46.
38. Coin, A., et al., *Total and regional body composition and energy expenditure in multiple symmetric lipomatosis.* Clin Nutr, 2005. **24**(3): p. 367-74.
39. Keskin, D., N. Ezirmik, and H. Celik, *Familial multiple lipomatosis.* Isr Med Assoc J, 2002. **4**(12): p. 1121-3.
40. Mc Kusik, V., *Mendelian inheritance in man.* John Hopkins University Press, 1978.
41. Chalk, C.H., et al., *Familial multiple symmetric lipomatosis with peripheral neuropathy.* Neurology, 1990. **40**(8): p. 1246-50.
42. Dal Cin, P., C. Turc-Carel, and A.A. Sandberg, *Consistent involvement of band 12q14 in two different translocations in three lipomas from the same patient.* Cancer Genet Cytogenet, 1988. **31**(2): p. 237-40.
43. Sreekantaiah, C. and A.A. Sandberg, *Clustering of aberrations to specific chromosome regions in benign neoplasms.* Int J Cancer, 1991. **48**(2): p. 194-8.
44. Heim, S., et al., *Different karyotypic features characterize different clinico-pathologic subgroups of benign lipogenic tumors.* Int J Cancer, 1988. **42**(6): p. 863-7.
45. Ligon, A.H., et al., *Constitutional rearrangement of the architectural factor HMGA2: a novel human phenotype including overgrowth and lipomas.* Am J Hum Genet, 2005. **76**(2): p. 340-8.
46. Cypess, A.M., et al., *Identification and importance of brown adipose tissue in adult humans.* N Engl J Med, 2009. **360**(15): p. 1509-17.
47. van Marken Lichtenbelt, W.D., et al., *Cold-activated brown adipose tissue in healthy men.* N Engl J Med, 2009. **360**(15): p. 1500-8.
48. Virtanen, K.A., et al., *Functional brown adipose tissue in healthy adults.* N Engl J Med, 2009. **360**(15): p. 1518-25.
49. Enzi, G., et al., *Multiple symmetric lipomatosis: a defect in adrenergic-stimulated lipolysis.* J Clin Invest, 1977. **60**(6): p. 1221-9.

50. Kodish, M.E., R.N. Alsever, and M.B. Block, *Benign symmetric lipomatosis: functional sympathetic denervation of adipose tissue and possible hypertrophy of brown fat.* Metabolism, 1974. **23**(10): p. 937-45.
51. Nisoli, E., et al., *Multiple symmetric lipomatosis may be the consequence of defective noradrenergic modulation of proliferation and differentiation of brown fat cells.* J Pathol, 2002. **198**(3): p. 378-87.
52. Gamez, J., et al., *Familial multiple symmetric lipomatosis associated with the A8344G mutation of mitochondrial DNA.* Neurology, 1998. **51**(1): p. 258-60.
53. Holme, E., et al., *Multiple symmetric lipomas with high levels of mtDNA with the tRNA(Lys) A-->G(8344) mutation as the only manifestation of disease in a carrier of myoclonus epilepsy and ragged-red fibers (MERRF) syndrome.* Am J Hum Genet, 1993. **52**(3): p. 551-6.
54. Mancuso, M., et al., *Encephalomyopathy with multiple mitochondrial DNA deletions and multiple symmetric lipomatosis: further evidence of a possible association.* J Neurol, 1999. **246**(12): p. 1197-8.
55. Guallar, J.P., et al., *Altered expression of master regulatory genes of adipogenesis in lipomas from patients bearing tRNA(Lys) point mutations in mitochondrial DNA.* Mol Genet Metab, 2006. **89**(3): p. 283-5.
56. Sawyer, S.L., et al., *Homozygous mutations in MFN2 cause multiple symmetric lipomatosis associated with neuropathy.* Hum Mol Genet, 2015. **24**(18): p. 5109-14.
57. Munoz-Malaga, A., et al., *Lipomatosis, proximal myopathy, and the mitochondrial 8344 mutation. A lipid storage myopathy?* Muscle Nerve, 2000. **23**(4): p. 538-42.
58. Becker-Wegerich, P., et al., *Defects of mitochondrial respiratory chain in multiple symmetric lipomatosis.* Arch Dermatol Res, 1998. **290**(12): p. 652-5.
59. Finsterer, J., *Mitochondrial neuropathy.* Clin Neurol Neurosurg, 2005. **107**(3): p. 181-6.
60. Canto, C., et al., *The NAD(+) precursor nicotinamide riboside enhances oxidative metabolism and protects against high-fat diet-induced obesity.* Cell Metab, 2012. **15**(6): p. 838-47.
61. Sanchez-Gurmaches, J., et al., *PTEN loss in the Myf5 lineage redistributes body fat and reveals subsets of white adipocytes that arise from Myf5 precursors.* Cell Metab, 2012. **16**(3): p. 348-62.
62. Prantl, L., et al., *Transcription Profile in Sporadic Multiple Symmetric Lipomatosis Reveals Differential Expression at the Level of Adipose Tissue-Derived Stem Cells.* Plast Reconstr Surg, 2016. **137**(4): p. 1181-90.
63. Zancanaro, C., et al., *Multiple symmetric lipomatosis. Ultrastructural investigation of the tissue and preadipocytes in primary culture.* Lab Invest, 1990. **63**(2): p. 253-8.
64. Meresse, T.G., J.L.; Garrido, I**.**, 2013.
65. Busetto, L.E., G. , *Multiple Symmetric Lipomatosis. Encyclopedia of Molecular Mechanisms of Disease.* Lang F. Ed ed. 2009: Springer-Verlag Gmbh.
66. Nielsen, S., et al., *Adipose tissue metabolism in benign symmetric lipomatosis.* J Clin Endocrinol Metab, 2001. **86**(6): p. 2717-20.
67. Cinti, S., et al., *Ultrastructural features of cultured mature adipocyte precursors from adipose tissue in multiple symmetric lipomatosis.* Ultrastruct Pathol, 1983. **5**(2-3): p. 145-52.
68. Chen, K., et al., *Profiling of differentially expressed genes in adipose tissues of multiple symmetric lipomatosis.* Mol Med Rep, 2017. **16**(5): p. 6570-6579.
69. Kveiborg, M., et al., *DeltaFosB induces osteosclerosis and decreases adipogenesis by two independent cell-autonomous mechanisms.* Mol Cell Biol, 2004. **24**(7): p. 2820-30.
70. Luther, J., et al., *Elevated Fra-1 expression causes severe lipodystrophy.* J Cell Sci, 2011. **124**(Pt 9): p. 1465-76.
71. Chen, K., et al., *miR-125a-3p and miR-483-5p promote adipogenesis via suppressing the RhoA/ROCK1/ERK1/2 pathway in multiple symmetric lipomatosis.* Sci Rep, 2015. **5**: p. 11909.
72. Prusty, D., et al., *Activation of MEK/ERK signaling promotes adipogenesis by enhancing peroxisome proliferator-activated receptor gamma (PPARgamma) and C/EBPalpha gene expression during the differentiation of 3T3-L1 preadipocytes.* J Biol Chem, 2002. **277**(48): p. 46226-32.
73. Huang, B., et al., *MiRNA-125a-3p is a negative regulator of the RhoA-actomyosin pathway in A549 cells.* Int J Oncol, 2013. **42**(5): p. 1734-42.

74. Bassetto, F., et al., *Surgical Treatment of Multiple Symmetric Lipomatosis With Ultrasound-Assisted Liposuction.* Ann Plast Surg, 2013.
75. Verhelle, N.A., et al., *Liposuction in benign symmetric lipomatosis: sense or senseless?* Aesthetic Plast Surg, 2003. **27**(4): p. 319-21.
76. Constantinidis, J., et al., *Combined surgical lipectomy and liposuction in the treatment of benign symmetrical lipomatosis of the head and neck.* Scand J Plast Reconstr Surg Hand Surg, 2003. **37**(2): p. 90-6.
77. Ujpal, M., et al., *Long-term results following surgical treatment of benign symmetric lipomatosis (BSL).* Int J Oral Maxillofac Surg, 2001. **30**(6): p. 479-83.
78. Zeitler, H., et al., *Multiple benign symmetric lipomatosis--a differential diagnosis of obesity. Is there a rationale for fibrate treatment?* Obes Surg, 2008. **18**(10): p. 1354-6.
79. Hasegawa, T., T. Matsukura, and S. Ikeda, *Mesotherapy for benign symmetric lipomatosis.* Aesthetic Plast Surg, 2010. **34**(2): p. 153-6.
80. Rosato, L., et al., *Mesotherapy should not replace the surgical approach in the treatment of benign symmetric lipomatosis.* Aesthetic Plast Surg, 2011. **35**(2): p. 278-80.
81. Leung, N.W., et al., *Multiple symmetric lipomatosis (Launois-Bensaude syndrome): effect of oral salbutamol.* Clin Endocrinol (Oxf), 1987. **27**(5): p. 601-6.
82. Keppler-Noreuil, K.M., et al., *PIK3CA-related overgrowth spectrum (PROS): diagnostic and testing eligibility criteria, differential diagnosis, and evaluation.* Am J Med Genet A, 2015. **167A**(2): p. 287-95.
83. Keppler-Noreuil, K.M., et al., *Somatic overgrowth disorders of the PI3K/AKT/mTOR pathway & therapeutic strategies.* Am J Med Genet C Semin Med Genet, 2016. **172**(4): p. 402-421.
84. Wu, J., et al., *Beige adipocytes are a distinct type of thermogenic fat cell in mouse and human.* Cell, 2012. **150**(2): p. 366-76.
85. Wang, W. and P. Seale, *Control of brown and beige fat development.* Nat Rev Mol Cell Biol, 2016. **17**(11): p. 691-702.
86. Seale, P., et al., *PRDM16 controls a brown fat/skeletal muscle switch.* Nature, 2008. **454**(7207): p. 961-7.
87. Berry, D.C., Y. Jiang, and J.M. Graff, *Emerging Roles of Adipose Progenitor Cells in Tissue Development, Homeostasis, Expansion and Thermogenesis.* Trends Endocrinol Metab, 2016. **27**(8): p. 574-85.
88. Rosen, E.D. and B.M. Spiegelman, *What we talk about when we talk about fat.* Cell, 2014. **156**(1-2): p. 20-44.
89. Lee, Y.H., et al., *In vivo identification of bipotential adipocyte progenitors recruited by beta3-adrenoceptor activation and high-fat feeding.* Cell Metab, 2012. **15**(4): p. 480-91.
90. Wang, Q.A., et al., *Tracking adipogenesis during white adipose tissue development, expansion and regeneration.* Nat Med, 2013. **19**(10): p. 1338-44.
91. Barbatelli, G., et al., *The emergence of cold-induced brown adipocytes in mouse white fat depots is determined predominantly by white to brown adipocyte transdifferentiation.* Am J Physiol Endocrinol Metab, 2010. **298**(6): p. E1244-53.
92. Himms-Hagen, J., et al., *Multilocular fat cells in WAT of CL-316243-treated rats derive directly from white adipocytes.* Am J Physiol Cell Physiol, 2000. **279**(3): p. C670-81.
93. Lee, Y.H., et al., *Cellular origins of cold-induced brown adipocytes in adult mice.* FASEB J, 2015. **29**(1): p. 286-99.
94. Vitali, A., et al., *The adipose organ of obesity-prone C57BL/6J mice is composed of mixed white and brown adipocytes.* J Lipid Res, 2012. **53**(4): p. 619-29.
95. Sharp, L.Z., et al., *Human BAT possesses molecular signatures that resemble beige/brite cells.* PLoS One, 2012. **7**(11): p. e49452.
96. Cypess, A.M., et al., *Anatomical localization, gene expression profiling and functional characterization of adult human neck brown fat.* Nat Med, 2013. **19**(5): p. 635-9.

97. Di Franco, A., et al., *Dissecting the origin of inducible brown fat in adult humans through a novel adipose stem cell model from adipose tissue surrounding pheochromocytoma.* J Clin Endocrinol Metab, 2014. **99**(10): p. E1903-12.
98. Frontini, A., et al., *White-to-brown transdifferentiation of omental adipocytes in patients affected by pheochromocytoma.* Biochim Biophys Acta, 2013. **1831**(5): p. 950-9.
99. Jespersen, N.Z., et al., *A classical brown adipose tissue mRNA signature partly overlaps with brite in the supraclavicular region of adult humans.* Cell Metab, 2013. **17**(5): p. 798-805.
100. Walden, T.B., et al., *Recruited vs. nonrecruited molecular signatures of brown, "brite," and white adipose tissues.* Am J Physiol Endocrinol Metab, 2011. **302**(1): p. E19-31.
101. Westerberg, R., et al., *ELOVL3 is an important component for early onset of lipid recruitment in brown adipose tissue.* J Biol Chem, 2006. **281**(8): p. 4958-68.
102. Rodeheffer, M.S., K. Birsoy, and J.M. Friedman, *Identification of white adipocyte progenitor cells in vivo.* Cell, 2008. **135**(2): p. 240-9.
103. Zuk, P.A., et al., *Multilineage cells from human adipose tissue: implications for cell-based therapies.* Tissue Eng, 2001. **7**(2): p. 211-28.
104. Baer, P.C., *Adipose-derived mesenchymal stromal/stem cells: An update on their phenotype in vivo and in vitro.* World J Stem Cells, 2014. **6**(3): p. 256-65.
105. Sidney, L.E., et al., *Concise review: evidence for CD34 as a common marker for diverse progenitors.* Stem Cells, 2014. **32**(6): p. 1380-9.
106. Tang, Q.Q. and M.D. Lane, *Adipogenesis: from stem cell to adipocyte.* Annu Rev Biochem, 2012. **81**: p. 715-36.
107. Garvey, W.T., *New tools for weight-loss therapy enable a more robust medical model for obesity treatment: rationale for a complications-centric approach.* Endocr Pract, 2013. **19**(5): p. 864-74.
108. Buchwald, H., J.N. Buchwald, and T.W. McGlennon, *Systematic review and meta-analysis of medium-term outcomes after banded Roux-en-Y gastric bypass.* Obes Surg, 2014. **24**(9): p. 1536-51.
109. Buchwald, H. and D.M. Oien, *Metabolic/bariatric surgery worldwide 2011.* Obes Surg, 2013. **23**(4): p. 427-36.
110. Hossain, P., B. Kawar, and M. El Nahas, *Obesity and diabetes in the developing world--a growing challenge.* N Engl J Med, 2007. **356**(3): p. 213-5.
111. Ertunc, M.E. and G.S. Hotamisligil, *Lipid signaling and lipotoxicity in metaflammation: indications for metabolic disease pathogenesis and treatment.* J Lipid Res, 2016. **57**(12): p. 2099-2114.
112. Czech, M.P., *Insulin action and resistance in obesity and type 2 diabetes.* Nat Med, 2017. **23**(7): p. 804-814.
113. Erion, K.A., et al., *Chronic Exposure to Excess Nutrients Left-shifts the Concentration Dependence of Glucose-stimulated Insulin Secretion in Pancreatic beta-Cells.* J Biol Chem, 2015. **290**(26): p. 16191-201.
114. Taniguchi, C.M., B. Emanuelli, and C.R. Kahn, *Critical nodes in signalling pathways: insights into insulin action.* Nat Rev Mol Cell Biol, 2006. **7**(2): p. 85-96.
115. Avruch, J., *Insulin signal transduction through protein kinase cascades.* Mol Cell Biochem, 1998. **182**(1-2): p. 31-48.
116. Manning, B.D. and L.C. Cantley, *AKT/PKB signaling: navigating downstream.* Cell, 2007. **129**(7): p. 1261-74.
117. Brady, M.J., F.J. Bourbonais, and A.R. Saltiel, *The activation of glycogen synthase by insulin switches from kinase inhibition to phosphatase activation during adipogenesis in 3T3-L1 cells.* J Biol Chem, 1998. **273**(23): p. 14063-6.
118. Cross, D.A., et al., *Inhibition of glycogen synthase kinase-3 by insulin mediated by protein kinase B.* Nature, 1995. **378**(6559): p. 785-9.
119. Kane, S., et al., *A method to identify serine kinase substrates. Akt phosphorylates a novel adipocyte protein with a Rab GTPase-activating protein (GAP) domain.* J Biol Chem, 2002. **277**(25): p. 22115-8.
120. Sano, H., et al., *Insulin-stimulated phosphorylation of a Rab GTPase-activating protein regulates GLUT4 translocation.* J Biol Chem, 2003. **278**(17): p. 14599-602.

121. Liu, L.B., et al., *The SUMO conjugating enzyme Ubc9 is a regulator of GLUT4 turnover and targeting to the insulin-responsive storage compartment in 3T3-L1 adipocytes.* Diabetes, 2007. **56**(8): p. 1977-85.
122. Sargeant, R.J. and M.R. Paquet, *Effect of insulin on the rates of synthesis and degradation of GLUT1 and GLUT4 glucose transporters in 3T3-L1 adipocytes.* Biochem J, 1993. **290 (Pt 3)**: p. 913-9.
123. Puigserver, P., et al., *Insulin-regulated hepatic gluconeogenesis through FOXO1-PGC-1alpha interaction.* Nature, 2003. **423**(6939): p. 550-5.
124. Nakae, J., et al., *The forkhead transcription factor Foxo1 regulates adipocyte differentiation.* Dev Cell, 2003. **4**(1): p. 119-29.
125. Kimmel, A.R. and C. Sztalryd, *The Perilipins: Major Cytosolic Lipid Droplet-Associated Proteins and Their Roles in Cellular Lipid Storage, Mobilization, and Systemic Homeostasis.* Annu Rev Nutr, 2016. **36**: p. 471-509.
126. Choi, S.M., et al., *Insulin regulates adipocyte lipolysis via an Akt-independent signaling pathway.* Mol Cell Biol, 2010. **30**(21): p. 5009-20.
127. Caron, A., D. Richard, and M. Laplante, *The Roles of mTOR Complexes in Lipid Metabolism.* Annu Rev Nutr, 2015. **35**: p. 321-48.
128. Chan, T.O., S.E. Rittenhouse, and P.N. Tsichlis, *AKT/PKB and other D3 phosphoinositide-regulated kinases: kinase activation by phosphoinositide-dependent phosphorylation.* Annu Rev Biochem, 1999. **68**: p. 965-1014.
129. Fischer-Posovszky, P., et al., *Differential function of Akt1 and Akt2 in human adipocytes.* Mol Cell Endocrinol, 2012. **358**(1): p. 135-43.
130. Jiang, Z.Y., et al., *Insulin signaling through Akt/protein kinase B analyzed by small interfering RNA-mediated gene silencing.* Proc Natl Acad Sci U S A, 2003. **100**(13): p. 7569-74.
131. Garofalo, R.S., et al., *Severe diabetes, age-dependent loss of adipose tissue, and mild growth deficiency in mice lacking Akt2/PKB beta.* J Clin Invest, 2003. **112**(2): p. 197-208.
132. George, S., et al., *A family with severe insulin resistance and diabetes due to a mutation in AKT2.* Science, 2004. **304**(5675): p. 1325-8.
133. Hussain, K., et al., *An activating mutation of AKT2 and human hypoglycemia.* Science, 2011. **334**(6055): p. 474.
134. Tschopp, O., et al., *Essential role of protein kinase B gamma (PKB gamma/Akt3) in postnatal brain development but not in glucose homeostasis.* Development, 2005. **132**(13): p. 2943-54.
135. Wijesekara, N., et al., *Muscle-specific Pten deletion protects against insulin resistance and diabetes.* Mol Cell Biol, 2005. **25**(3): p. 1135-45.
136. Klotz, L.O., et al., *Redox regulation of FoxO transcription factors.* Redox Biol, 2015. **6**: p. 51-72.
137. Bar-Peled, L. and D.M. Sabatini, *Regulation of mTORC1 by amino acids.* Trends Cell Biol, 2014. **24**(7): p. 400-6.
138. Ryder, J.W., M. Gilbert, and J.R. Zierath, *Skeletal muscle and insulin sensitivity: pathophysiological alterations.* Front Biosci, 2001. **6**: p. D154-63.
139. Titchenell, P.M., et al., *Direct Hepatocyte Insulin Signaling Is Required for Lipogenesis but Is Dispensable for the Suppression of Glucose Production.* Cell Metab, 2016. **23**(6): p. 1154-1166.
140. Schoiswohl, G., et al., *Impact of Reduced ATGL-Mediated Adipocyte Lipolysis on Obesity-Associated Insulin Resistance and Inflammation in Male Mice.* Endocrinology, 2015. **156**(10): p. 3610-24.
141. Parker, V.E., et al., *Mechanistic insights into insulin resistance in the genetic era.* Diabet Med, 2011. **28**(12): p. 1476-86.
142. Chaurasia, B. and S.A. Summers, *Ceramides - Lipotoxic Inducers of Metabolic Disorders.* Trends Endocrinol Metab, 2015. **26**(10): p. 538-50.
143. Hoehn, K.L., et al., *IRS1-independent defects define major nodes of insulin resistance.* Cell Metab, 2008. **7**(5): p. 421-33.
144. Turner, N., et al., *Distinct patterns of tissue-specific lipid accumulation during the induction of insulin resistance in mice by high-fat feeding.* Diabetologia, 2013. **56**(7): p. 1638-48.
145. Williams, A.S., L. Kang, and D.H. Wasserman, *The extracellular matrix and insulin resistance.* Trends Endocrinol Metab, 2015. **26**(7): p. 357-66.

146. Pinna, L.A. and A. Donella-Deana, *Phosphorylated synthetic peptides as tools for studying protein phosphatases.* Biochim Biophys Acta, 1994. **1222**(3): p. 415-31.
147. Salvi, M., et al., *Extraordinary pleiotropy of protein kinase CK2 revealed by weblogo phosphoproteome analysis.* Biochim Biophys Acta, 2009. **1793**(5): p. 847-59.
148. Issinger, O.G., *Casein kinases: pleiotropic mediators of cellular regulation.* Pharmacol Ther, 1993. **59**(1): p. 1-30.
149. Ruzzene, M. and L.A. Pinna, *Addiction to protein kinase CK2: a common denominator of diverse cancer cells?* Biochim Biophys Acta, 2010. **1804**(3): p. 499-504.
150. Escalier, D., D. Silvius, and X. Xu, *Spermatogenesis of mice lacking CK2alpha': failure of germ cell survival and characteristic modifications of the spermatid nucleus.* Mol Reprod Dev, 2003. **66**(2): p. 190-201.
151. Niefind, K., et al., *Crystal structure of human protein kinase CK2: insights into basic properties of the CK2 holoenzyme.* EMBO J, 2001. **20**(19): p. 5320-31.
152. Sarno, S., et al., *Cooperative modulation of protein kinase CK2 by separate domains of its regulatory beta-subunit.* Biochemistry, 2000. **39**(40): p. 12324-9.
153. Boldyreff, B., et al., *Reconstitution of normal and hyperactivated forms of casein kinase-2 by variably mutated beta-subunits.* Biochemistry, 1993. **32**(47): p. 12672-7.
154. Litchfield, D.W., *Protein kinase CK2: structure, regulation and role in cellular decisions of life and death.* Biochem J, 2003. **369**(Pt 1): p. 1-15.
155. Zhang, C., et al., *Phosphorylation regulates the stability of the regulatory CK2beta subunit.* Oncogene, 2002. **21**(23): p. 3754-64.
156. Leroy, D., et al., *Binding of polyamines to an autonomous domain of the regulatory subunit of protein kinase CK2 induces a conformational change in the holoenzyme. A proposed role for the kinase stimulation.* J Biol Chem, 1997. **272**(33): p. 20820-7.
157. Meggio, F., O. Marin, and L.A. Pinna, *Substrate specificity of protein kinase CK2.* Cell Mol Biol Res, 1994. **40**(5-6): p. 401-9.
158. Sarno, S., P. Ghisellini, and L.A. Pinna, *Unique activation mechanism of protein kinase CK2. The N-terminal segment is essential for constitutive activity of the catalytic subunit but not of the holoenzyme.* J Biol Chem, 2002. **277**(25): p. 22509-14.
159. Olsten, M.E. and D.W. Litchfield, *Order or chaos? An evaluation of the regulation of protein kinase CK2.* Biochem Cell Biol, 2004. **82**(6): p. 681-93.
160. Nunez de Villavicencio-Diaz, T., A.J. Rabalski, and D.W. Litchfield, *Protein Kinase CK2: Intricate Relationships within Regulatory Cellular Networks.* Pharmaceuticals (Basel), 2017. **10**(1).
161. Lupp, S., et al., *CK2 kinase activity but not its binding to CK2 promoter regions is implicated in the regulation of CK2alpha and CK2beta gene expressions.* Mol Cell Biochem, 2013. **384**(1-2): p. 71-82.
162. St-Denis, N., et al., *Systematic investigation of hierarchical phosphorylation by protein kinase CK2.* J Proteomics, 2015. **118**: p. 49-62.
163. Al Quobaili, F. and M. Montenarh, *CK2 and the regulation of the carbohydrate metabolism.* Metabolism, 2012. **61**(11): p. 1512-7.
164. Di Maira, G., et al., *Dephosphorylation and inactivation of Akt/PKB is counteracted by protein kinase CK2 in HEK 293T cells.* Cell Mol Life Sci, 2009. **66**(20): p. 3363-73.
165. Girardi, C., et al., *Differential phosphorylation of Akt1 and Akt2 by protein kinase CK2 may account for isoform specific functions.* Biochim Biophys Acta, 2014. **1843**(9): p. 1865-74.
166. Torres, J. and R. Pulido, *The tumor suppressor PTEN is phosphorylated by the protein kinase CK2 at its C terminus. Implications for PTEN stability to proteasome-mediated degradation.* J Biol Chem, 2001. **276**(2): p. 993-8.
167. Cohen, P., *The twentieth century struggle to decipher insulin signalling.* Nat Rev Mol Cell Biol, 2006. **7**(11): p. 867-73.
168. Wong, J.T., et al., *Pten (phosphatase and tensin homologue gene) haploinsufficiency promotes insulin hypersensitivity.* Diabetologia, 2007. **50**(2): p. 395-403.
169. Pal, A., et al., *PTEN mutations as a cause of constitutive insulin sensitivity and obesity.* N Engl J Med, 2012. **367**(11): p. 1002-11.

170. Ma, J., et al., *Prolonged insulin stimulation down-regulates GLUT4 through oxidative stress-mediated retromer inhibition by a protein kinase CK2-dependent mechanism in 3T3-L1 adipocytes.* J Biol Chem, 2014. **289**(1): p. 133-42.
171. Meng, R., C. Gotz, and M. Montenarh, *The role of protein kinase CK2 in the regulation of the insulin production of pancreatic islets.* Biochem Biophys Res Commun, 2010. **401**(2): p. 203-6.
172. Welker, S., et al., *Glucose regulates protein kinase CK2 in pancreatic beta-cells and its interaction with PDX-1.* Int J Biochem Cell Biol, 2013. **45**(12): p. 2786-95.
173. Rossi, M., et al., *CK2 acts as a potent negative regulator of receptor-mediated insulin release in vitro and in vivo.* Proc Natl Acad Sci U S A, 2015. **112**(49): p. E6818-24.
174. Marselli, L., et al., *Gene expression profiles of Beta-cell enriched tissue obtained by laser capture microdissection from subjects with type 2 diabetes.* PLoS One, 2010. **5**(7): p. e11499.
175. Sommercorn, J. and E.G. Krebs, *Induction of casein kinase II during differentiation of 3T3-L1 cells.* J Biol Chem, 1987. **262**(8): p. 3839-43.
176. Wilhelm, N., et al., *Protein kinase CK2 is implicated in early steps of the differentiation of pre-adipocytes into adipocytes.* Mol Cell Biochem, 2012. **365**(1-2): p. 37-45.
177. Schwind, L., et al., *Quinalizarin inhibits adipogenesis through down-regulation of transcription factors and microRNA modulation.* Biochim Biophys Acta, 2017. **1861**(12): p. 3272-3281.
178. Schwind, L., S. Schetting, and M. Montenarh, *Inhibition of Protein Kinase CK2 Prevents Adipogenic Differentiation of Mesenchymal Stem Cells Like C3H/10T1/2 Cells.* Pharmaceuticals (Basel), 2017. **10**(1).
179. Chen, Q., et al., *SIRT6 Is Essential for Adipocyte Differentiation by Regulating Mitotic Clonal Expansion.* Cell Rep, 2017. **18**(13): p. 3155-3166.
180. Shinoda, K., et al., *Phosphoproteomics Identifies CK2 as a Negative Regulator of Beige Adipocyte Thermogenesis and Energy Expenditure.* Cell Metab, 2015. **22**(6): p. 997-1008.
181. Hubert, A., et al., *Casein kinase 2 inhibition decreases hypoxia-inducible factor-1 activity under hypoxia through elevated p53 protein level.* J Cell Sci, 2006. **119**(Pt 16): p. 3351-62.
182. Mottet, D., et al., *Role for casein kinase 2 in the regulation of HIF-1 activity.* Int J Cancer, 2005. **117**(5): p. 764-74.
183. Schaefer, S., et al., *D11-Mediated Inhibition of Protein Kinase CK2 Impairs HIF-1alpha-Mediated Signaling in Human Glioblastoma Cells.* Pharmaceuticals (Basel), 2017. **10**(1).
184. Ampofo, E., et al., *Phosphorylation of the von Hippel-Lindau protein (VHL) by protein kinase CK2 reduces its protein stability and affects p53 and HIF-1alpha mediated transcription.* Int J Biochem Cell Biol, 2010. **42**(10): p. 1729-35.
185. Feng, D., et al., *Protein kinase CK2 is a regulator of angiogenesis in endometriotic lesions.* Angiogenesis, 2012. **15**(2): p. 243-52.
186. Afonyushkin, T., et al., *Involvement of CK2 in activation of electrophilic genes in endothelial cells by oxidized phospholipids.* J Lipid Res, 2011. **52**(1): p. 98-103.
187. Noy, P., et al., *Protein kinase CK2 inactivates PRH/Hhex using multiple mechanisms to de-repress VEGF-signalling genes and promote cell survival.* Nucleic Acids Res, 2012. **40**(18): p. 9008-20.
188. Pollreisz, A., et al., *Retinal pigment epithelium cells produce VEGF in response to oxidized phospholipids through mechanisms involving ATF4 and protein kinase CK2.* Exp Eye Res, 2013. **116**: p. 177-84.
189. Garat, C.V., et al., *Thiazolidinediones prevent PDGF-BB-induced CREB depletion in pulmonary artery smooth muscle cells by preventing upregulation of casein kinase 2 alpha' catalytic subunit.* J Cardiovasc Pharmacol, 2010. **55**(5): p. 469-80.
190. Maik-Rachline, G. and R. Seger, *Variable phosphorylation states of pigment-epithelium-derived factor differentially regulate its function.* Blood, 2006. **107**(7): p. 2745-52.
191. Lee, N.Y., et al., *Casein kinase 2beta as a novel enhancer of activin-like receptor-1 signaling.* FASEB J, 2009. **23**(11): p. 3712-21.
192. Heiker, J.T., et al., *Protein kinase CK2 interacts with adiponectin receptor 1 and participates in adiponectin signaling.* Cell Signal, 2009. **21**(6): p. 936-42.

193. Juhl, C., K. Morl, and A.G. Beck-Sickinger, *Adiponectin receptor 1 interacts with both subunits of protein kinase CK2.* Mol Cell Biochem, 2011. **356**(1-2): p. 185-9.
194. Sassa, T., T. Hirayama, and A. Kihara, *Enzyme Activities of the Ceramide Synthases CERS2-6 Are Regulated by Phosphorylation in the C-terminal Region.* J Biol Chem, 2016. **291**(14): p. 7477-87.
195. Raichur, S., et al., *CerS2 haploinsufficiency inhibits beta-oxidation and confers susceptibility to diet-induced steatohepatitis and insulin resistance.* Cell Metab, 2014. **20**(4): p. 687-95.
196. Turpin, S.M., et al., *Obesity-induced CerS6-dependent C16:0 ceramide production promotes weight gain and glucose intolerance.* Cell Metab, 2014. **20**(4): p. 678-86.
197. Kanfi, Y., et al., *SIRT6 protects against pathological damage caused by diet-induced obesity.* Aging Cell, 2010. **9**(2): p. 162-73.
198. Kim, H.S., et al., *Hepatic-specific disruption of SIRT6 in mice results in fatty liver formation due to enhanced glycolysis and triglyceride synthesis.* Cell Metab, 2010. **12**(3): p. 224-36.
199. Finkel, T., C.X. Deng, and R. Mostoslavsky, *Recent progress in the biology and physiology of sirtuins.* Nature, 2009. **460**(7255): p. 587-91.
200. Gillum, M.P., et al., *SirT1 regulates adipose tissue inflammation.* Diabetes, 2011. **60**(12): p. 3235-45.
201. Kemper, J.K., S.E. Choi, and D.H. Kim, *Sirtuin 1 deacetylase: a key regulator of hepatic lipid metabolism.* Vitam Horm, 2013. **91**: p. 385-404.
202. Pfluger, P.T., et al., *Sirt1 protects against high-fat diet-induced metabolic damage.* Proc Natl Acad Sci U S A, 2008. **105**(28): p. 9793-8.
203. Purushotham, A., et al., *Hepatocyte-specific deletion of SIRT1 alters fatty acid metabolism and results in hepatic steatosis and inflammation.* Cell Metab, 2009. **9**(4): p. 327-38.
204. Choi, S.E., et al., *Obesity-Linked Phosphorylation of SIRT1 by Casein Kinase 2 Inhibits Its Nuclear Localization and Promotes Fatty Liver.* Mol Cell Biol, 2017. **37**(15).
205. Huang, J., et al., *Protein kinase CK2alpha catalytic subunit ameliorates diabetic renal inflammatory fibrosis via NF-kappaB signaling pathway.* Biochem Pharmacol, 2017. **132**: p. 102-117.
206. Ahmed, K., et al., *Significance of protein kinase CK2 nuclear signaling in neoplasia.* J Cell Biochem Suppl, 2000. **Suppl 35**: p. 130-5.
207. Pinna, L.A., *Protein kinase CK2.* Int J Biochem Cell Biol, 1997. **29**(4): p. 551-4.
208. Izeradjene, K., et al., *Casein kinase I attenuates tumor necrosis factor-related apoptosis-inducing ligand-induced apoptosis by regulating the recruitment of fas-associated death domain and procaspase-8 to the death-inducing signaling complex.* Cancer Res, 2004. **64**(21): p. 8036-44.
209. Yamane, K. and T.J. Kinsella, *CK2 inhibits apoptosis and changes its cellular localization following ionizing radiation.* Cancer Res, 2005. **65**(10): p. 4362-7.
210. Torres, J., et al., *Phosphorylation-regulated cleavage of the tumor suppressor PTEN by caspase-3: implications for the control of protein stability and PTEN-protein interactions.* J Biol Chem, 2003. **278**(33): p. 30652-60.
211. Tawfic, S., et al., *Protein kinase CK2 signal in neoplasia.* Histol Histopathol, 2001. **16**(2): p. 573-82.
212. Trembley, J.H., et al., *Emergence of protein kinase CK2 as a key target in cancer therapy.* Biofactors, 2010. **36**(3): p. 187-95.
213. Ahmad, K.A., et al., *Protein kinase CK2--a key suppressor of apoptosis.* Adv Enzyme Regul, 2008. **48**: p. 179-87.
214. St-Denis, N.A. and D.W. Litchfield, *Protein kinase CK2 in health and disease: From birth to death: the role of protein kinase CK2 in the regulation of cell proliferation and survival.* Cell Mol Life Sci, 2009. **66**(11-12): p. 1817-29.
215. Dovat, S., et al., *Ikaros, CK2 kinase, and the road to leukemia.* Mol Cell Biochem, 2011. **356**(1-2): p. 201-7.
216. Song, C., et al., *Regulation of Ikaros function by casein kinase 2 and protein phosphatase 1.* World J Biol Chem, 2011. **2**(6): p. 126-31.
217. Cozza, G. and L.A. Pinna, *Casein kinases as potential therapeutic targets.* Expert Opin Ther Targets, 2016. **20**(3): p. 319-40.

218. Siddiqui-Jain, A., et al., *CX-4945, an orally bioavailable selective inhibitor of protein kinase CK2, inhibits prosurvival and angiogenic signaling and exhibits antitumor efficacy.* Cancer Res, 2010. **70**(24): p. 10288-98.
219. Chon, H.J., et al., *The casein kinase 2 inhibitor, CX-4945, as an anti-cancer drug in treatment of human hematological malignancies.* Front Pharmacol, 2015. **6**: p. 70.
220. Hung, M.S., et al., *Identification of hematein as a novel inhibitor of protein kinase CK2 from a natural product library.* BMC Cancer, 2009. **9**: p. 135.
221. Borgo, C., et al., *Aberrant signalling by protein kinase CK2 in imatinib-resistant chronic myeloid leukaemia cells: biochemical evidence and therapeutic perspectives.* Mol Oncol, 2013. **7**(6): p. 1103-15.
222. Yumuk, V., et al., *European Guidelines for Obesity Management in Adults.* Obes Facts, 2015. **8**(6): p. 402-24.
223. Matthews, D.R., et al., *Homeostasis model assessment: insulin resistance and beta-cell function from fasting plasma glucose and insulin concentrations in man.* Diabetologia, 1985. **28**(7): p. 412-9.
224. Chen, G., et al., *Glucosamine-induced insulin resistance is coupled to O-linked glycosylation of Munc18c.* FEBS Lett, 2003. **534**(1-3): p. 54-60.
225. Hu, Y. and G.K. Smyth, *ELDA: extreme limiting dilution analysis for comparing depleted and enriched populations in stem cell and other assays.* J Immunol Methods, 2009. **347**(1-2): p. 70-8.
226. Ginsberg, M., et al., *Efficient direct reprogramming of mature amniotic cells into endothelial cells by ETS factors and TGFbeta suppression.* Cell, 2012. **151**(3): p. 559-75.
227. Tremp, M., et al., *Adipose-Derived Stromal Cells from Lipomas: Isolation, Characterisation and Review of the Literature.* Pathobiology, 2016. **83**(5): p. 258-66.
228. Jorgensen, J.A., D. Zadravec, and A. Jacobsson, *Norepinephrine and rosiglitazone synergistically induce Elovl3 expression in brown adipocytes.* Am J Physiol Endocrinol Metab, 2007. **293**(5): p. E1159-68.
229. Jakobsson, A., J.A. Jorgensen, and A. Jacobsson, *Differential regulation of fatty acid elongation enzymes in brown adipocytes implies a unique role for Elovl3 during increased fatty acid oxidation.* Am J Physiol Endocrinol Metab, 2005. **289**(4): p. E517-26.
230. Kobayashi, T. and K. Fujimori, *Very long-chain-fatty acids enhance adipogenesis through coregulation of Elovl3 and PPARgamma in 3T3-L1 cells.* Am J Physiol Endocrinol Metab, 2012. **302**(12): p. E1461-71.
231. Ji, L., M. Gupta, and B.J. Feldman, *Vitamin D Regulates Fatty Acid Composition in Subcutaneous Adipose Tissue Through Elovl3.* Endocrinology, 2016. **157**(1): p. 91-7.
232. Hei, Y.J., et al., *Characterization of insulin-stimulated seryl/threonyl protein kinases in rat skeletal muscle.* J Biol Chem, 1993. **268**(18): p. 13203-13.
233. Maeda, R., et al., *Activation of skeletal muscle casein kinase II by insulin is not diminished in subjects with insulin resistance.* J Clin Invest, 1991. **87**(3): p. 1017-22.
234. Roher, N., et al., *Protein kinase CK2 is altered in insulin-resistant genetically obese (fa/fa) rats.* FEBS Lett, 1998. **437**(3): p. 211-5.
235. Kusminski, C.M., P.E. Bickel, and P.E. Scherer, *Targeting adipose tissue in the treatment of obesity-associated diabetes.* Nat Rev Drug Discov, 2016. **15**(9): p. 639-60.
236. Samuel, V.T. and G.I. Shulman, *The pathogenesis of insulin resistance: integrating signaling pathways and substrate flux.* J Clin Invest, 2016. **126**(1): p. 12-22.
237. Dominguez, I., G.E. Sonenshein, and D.C. Seldin, *Protein kinase CK2 in health and disease: CK2 and its role in Wnt and NF-kappaB signaling: linking development and cancer.* Cell Mol Life Sci, 2009. **66**(11-12): p. 1850-7.
238. Gilbert, C.A. and J.M. Slingerland, *Cytokines, obesity, and cancer: new insights on mechanisms linking obesity to cancer risk and progression.* Annu Rev Med, 2013. **64**: p. 45-57.